Nuclear Safety
NEA/CSNI/R(2017)19
February 2019
www.oecd-nea.org

NEA Benchmark Exercise: Computational Fluid Dynamic Prediction and Uncertainty Quantification of a GEMIX Mixing Layer Test

OECD
BETTER POLICIES FOR BETTER LIVES

NEA
NUCLEAR ENERGY AGENCY

Nuclear Energy Agency

NEA/CSNI/R(2017)19

Unclassified

English text only

6 February 2019

NUCLEAR ENERGY AGENCY
COMMITTEE ON THE SAFETY OF NUCLEAR INSTALLATIONS

NEA Benchmark Exercise: Computational Fluid Dynamic Prediction and Uncertainty Quantification of a GEMIX Mixing Layer Test

JT03442730

ORGANISATION FOR ECONOMIC CO-OPERATION AND DEVELOPMENT

The OECD is a unique forum where the governments of 36 democracies work together to address the economic, social and environmental challenges of globalisation. The OECD is also at the forefront of efforts to understand and to help governments respond to new developments and concerns, such as corporate governance, the information economy and the challenges of an ageing population. The Organisation provides a setting where governments can compare policy experiences, seek answers to common problems, identify good practice and work to co-ordinate domestic and international policies.

The OECD member countries are: Australia, Austria, Belgium, Canada, Chile, the Czech Republic, Denmark, Estonia, Finland, France, Germany, Greece, Hungary, Iceland, Ireland, Israel, Italy, Japan, Korea, Latvia, Lithuania, Luxembourg, Mexico, the Netherlands, New Zealand, Norway, Poland, Portugal, the Slovak Republic, Slovenia, Spain, Sweden, Switzerland, Turkey, the United Kingdom and the United States. The European Commission takes part in the work of the OECD.

OECD Publishing disseminates widely the results of the Organisation's statistics gathering and research on economic, social and environmental issues, as well as the conventions, guidelines and standards agreed by its members.

NUCLEAR ENERGY AGENCY

The OECD Nuclear Energy Agency (NEA) was established on 1 February 1958. Current NEA membership consists of 33 countries: Argentina, Australia, Austria, Belgium, Canada, the Czech Republic, Denmark, Finland, France, Germany, Greece, Hungary, Iceland, Ireland, Italy, Japan, Korea, Luxembourg, Mexico, the Netherlands, Norway, Poland, Portugal, Romania, Russia, the Slovak Republic, Slovenia, Spain, Sweden, Switzerland, Turkey, the United Kingdom and the United States. The European Commission also takes part in the work of the Agency.

The mission of the NEA is:

– to assist its member countries in maintaining and further developing, through international co-operation, the scientific, technological and legal bases required for a safe, environmentally sound and economical use of nuclear energy for peaceful purposes;

– to provide authoritative assessments and to forge common understandings on key issues as input to government decisions on nuclear energy policy and to broader OECD analyses in areas such as energy and the sustainable development of low-carbon economies.

Specific areas of competence of the NEA include the safety and regulation of nuclear activities, radioactive waste management and decommissioning, radiological protection, nuclear science, economic and technical analyses of the nuclear fuel cycle, nuclear law and liability, and public information. The NEA Data Bank provides nuclear data and computer program services for participating countries.

COMMITTEE ON THE SAFETY OF NUCLEAR INSTALLATIONS

The Committee on the Safety of Nuclear Installations (CSNI) is responsible for the Nuclear Energy Agency (NEA) programmes and activities that support maintaining and advancing the scientific and technical knowledge base of the safety of nuclear installations.

The Committee constitutes a forum for the exchange of technical information and for collaboration between organisations, which can contribute, from their respective backgrounds in research, development and engineering, to its activities. It has regard to the exchange of information between member countries and safety R&D programmes of various sizes in order to keep all member countries involved in and abreast of developments in technical safety matters.

The Committee reviews the state of knowledge on important topics of nuclear safety science and techniques and of safety assessments, and ensures that operating experience is appropriately accounted for in its activities. It initiates and conducts programmes identified by these reviews and assessments in order to confirm safety, overcome discrepancies, develop improvements and reach consensus on technical issues of common interest. It promotes the co-ordination of work in different member countries that serve to maintain and enhance competence in nuclear safety matters, including the establishment of joint undertakings (e.g. joint research and data projects), and assists in the feedback of the results to participating organisations. The Committee ensures that valuable end-products of the technical reviews and analyses are provided to members in a timely manner, and made publicly available when appropriate, to support broader nuclear safety.

The Committee focuses primarily on the safety aspects of existing power reactors, other nuclear installations and new power reactors; it also considers the safety implications of scientific and technical developments of future reactor technologies and designs. Further, the scope for the Committee includes human and organisational research activities and technical developments that affect nuclear safety.

ACKNOWLEDGEMENTS

This report was written by J. Fokken, B. Krohn, R. Kapulla, B. Niceno, H.-M. Prasser and A. Badillo, from the Laboratory of Thermal Hydraulics, Paul Scherrer Institute, Switzerland.

TABLE OF CONTENTS

LIST OF ABBREVIATIONS AND ACRONYMS

CFD	Computational fluid dynamic
CL	Cold leg
CSNI	Committee on the Safety of Nuclear Installations
DES	Detached eddy simulations
DNS	Direct numerical simulations
DS	Deterministic sampling
FoM	Figure of merit
FOV	Field of view
FP	Framework programme
GCI	Grid convergence index
GEMIX	Generic mixing experiment
IET	Integral effect test
k-Ɛ	k-epsilon
LDA	Laser Doppler anemometry
LES	Large eddy simulation
LHS	Latin hypercube sampling
LIF	Laser-induced fluorescence
MC	Monte Carlo
NEA	Nuclear Energy Agency
NRS	Nuclear reactor safety
NS	Navier Stokes
PC	Polynomial chaos
PCE	Polynomial chaos expansions
PDF	Probability distribution function
PIRT	Phenomena identification and ranking table
PIV	Particle image velocimetry
PSI	Paul Scherrer Institute
PTS	Pressurised thermal shock

RANS	Reynolds averaged Navier Stokes
RAP	Reliability analysis program
RMS	Root mean square
RNG	Renormalisation group
RPV	Reactor pressure vessel
R&D	Research and development
SNR	Signal to noise ratio
SST	Shear stress transport
TKE	Turbulent kinetic energy
UQ	Uncertainty quantification
UQCFD	Uncertainty quantification in computational fluid dynamic
UNICEP	Uncertainty identification, calibration, extrapolation and propagation
WMS	Wire mesh sensor
3D	Three-dimensional

EXECUTIVE SUMMARY

Background

The main objectives of the current activity are the promotion, test and evaluation of various methodologies for uncertainty quantification in computational fluid dynamics (UQCFD) for nuclear reactor safety (NRS) applications. The assessment of the UQ methodologies was based on a blind test case from an experiment with a density gradient, which is of practical interest to NRS. The product is a synthesis report presenting a detailed assessment of numerical predictions – including the uncertainty bands – with measured data. This report was presented at the CFD4NRS-6 Workshop held in Boston in 2016.

The numerical benchmark exercise is restricted to single-phase flow, with turbulent mixing in the presence of density gradients, which is a typical situation encountered in many reactor issues, where computational fluid dynamics (CFD) is currently used. The exercise was based on the GEMIX experiment, which was carried out at the Paul Scherrer Institute (PSI) in Switzerland. Participants submitted a calculation for the blind test case, where they presented their predictions for mean velocity, turbulence kinetic energy and concentration profiles. All the results included uncertainty bands. Since some methodologies for UQCFD use data from a validation step (for the definition of the model, its calibration and/or extrapolation of errors), three open tests cases were provided to the participants. It is noteworthy to mention that for the blind test, the density ratio between the two mixing streams was 1%, which is much lower than the values encountered, for example, in pressured thermal shocks.

In recent years, the use of CFD to address issues related to nuclear reactor safety has become very popular due to its higher (temporal and spatial) resolution compared to system codes. Reactor components where inherent three-dimensional phenomenaare taking place are particularly suited for these computational tools. For instance, the junction of the cold leg (CL) with the reactor pressure vessel (RPV) may be subjected to thermal stresses in pressurised thermal shock (PTS) scenarios. Accurately predicting three-dimensional (3D) flows with a sufficiently fine resolution cannot be handled by lump parameter codes, nor by system codes, which makes CFD the only option.

Despite the enormous advances in conventional CFD (which involves single-phase turbulent flows) there are still questions about the level of accuracy of these simulations, which acquires a special relevance for licensing purposes. Although in CFD simulations, the number of parameters is much lower than that of system codes, the uncertainties associated with the mesh resolution, turbulence models, boundary conditions and numerical schemes still renders the use of these advanced tools to mere “demonstrations” in the context of NRS.

There are several methodologies available nowadays for UQCFD, and most of them involve sampling the parameter space. Compared to system code, each CFD realisation might be orders of magnitude more expensive, and thus efficient methods, which can obtain a good estimation of the uncertainties with few samples, are needed. Therefore, the GEMIX benchmark exercise presents a unique opportunity to investigate the advantages and disadvantages of each method, which can provide valuable information when selecting a UQCFD for NRS applications.

Methods to assess model uncertainties can be divided into two classes: propagation methods and extrapolation methods. Propagation of uncertainty methods requires several steps:

- identification of all uncertain input parameters;
- determination of the uncertainty of all uncertain input parameters;
- calculating a number of runs with each uncertain parameter being sampled according to the established probability distribution function (PDF);
- from the runs, determination of the PDF of the figure(s) of merit or of any code response.

Various propagation methods may differ by the use of random sampling or deterministic sampling, and by a possible use of meta-models (e.g. polynomial chaos expansion).

Extrapolation methods measure the accuracy of predictions on some experiments (here on open GEMIX tests) and extrapolate the accuracy to the blind problem.

There are also methods combining extrapolation for some sources of uncertainty (e.g. uncertainty due to physical model) with propagation of uncertainty for other sources of uncertainty (e.g. initial and boundary conditions). Extrapolation methods may also use some meta-models.

Extrapolation methods may need a lower number of runs than propagation methods. Propagation methods may reduce the number of runs by using deterministic sampling rather than random sampling. The use of meta-models may reduce the number of runs if the number of uncertain parameters is not too high.

Deliverables, expected results and users

- Mean velocity, turbulence kinetic energy, and concentration profiles were predicted and compared to experimental values (GEMIX).
- A synthesis was presented at the CFD4NRS-6 Workshop held in September 2016 and a detailed synthesis report on comparisons between numerical and measured data was produced.
- Users are all actors in safety analysis and in nuclear fuel design.

The exercise complements ongoing national programmes for the study nuclear safety, and European initiatives, such as NURESAFE (7^{th} EU – FP).

Safety significance of the current results

The absence of UQCFD application to nuclear safety is a major limitation in the use of mature single-phase CFD tools in safety demonstrations for licensing.

Most single-phase issues – for which it was recognised that CFD may bring benefits – are mixing problems with or without density effects (buoyancy/stratification). The proposed activity addresses UQ for mixing problems in the presence of such effects, though with a limited density ratio and some incomplete experimental uncertainties.

Main conclusions

- Actors should be aware of the limitations of particle image velocimetry (PIV) when working with slightly inhomogeneous fluids. In this benchmark, we could not prove if the high values for the turbulence kinetic energy in the mixing layer, for a slightly inhomogeneous medium, is physical or not, but there is a suspicion of a measuring artefact. Turbulence kinetic energy was

therefore not considered in the evaluation and ranking of code predictions and of uncertainty quantifications.

- A new measure (fidelity) has been proposed to assess UQCFD results. It is given by the convolution of the probability distributions of a predicted value and the corresponding experimental value, both assumed to be Gaussian.
- The scatter in the results is less than expected given the complexity of the problem. For example, velocity profiles from all participants fall within a narrow band (±7%), close to experimental values.
- Although the shape of concentration profiles was in general well predicted, a larger scatter was observed for the thickness of the mixing layer, indicating some problems when selecting the turbulent Schmidt number. Since the spreading of the mixing layer is primarily controlled by the turbulent Schmidt number, it seems logical to include this parameter as a source of uncertainty in future UQCFD analyses.
- Very good results could be obtained with both uncertainty propagation method and combined accuracy extrapolation and uncertainty propagation methods. The top 3 users needed 6, 15 and 836 simulations of the blind test showing that some methods may be used successfully with a low number of calculations at least in this rather simple case. Extrapolation methods may need a lower number of runs than propagation methods and propagation methods may reduce the number of runs by using meta-models, provided that the number of uncertain parameters is not too high. Such low numbers of runs may thus not be generalisable to other more complex problems, with more challenging geometries and boundary conditions. In addition, many preliminary calculations of open tests may have been necessary when using extrapolation methods, before the application to the blind test.
- The participants using a combined method (propagation and extrapolation) obtained the best agreement with the blind data. However, this should be analysed with care, because if the experimental results – on which the extrapolated errors are based – have a large bias, the numerical results will reflect that, as seen with the (most likely) unphysically value for the turbulence kinetic energy.
- Some methods give a very narrow band of uncertainties, while some others give a rather wide band of uncertainties. It may be linked to the input uncertainties taken into account, but possibly also to the characteristics of the methods themselves. The applicability of these methods, in the field of nuclear safety assessment, still raises questions to be further discussed and requires at least further testing and benchmarking.
- The most important step in the UQCFD analysis is the proper characterisation of the input uncertainties. When analysing the scattering in the rankings from users employing the same turbulence model (e.g. k-Ɛ), it is clear that the turbulence model alone cannot be responsible for such variability in the results. As explained in the text, if we focus only on propagating a probability distribution function (PDF) through a mathematical model, the output PDF should be independent of the propagation method. The propagation method and turbulence model therefore must have a marginal influence in the present exercise. Since the users' results were not used to perform a sensitivity analysis to determine the most influential variables, the last statement should be taken with precaution, as there is no definitive scientific proof to support it.
- In the present exercise, it is clear that the results of some participants increase confidence in the applicability of UQCFD, for more realistic scenarios relevant for NRS.

- As a result of small density effects in the benchmark and small differences between open and blind tests, the extrapolation from open tests made the benchmark somewhat easier. Future benchmarks should investigate situations with stronger density effects and with more different conditions between open and blind tests.

1. INTRODUCTION

Claude-Louis Navier and Augustin-Louis Cauchy were born in 1785 and 1789 respectively. The world would have to wait another 30 years for George Gabriel Stokes to be born, to later complete the foundation of what would become known as the Navier-Stokes (NS) equations. This elemental set of equations constitutes, nowadays, the best mathematical description of fluid motion at the continuum level. These equations are thought to hold the mysteries of one of the unsolved problems in physics: turbulence. Much effort has been made to understand the mathematical behaviour of these equations, but their complexity has stubbornly deprived mathematicians from even being able to prove the existence of smooth solutions for three-dimensional (3D) flows. With the advancement of digital computers in the last decades, we have been able to solve discrete representations of the Navier-Stokes equations, with a high level of "accuracy". Direct numerical simulations (DNS) have become the workhorse of many scientists, working on the most fundamental aspects of turbulence (e.g. intermittency). However, we must always bear in mind that as accurate a DNS solution might be, it will never be a real solution of the Navier-Stokes equations. Without formal mathematical proof for the existence of smooth solutions, there is always the possibility that in those unresolved scales, singularities might exist. Thus, to study turbulence with our rudimentary numerical tools, we must accept the fact that our simulations might not be as accurate as we would like to think. In the eventuality that solutions are indeed smooth, then the only uncertainties that would arise in DNS are from numerical errors, which can easily be quantified. On the contrary, this sort of uncertainties would be of second order (or much lower) in the unfortunate case that there are some singularities in the solutions. This kind of uncertainty refers to how reliable are our numerical results, compared to a true solution of the NS equations. Not being certain of the existence of smooth solutions, this question does not have an answer.

A different sort of uncertainty arises when evaluating the quality of the NS equations in representing the real world. The uncertainties described in the previous paragraph belong only to the mathematical realm, but when we want to assess how good the NS equations describe turbulence in real systems, additional sources of uncertainty appear. For instance, the need of physical properties such as density and viscosity, introduces instantaneously a certain level of uncertainty in our numerical solution. Whenever we use parameters that must be determined from experiments, we are introducing stochastic variables in our models. Thus, the naive notion that DNS simulations could predict perfectly experimental observations (even is the theoretical case of infinite computational power), dissipates quickly. Most of the practical work associated with turbulent flow, is currently carried out with the aim of a different mathematical representation of the NS equations. These are the so-called Reynolds Averaged Navier Stokes (RANS) equations, which are obtained by eliminating the time dependency through a time average. If the physical properties if the fluid are considered constant, a time average leads to a set of time correlation functions that are commonly known as the Reynolds stresses. Thus, the problems of turbulence only resort to finding the appropriate forms of these correlations. If we leave aside our worries about the existence of singularities in the NS equations, then if we could measure individually the Reynolds stresses everywhere in the domain and then use this results as parameters in the RANS equations (very much like the density and viscosity), then our computational fluid dynamic (CFD) results for mean velocity profiles should match those from the experiments very accurately (there would still be some uncertainties associated to numerical errors). Similar correlations appear when we filter the NS in

space, which account for subgrid scale turbulence in large eddy simulations (LES). Finally, uncertainties from initial and boundary conditions will also introduce a level of stochasticity in our CFD solutions.

For practical applications to nuclear reactor safety, Direct Numerical (and to a less extent LES) simulation, require a computational power not currently available. Thus, most CFD analyses are carried out with RANS models. The GEMIX facility was originally designed to study the fundamentals of turbulent mixing, for a variety of Reynolds and Froude numbers. However, despite the fact that GEMIX was not initially intended for uncertainty quantification (UQ) studies, its small and simple geometry makes it a prime candidate for this purpose. Because all GEMIX test cases are steady state, this experimental facility offers an unparalleled advantage to assess UQ methodologies, at a relatively low computational cost. This is the main reason for selecting GEMIX for the first international benchmark on UQCFD.

2. UNCERTAINTY SOURCES IN COMPUTATIONAL FLUID DYNAMICS

We will start our discussion with the basic equations for fluid dynamics, that is, conservation of mass and momentum:

Mass $$\frac{\partial \rho}{\partial t} + \nabla \cdot \mathbf{p} = 0 \quad (1)$$

Momentum $$\frac{\partial \mathbf{p}}{\partial t} + \nabla \cdot (\mathbf{up}) = -\nabla \cdot \overleftrightarrow{\sigma} + \mathbf{f} \quad (2)$$

with ρ the density, $\mathbf{p} = \rho\mathbf{u}$ the linear momentum. The stress tensor $\overleftrightarrow{\sigma} = P\overleftrightarrow{\mathbf{I}} - \overleftrightarrow{\tau}$ is expressed in terms of the pressure P and the deviatoric stress tensor $\overleftrightarrow{\tau} = \mu\left(\nabla\mathbf{u} + \nabla\mathbf{u}^{\boldsymbol{T}}\right) + \lambda\nabla \cdot \mathbf{u}$, where μ and λ are the shear and second viscosities respectively. In this section, we will neglect possible uncertainties related to singularities in the Navier-Stokes equations and, thus, we will center our attention on physical properties, turbulence models, and boundary and initial conditions.

2.1. Uncertainties in the physical properties

Measuring physical properties with a high level of accuracy is not an easy task, even for straightforward properties such as density. For instance, measuring the density of water with an accuracy of ± 0.001 gr/cm^3 has already been an important challenge [1]. In the case of water viscosity, different measurement techniques lead to slightly different values, whose difference is larger than the experimental uncertainties reported by each individual technique [2]. Although small, physical uncertainties could have an impact, for example, on high-fidelity DNS and/or simulations of extremely large systems (e.g. oceanic simulations). To the best of our knowledge, no UQ analysis assessing the influence of uncertainties in physical properties on DNS has ever been presented in the open literature. For conventional CFD simulations (i.e. RANS and LES), uncertainties in the physical properties appear to have a lower relevance compared to the uncertainties in the turbulence modes used to estimate the Reynolds stresses. However, no such assessment has ever been carried out.

2.2. Uncertainties in turbulence models

The dominant uncertainties in turbulence models arise from the lack of knowledge of the pair correlation functions obtained from applying a time averaging or space/time filtering to the Navier-Stokes equations. A filtered velocity field is defined as

$$\langle \mathbf{u}(\mathbf{x}, t) \rangle = \lim_{T\to\infty} \int_{-T/2}^{T/2} \mathbf{u}(\mathbf{x}, \tau) g(t - \tau) d\tau = \mathbf{U}(\mathbf{x}, t) \quad (3)$$

Since the kernel function must satisfy $\lim_{T\to\infty} \int_{-T/2}^{T/2} g(t - \tau) d\tau = 1$, we obtain a time average by taking $g(t - \tau) = 1/T$. This results in an averaged velocity field that is time independent. Thus, any further filtering operation will not change the averaged field. If we now use a rectangular pulse with a finite width T_0, then the kernel function is given by

$$g(t-\tau) = \begin{cases} 1/T_0 & for \ \ |t-\tau| \le T_0/2 \\ 0 & otherwise \end{cases} \quad (4)$$

The operation defined in Eq. (3) is a convolution and, thus, the spectrum of the filtered field is given by the multiplication of the individual spectra:

$$\breve{\mathbf{U}}(x,q) = \breve{\mathbf{u}}(x,q)\breve{g}(x,q) \quad (5)$$

The spectrum of the square pulse is shown in Figure 1and is given by $\breve{g}(x,q) = \sin(\pi q T_0)/\pi q T_0$. Although highly attenuated, harmonics with frequencies higher than $q_0 = 1/T_0$ are still present in the spectrum of the filtered velocity field.

Figure 1. Spectrum of the unitary square pulse

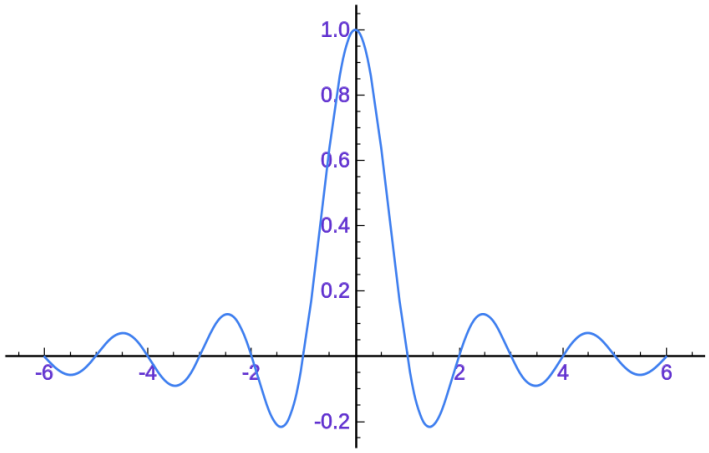

Despite that using a square pulse—as the filter kernel—may appears analogous to using a uniform mesh (in time and/or space), this is not the case. Even experienced CFD practitioners have misinterpreted the use a numerical mesh to be equivalent to a filtering operation with a pulse width equal to the mesh spacing. Although the use of high order polynomials might help us in reconstructing a continuous filtered velocity field from a set of discrete points, the resultant velocity field will never be the same as the true continuous filtered field. Even in the case of spectral methods, the reconstructed field will not match the true one due to a truncation error in the polynomial series.

When we apply a time average, the mathematical operation can be represented by a Reynolds operator $\mathcal{R}$, which satisfy a given set of rules. However, when filtering the Navier Stokes equations over a finite time/space interval, the applied operator does not satisfy invariance upon successive operations and, thus, it cannot be considered a Reynolds operator. The invariance upon successive applications is expressed mathematically as

$$\mathcal{R}\big(\mathcal{R}(\phi)\big) = \mathcal{R}(\phi) \quad (6)$$

This rule is not strictly satisfied in Unsteady RANS or LES formulations respectively (see details in the Appendix A). To simplify the analysis, we will write the filtered momentum equation in its more recognisable form,

$$\frac{\partial \overline{\mathbf{u}}}{\partial t} + \nabla \cdot \langle \overline{\mathbf{u}}\overline{\mathbf{u}} \rangle + \nabla \cdot \langle \mathbf{u}'\mathbf{u}' \rangle = -\frac{1}{\rho}\nabla \bar{P} + \nabla \cdot (\nu \nabla \overline{\mathbf{u}} + \nu \nabla \overline{\mathbf{u}}^T) + \frac{1}{\rho}\bar{\mathbf{f}} + \mathbf{f}_{correction} \quad (7)$$

where we have put all the missing terms in the correcting force $\mathbf{f}_{correction}$. The dominant uncertainty in turbulence models arise from the Reynolds stresses (we will use this term indistinctly to refer to the averaged fluctuating tensor correlation obtained from RANS or LES filters). We can express the Reynolds stresses in terms of the mean/filtered velocity field through the following relation

$$-\langle \mathbf{u}'\mathbf{u}' \rangle \equiv \overleftrightarrow{\nu}_t \circ (\nabla \overline{\mathbf{u}} + \nabla \overline{\mathbf{u}}^T) - \frac{2}{3} k_{TKE} \overleftrightarrow{\mathbf{I}} \qquad (8)$$

where $\overleftrightarrow{\nu}_t$ is a second rank symmetric tensor. Expressing the Reynolds stresses in this manner would allow us to obtain the viscosity tensor from DNS,

$$\overleftrightarrow{\nu}_t = \left(\frac{2}{3} k_{TKE} \overleftrightarrow{\mathbf{I}} - \langle \mathbf{u}'\mathbf{u}' \rangle \right) \circ (\nabla \overline{\mathbf{u}} + \nabla \overline{\mathbf{u}}^T)^{-1} \qquad (9)$$

DNS data could be used to test several assumptions made on turbulence models. This expression has a direct connection to the Reynolds Stress Model, where individual equations are solved for each of the components of the Reynolds stress tensor. The viscosity tensor gives us information about how correlated the pair correlation functions are with the strain rate of the mean velocity field. A tensor with no off-diagonal terms and a constant value in the diagonal, would indicate that the fluctuating correlation function can be represented exactly as an isotropic diffusional phenomenon. This is the assumption in the Boussinesq approximation, which is used in most of the conventional RANS models and subgrid scale models in LES. Since the viscosity tensor has the same units as its kinematic molecular counterpart, an isotropic tensor can be expressed in terms of a velocity and a length scale. For an isotropic tensor, we have

$$\overleftrightarrow{\nu}_t = \nu_t \overleftrightarrow{\mathbf{I}} \qquad (10)$$

with the turbulent eddy viscosity, proportional to

$$\nu_t \propto V \times L \qquad (11)$$

Since we assume that the fluctuating part of the velocity field is responsible for transporting momentum in a diffusion like manner, it is logical to consider that the velocity scale should be obtained from velocity fluctuations. For an incompressible flow, the trace of the Reynolds stress tensor is equal to twice the turbulence kinetic energy, that is,

$$Tr(\langle \mathbf{u}'\mathbf{u}' \rangle) \equiv 2k_{TKE} \qquad (12)$$

The trace of a tensor is a fundamental quantity that represents an invariant upon rotation, even for anisotropic tensor fields. A quantity that is invariant upon rotation is highly desirable when looking for a proper velocity and length scale. We would not want to have our fundamental scales defined in terms of quantities that change upon rotation of the co-ordinate system. Thus, an evident velocity scale based on the turbulence kinetic energy satisfy two conditions: Rotational invariance and a direct association to the fluctuating velocity field,

$$V = \sqrt{k_{TKE}} \qquad (13)$$

For isotropic turbulence, this definition coincides with the RMS value of the velocity fluctuations. A more delicate situation arises when determining the appropriate length scale. Based purely on dimensional grounds, a length scale can be obtained by combining the viscous dissipation and the turbulence kinetic energy

$$L = \frac{{k_{TKE}}^{3/2}}{\varepsilon} \qquad (14)$$

where the viscous dissipation of the fluctuating field is defined as $\varepsilon = \nu\langle\nabla\mathbf{u}' : (\nabla\mathbf{u}' + \nabla\mathbf{u}'^{T})\rangle$. Although dimensionally correct, this length scale does not appear to be the most appropriate one. The term $\langle\nabla\mathbf{u}' : (\nabla\mathbf{u}' + \nabla\mathbf{u}'^{T})\rangle$ has units of frequency square and, thus, provides a measure of the RMS frequency of eddies. Hence, this term appears to be more appropriate for a time scale. Utilising this time scale, we could define a new length scale (Taylor scale) as

$$L = \sqrt{\frac{k_{TKE}}{\langle\nabla\mathbf{u}' : (\nabla\mathbf{u}' + \nabla\mathbf{u}'^{T})\rangle}} = \sqrt{\frac{k_{TKE}}{\varepsilon/\nu}} \qquad (15)$$

Considering the conventional length scale used in RANS models Eq.(14), the eddy viscosity is written as

$$\nu_t = C_\mu \frac{k_{TKE}^2}{\varepsilon} \qquad (16)$$

Using the new length scale Eq. (15), this quantity would be given by

$$\nu_t = B_\mu \frac{k_{TKE}}{\langle\nabla\mathbf{u}' : (\nabla\mathbf{u}' + \nabla\mathbf{u}'^{T})\rangle^{1/2}} = B_\mu \frac{k_{TKE}}{\sqrt{\varepsilon/\nu}} \qquad (17)$$

This short analysis is only intended to show that uncertainties in the most fundamental quantities in RANS models (i.e. eddy viscosity), arise not only from uncertainties in the constant C_μ, but also from the very definition of the length scale.

2.3. Boundary and initial conditions

Uncertainties in boundary and initial conditions are usually neglected in CFD simulations. The lack of knowledge of boundary condition, plus the tediousness of UQ analyses, render their study essentially to the academic world. However, we have seen in the present benchmark that the inlet boundary condition plays a relevant role in the final measure of uncertainty. Aside from this type of uncertainties, there might be uncertainties related to the geometry due to, for instance, manufacturing tolerance. Initial conditions can also be important. For example, it is well known that when emptying a container with a liquid (e.g. a bottle full of water), the flow pattern of the liquid exiting the container, will be quite different if the fluid is initially still or has a strong rotational velocity. Thus, neglecting an initial rotational component will most likely lead to large errors.

2.4. Numerical errors

Although numerical errors do not constitute an uncertainty source, they also affect the level of accuracy of a numerical simulation. The most dominant errors derive from the discretisation of the differential operators in partial differential equations (e.g. Laplacian, gradient, partial derivative respect to time, etc.). Rounding errors, such as those found in the solution of the linear systems, might also contribute substantially to numerical errors if the solutions are not fully converged. Numerical errors are strongly correlated to the user's experience, where for instance, a good quality mesh can make a big difference in the final results. The use of a Best Practice Guideline can mitigate, to a certain extent, the influence of numerical errors. However, these guidelines must not be considered as CFD laws and should be reviewed case by case. Ultimately, the experience of the CFD practitioner is the best tool for error optimisation.

Figure 2. Sources of errors and uncertainties in CFD.

Type the subtitle here. If you do not need a subtitle, please delete this line.

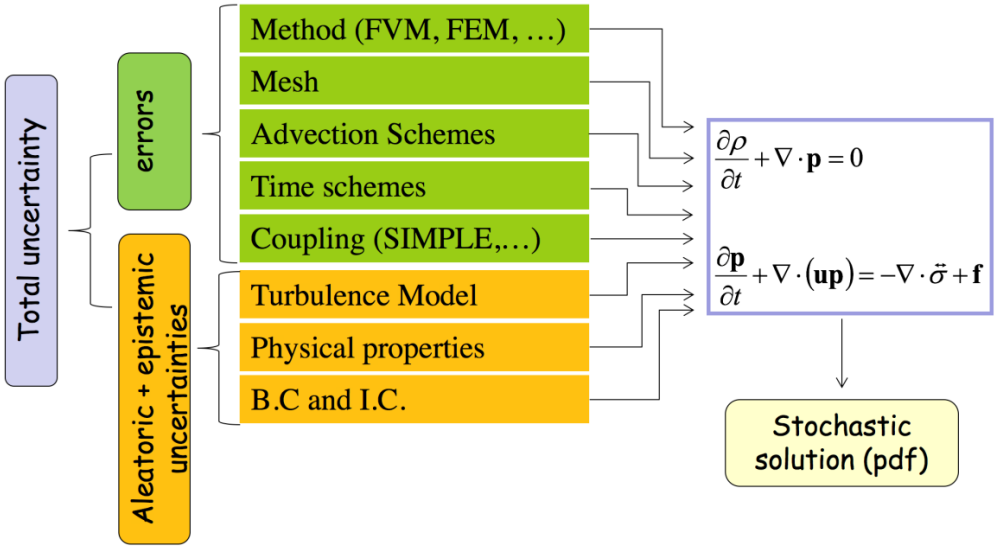

3. UNCERTAINTY QUANTIFICATION IN COMPUTATIONAL FLUID DYNAMICS

There is a plethora of articles addressing uncertainty in numerical simulations in general. However, the literature is much more reduced when it comes to computational fluid dynamic (CFD) due to the computational cost associated to it. More details about uncertainty methods currently used in CFD can be found in (NEA/CSNI/R(2016)4). Nowadays, uncertainty quantification (UQ) methods can be split into two groups: Propagation and extrapolation. The former propagates uncertainties in input parameters to the CFD solution, while the latter extrapolate physical errors in the model –estimated from integral effect test (IET)– to a different case scenario. These two methodologies have negative and positive aspects associated to them. For instance, in propagation methods the determination of input uncertainties is a major challenge, while the propagation of these uncertainties through the mathematical model is usually straightforward. For extrapolation methods, the main problem lies on the quality of the experimental data and how representative are the IETs of the new case scenario. For example, if we use a database for fully turbulent flows to find the accuracy of CFD simulations, the error will not be representative when the same model is used to simulate transitional flows. The IETs can additionally be used to calibrate the numerical models. It is also possible to combine these two techniques, as some of the users already did in the present benchmark, to arrive at a very robust uncertainty quantification in computational fluid dynamic (UQCFD) methodology.

4. EXPERIMENTAL TEST SECTION

The confined wake flow water mixing experiments in the GEMIX facility, focus on the basic turbulent mixing mechanisms for unstratified and stably stratified conditions. A simplified schematic of the test rig is shown in Figure 3. The flow channel is made of acrylic glass to enable optical access, except for the last 80 mm of the splitter plate, which is made of stainless steel to avoid deformation of the splitter plate tip. The main design parameters for the GEMIX flow channel are listed in Table 1. The co-ordinate system to describe the velocity and concentration fields is located at the tip of the splitter plate and its origin is placed in the middle of the channel. The x-co-ordinate represents the stream-wise direction, the y-coordinate the crosswise and the z-co-ordinate the spanwise direction (see Figure 3).

Figure 3. Schematic of the GEMIX test rig

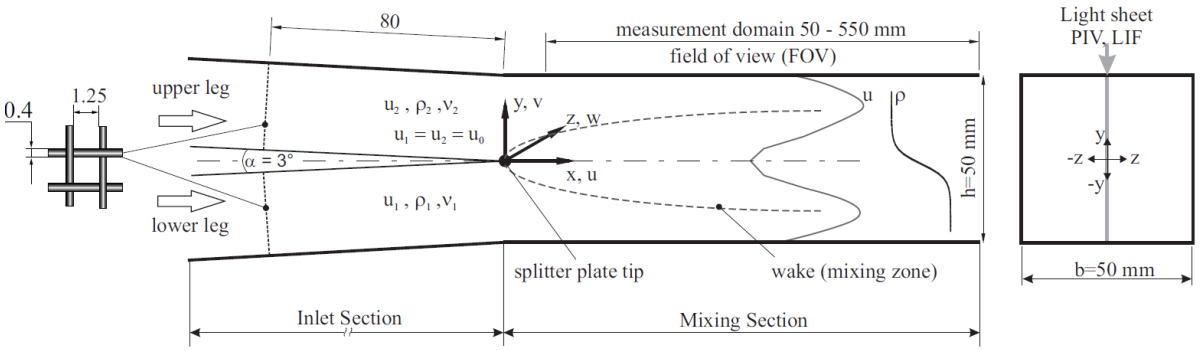

The inlet section comprises the lower and upper legs, where the two co-flowing water streams are initially separated by the splitter plate. Upper and lower legs are equipped with flow conditioning devices, where both streams pass through a single honeycomb, two identical coarse grids and a single fine grid, such that the velocity profiles at the splitter plate tip appear almost equal in shape and free from rotational components. The wire diameter d, mesh width w and upstream location of the braided flow conditioning grids as well as the diameter d, length l and rear edge position of the circular cell honeycombs are listed in Table 1. For the experiments, each leg of the inlet section is supplied with the same volumetric flow rate from an individual pumping line connected to its own individual water storage tank of 2 000 l capacity, enabling separate conditioning for each stream. One storage tank contains tap water, while the other one contains either de-ionised water or a solution of de-ionised water and sucrose to increase the density of the lower stream to establish stable stratified flow conditions. Sucrose is used to increase the density of the lower stream instead of salt, because it makes only minor changes to the electrical conductance of the water. However, and due to the decrease in the mobility of charge carrying ions in the presence of sucrose, a complex calibration procedure – taking into account the initial conductivity of the applied water as well as both sugar concentration and temperature – was used to convert primary measuring signals of wire mesh sensor (WMS) into dimensionless transport scalars [4]. The mass fraction of sucrose in conjunction with a temperature adjustment is used to compensate partially for changes in the electrical conductance, and to alter the density differences between the

streams while keeping the kinematic viscosity (and therefore the Reynolds Numbers Re_0) of the two streams approximately identical to that of pure water at 1 bar, 20°C (see Table 1).

Figure 4. Inlet conditioning section

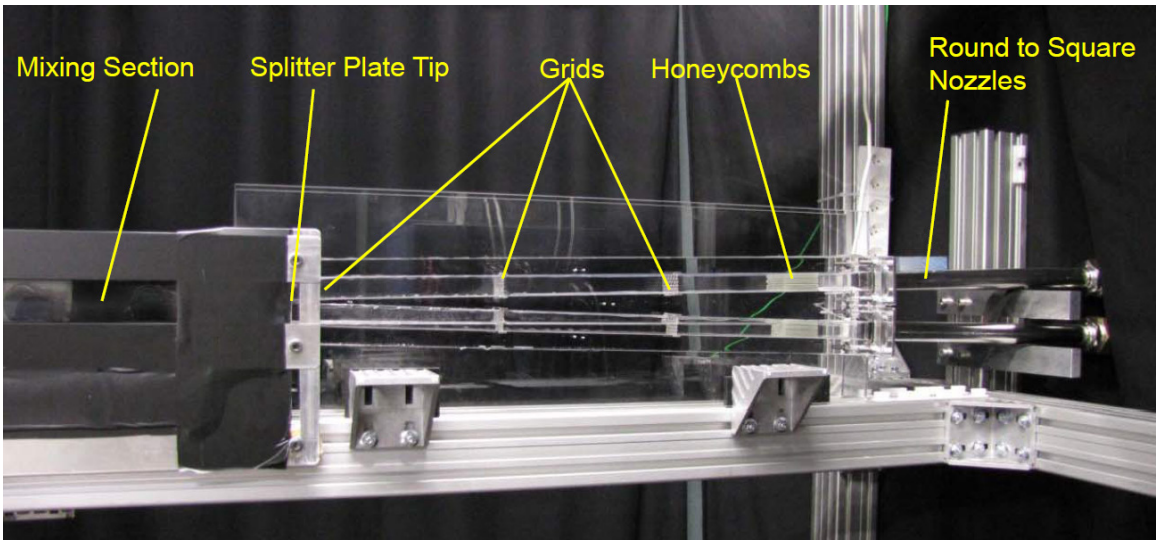

Figure 5. Mixing section

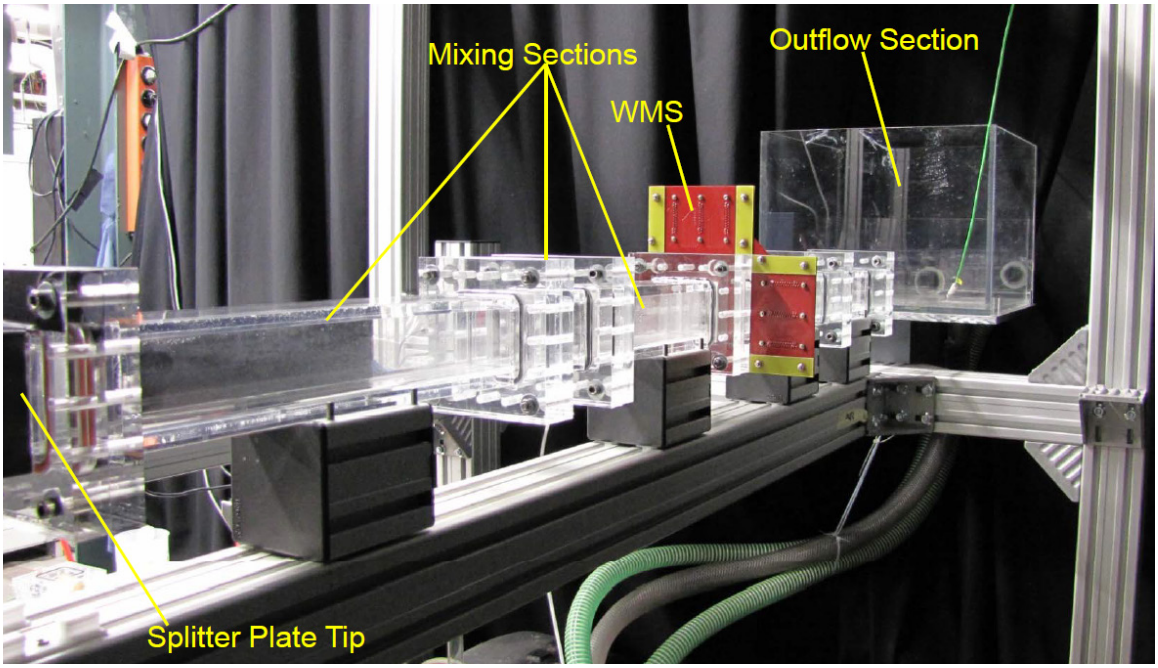

The mixing section assembly in which both streams interact and form the wake mixing zone past the splitter plate tip, is attached to the inlet section. The square mixing section is composed by non-adjustable walls with a cross-sectional area of 50×50 mm^2 and a length of 550 mm. The mixing section can be assembled by a single segment of 550 mm in length when particle image velocimetry (PIV) or laser-induced fluorescence (LIF) is applied to measure the mixing process, or by two segments of

different length to place a wire-mesh sensor in the cross-sectional area at various downstream distances. Only one wire-mesh sensor is placed in the mixing section; therefore, to measure cross-sectional concentration profiles at several locations, different experiments are needed (one per each location of the wire-mesh sensor). The outlet section is aligned to the mixing section and consists of an additional straight channel segment of 1 m in length, a flow splitter device and a water box with a spillover weir. At the end of the additional straight channel segment, the flow is split again into two streams to minimise possible feedback effects of the water box to the developing wake flow upstream. The rectangular water box has a volume of 40 l and a spillover weir that maintains constant back pressure of 250 mm head in the channel for all flow rates. The mass flow rates, densities and temperatures of the two streams are recorded for each experimental run and the measured data is stored and processed on a computer.

Table 1. Main design parameters of the GEMIX flow channel geometric dimension in mm).The flow conditions correspond to those in the full experimental campaign.

Inlet section length	1 250
Inlet section height × width	25×50 (2×)
Splitter plate angle	3
Honeycomb $d = 2$, $l = 50$	@ $x = -670$
1. Grid $d = 1$, $w = 4$	@ $x = -520$
2. Grid $d = 1$, $w = 4$	@ $x = -300$
3. Grid $d = 0.4$, $w = 1.25$	@ $x = -80$
Mixing section length	550
Mixing section height × width	50×50
Total channel length	3000
Nominal inlet velocities	0.2-1.2 m/s
Re-Numbers in mixing section	10 000 – 60 000
Volumetric flow rate	15 – 90 l/min
Density difference	0 – 10%
Temperature difference	0 – 50K
Viscosity difference	0 – 100%
Streamwise turbulence level	5%

Figure 6. Schematic of GEMIX Geometrical information of the CFD domain is provided in the top image. Comparison between simulations and experimental results will be carried out using several profiles at the center plane of the mixing section

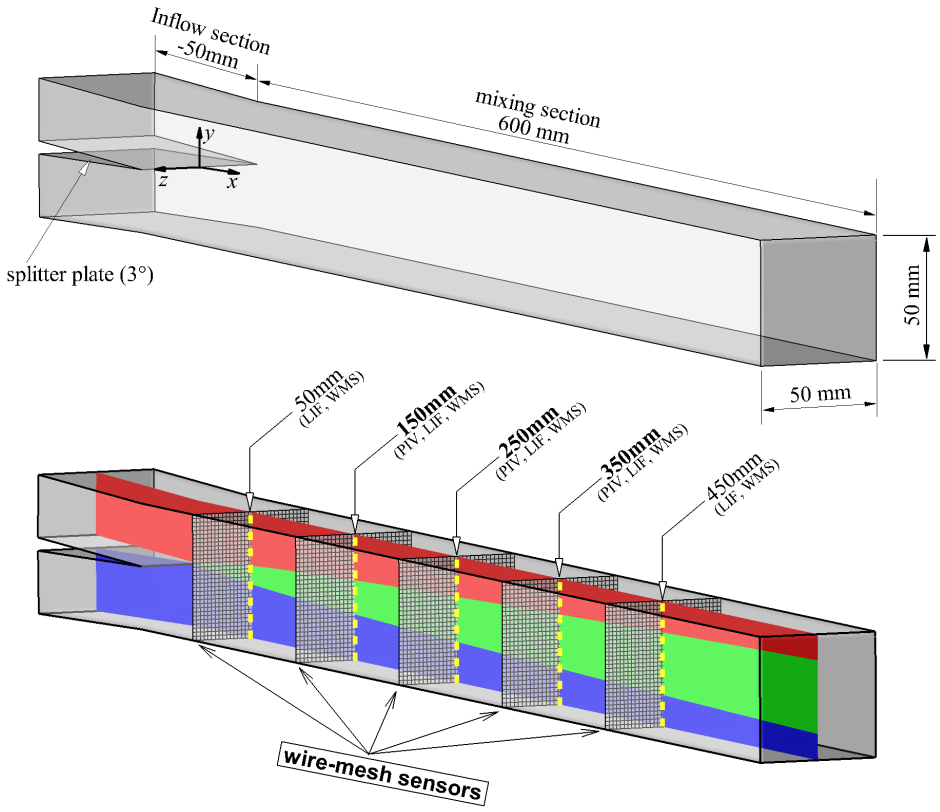

5. EXPERIMENTAL UNCERTAINTIES

The accuracy of volumetric flow rate –as monitored by the Coriolis flow metres– was ±0.15%. The error associated to the density measurement was estimated to be ±0.01 kg/m^3. The relative difference between the volumetric flows in the upper and lower legs of the inlet section, which determines the accuracy of the isokinetic condition $u_0 = u_1 = u_2$, was kept below $(\dot{V}_1 - \dot{V}_2)/\dot{V}_1 \cdot 100 \leq \pm 1\%$ for all experiments. Since we can only measure estimators for mean and RMS values from the experimental data (PIV, laser Doppler anemometry – LDA and LIF), a quantification of the statistical uncertainty associated to these estimators is required. Thus, the mean and RMS values provided in the experimental data files have a level of uncertainty, characterised by an interval of confidence. For mean values, the interval of confidence was determined from the Student's distribution, while for RMS values, a nonparametric X^2-test was applied. Since the Student's distribution is symmetric, the upper and lower bands – corresponding to the 95% interval of confidence – are also symmetric. However, the X^2distribution is not symmetric and therefore the upper and lower bands are slightly asymmetric with respect to the RMS value. The uncertainty for the turbulence kinetic energy was estimated by combining the individual uncertainties of the diagonal components of the Reynolds stress tensor, that is:

$$\Delta k = \sqrt{U_1^2 + U_2^2 + U_3^2}, \tag{18}$$

where each uncertainty was calculated as:

$$U_1 = \frac{\partial k}{\partial \langle u'u' \rangle} \cdot \sigma(\langle u'u' \rangle), \; U_2 = \frac{\partial k}{\partial \langle v'v' \rangle} \cdot \sigma(\langle v'v' \rangle), \; U_3 = \frac{\partial k}{\partial \langle w'w' \rangle} \cdot \sigma(\langle w'w' \rangle). \tag{19}$$

On locations where only the x- and y-components of the velocity could be measured (i.e. all PIV results and some LDA results), we assume the spanwise z-component to be equal to the vertical velocity component:

$$\Delta k = \sqrt{U_1^2 + 2 \cdot U_2^2} \tag{20}$$

In addition to the statistical uncertainty, the signal to noise ratio (SNR) introduces additional uncertainties to the LIF measurements of the concentration field. The SNR and statistical uncertainties were combined into a single value for LIF data. WMS data have been discarded for the present benchmark, because its associated uncertainty has not been fully clarified.

5.1. Other sources of uncertainties

As it will be seen in the results section, the values of the turbulence kinetic energy are rather high in the mixing layer for the cases with a small density difference (see Figure 17). Although we intensively discussed this issue at PSI, there is still not a satisfactory explanation for these results. For the test cases with density difference, the refraction index changes slightly within the mixing section, but its change is very small. Table 2 shows the refraction index for densities near the ones used in the experiments.

Table 2. Refraction index of water as a function of the sucrose content.
Source: http://homepages.gac.edu/~cellab/chpts/chpt3/table3-2.html

Sucrose concentration wt%	Density (g/cm^3)	Refraction index
0	0.9982	1.3330
1	1.0021	1.3344
2	1.0060	1.3359
3	1.0099	1.3374
4	1.0139	1.3388

The data shows that a change of 2.7 wt% in the sucrose content, leads to a change of 0.3% in the refraction index. To estimate the influence of such a small refraction index change, we made use of a simple model to calculate the trajectory of a light beam crossing an inhomogeneous medium. The differential equation reads:

$$\frac{\partial}{\partial l}\left(n\frac{\partial \mathbf{r}}{\partial l}\right) = \nabla n \qquad (21)$$

with $\mathbf{r}$ the light beam trajectory, n the refraction index and l the displacement along the light beam trajectory. More advanced models based on the geodesic path of a light beam crossing an inhomogeneous medium could be used [5], but we only needed an estimation of the error. The result of this calculation can be seen in Figure 7. When calculating the error in the particles' position, we must assume that the light source is located at the camera sensor and, thus, a good estimation of this error can be obtained by calculating the variation in position of a light beam at the boundary of the square channel (assuming the light source located at the centre of the channel). This simple calculation shows that even for a medium slightly inhomogeneous (small density difference), the fluctuating concentration introduces a small error in the particles position. Depending on the algorithm used to calculate the cross-correlation between two consecutive images, the error in the measurement of RMS values could be rather large. For the time being there are no established procedures to calculate/estimate the errors in RMS values for inhomogeneous media.

Figure 7. Calculated trajectory of a light beam across an inhomogeneous medium (black continuous line). The colour scale represents the instantaneous concentration obtained with a Wire Mesh Sensor. The red-dashed line corresponds to the case of a completely homogeneous medium (straight line).

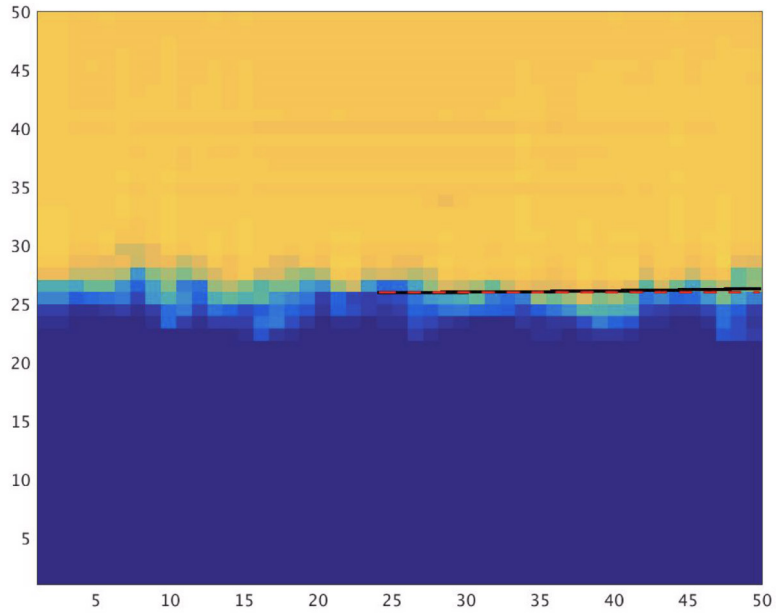

The results found in the GEMIX experiment –regarding the velocity fluctuations in slightly inhomogeneous media– is something to keep in mind for future experiments. PIV is a non-intrusive experimental technique that allows for obtaining important information about the velocity field (and its fluctuations). However, there are still many sources of uncertainties not fully clarified and usually neglected. For instance, PIV measurements are usually accompanied by error bars that contain only statistical uncertainty. Nonetheless, uncertainties regarding the algorithms for processing the images, interrogation windows size, the influence of the light intensity, seeding concentration and the influence of inhomogeneities in the propagating light media, are never accounted for. Although we should have included these uncertainties in the experimental results, a lack of human resources precluded us from doing so. In the impossibility of fully clarifying what are the uncertainties for the turbulence kinetic energy, we did not include the experimental points lying within the mixing layer in the elaboration of the ranking tables. Thus, the ranking table for the turbulence kinetic energy should be considered with precaution for the case of the density difference of 1%. The turbulence kinetic energy reported from the PIV measurements in the case without density stratification, is of course unaffected. In the future, experimental results – without all the sources of uncertainties clearly identified – should not be considered for a UQCFD analysis. This clearly poses an additional burden to the experimental teams preparing and designing CFD grade experiments, but if the experimental uncertainties are uncertain, then a UQCFD analysis becomes meaningless. Figure 8 shows a comparison of the velocity and turbulence kinetic energy profiles for blind test case (red) and its counterpart without density difference (blue). Although the average velocity profiles are very similar between the two experiments, the turbulence kinetic energy within the mixing layer differs greatly from one another. It is still unclear, from a theoretical point of view, how much a small density difference can affect the turbulence kinetic energy. In the RANS equations, there are double and triple correlation functions that are always omitted, but that could potentially have an impact on the results.

Figure 8. Mean velocity profiles and turbulence kinetic energy profiles at two locations inside the mixing section. Upper and lower profiles correspond to the mean velocities and turbulence kinetic energy respectively.

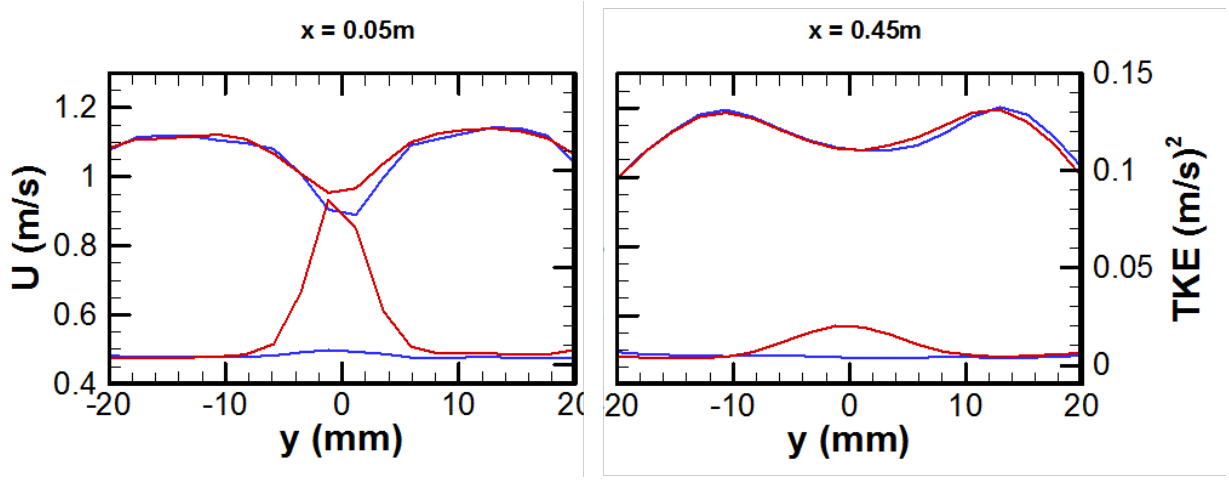

These correlations are obtained by applying a time average and the Reynolds decomposition to total kinetic energy,

$$\langle k \rangle = \frac{\bar{\rho}\bar{\mathbf{u}} \cdot \bar{\mathbf{u}}}{2} + \bar{\rho}\left(\frac{\langle \mathbf{u}' \cdot \mathbf{u}' \rangle}{2} + \frac{1}{\bar{\rho}}\langle \rho' \mathbf{u}' \rangle \cdot \bar{\mathbf{u}} + \frac{1}{2}\frac{1}{\bar{\rho}}\langle \rho' \mathbf{u}' \cdot \mathbf{u}' \rangle\right) \qquad (22)$$

Since for the blind test case the density difference is very mild, it is not clear whether these additional correlations may influence the results in a significant manner. Our feeling is that the high values for the turbulence kinetic energy within the mixing layer derives from an experimental artefact, but we cannot confirm this.

6. EXPERIMENTAL TEST MATRIX

The complete campaign in the GEMIX facility comprises experimental conditions with inlet mean velocities ranging from 0.2 to 1 m/s and density ratios of 0 to 10%, leading to a total of thirty independent cases. Nonetheless, for this benchmark exercise only four experiments will be considered – three will be disclosed and one will be kept secret for the blind calculations.

Table 3. Experimental matrix for this benchmark

Inlet mean velocity	0.6 m/s	1 m/s
Global Re-number	30 000	50 000
$\Delta\rho = 0\%$, $\Delta T = 0K$	N339	N337
$\Delta\rho = 1\%$, $\Delta T = 2.5K$	N320	**N318**

The selected experiment for the blind calculation is N318. Inlet boundary conditions will be provided for all the experiments. However, velocity, Reynolds stresses (*u'u', u'v', v'v'*) and concentration profiles inside the mixing section –at the locations shown in Figure 4– will be provided only for the other three cases. These data can be used freely by the participants, for instance, to calibrate physical models, mesh improvement or to obtain the uncertainty band in extrapolation methods.

7. PHYSICAL PROPERTIES

The physical properties of water for the experiments considered in this benchmark exercise are listed in Table 4. Properties of de-ionised as well as tap water were considered identical.

Table 4. Physical properties for tap/de-ionised water and for the mixture de-ionised water + sucrose 2.7 wt%

	Tap / de-ionised water @ 20C	De-ionised water + sucrose @ 22.5C
$k\,(W/mK)$	0.6	0.6
$Cp\,(kJ/kgK)$	4.18	4.18
$\rho\,(kg/m^3)$	998	1008
$\mu\,(N/m^2 s)$	1.002	0.991

8. MEASURING THE INLET BOUNDARY CONDITIONS

Mean velocities and their associated fluctuations were measured with LDA in one quadrant of the upper leg 50 mm upstream the tip of the splitter plate (see Figure 5). Figure 6 shows the location of the measuring points for the inlet boundary condition. Due to limitations in optical access, the three velocity components could only be measured at the locations marked in pink. The black markers correspond to the location were only two velocity components were measured (x,y). Hence, in the data files for the inlet boundary conditions, the RMS values of the z-component were filled with zeros for those locations.

To construct the whole upper leg inlet boundary condition, symmetry was assumed among the four quadrants. Because the Reynolds number for both legs is the same (even for a $\Delta\rho$ = 1%), the inlet boundary condition for the lower leg was obtained by applying symmetry once again along the z-co-ordinate. Since LDA measurements at each point are time consuming, it was decided to measure only the upper leg. The distribution of the measuring points in the cross-sectional area of the conditioning section is shown in Figure 6. The experiments were performed at room temperature and, therefore, heat losses can be considered negligible, even for the case with $\Delta\rho$ = 1% where the temperature in the lower leg is slightly higher (2.5 °C) than that of the upper leg.

Figure 9. Location of the LDA measurement plane. These measurements were used to determine the inlet boundary condition for the CFD simulations.

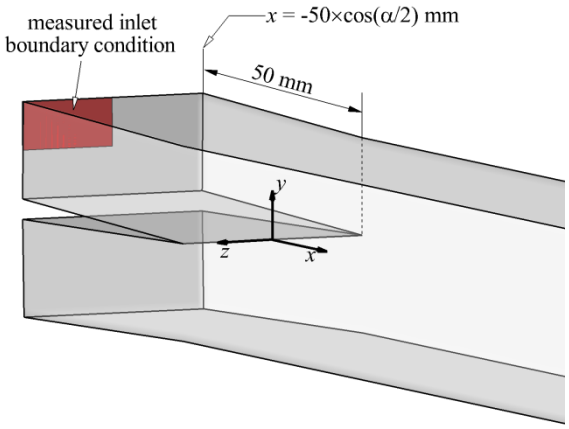

It is important to remark the LDA measuring plane for inlet boundary condition was inclined 1.5°respect to the yz-plane to obtain a streamwise velocity profile parallel to the surface of the splitter plate, hence, the x-co-ordinate of the measuring points changes slightly for each value of the y-co-ordinate. The files containing the experimental measurements of the inlet boundary conditions have the proper co-ordinates in the xyz Cartesian system. The time averaged velocity at each point was calculated according to:

$$\bar{u} = \frac{1}{N}\sum_{i=1}^{N} u_i, \qquad (23)$$

where N correspond to the total number of samples and u_i is the instantaneous velocity at a given point. The RMS of velocity fluctuations was calculated by:

$$\langle u' \rangle_{RMS} = \sqrt{\frac{1}{N-1}\sum_{i=1}^{N}(u_i - \bar{u})^2} \qquad (24)$$

Figure 10. Location of the measuring points for velocity inlet boundary conditions with LDA

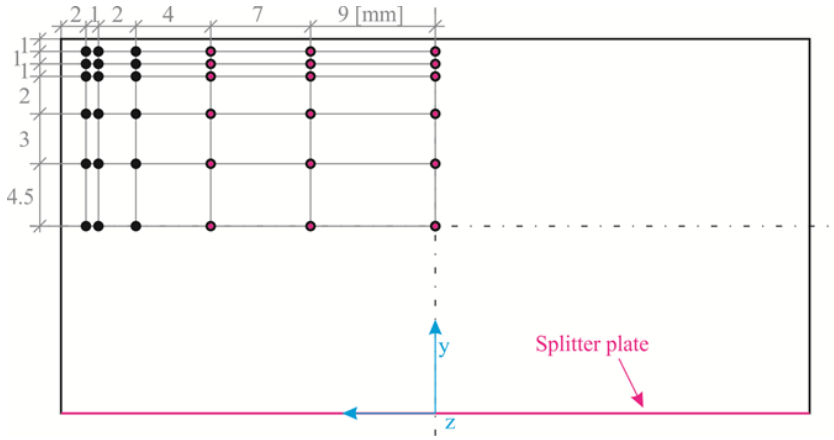

Since the available LDA system enables for one-dimensional pointwise measurements of the instantaneous velocities, the three components of the velocity fluctuations cannot be measured simultaneously. Hence, the three components of the velocity fluctuations were measured by re-orienting the LDA system in different directions. For the points where the three velocity components were measured (pink markers in Figure 10), the turbulence kinetic energy was calculated according to:

$$k = \frac{1}{2}\left(\langle u' \rangle_{RMS} + \langle v' \rangle_{RMS} + \langle w' \rangle_{RMS}\right) \qquad (25)$$

For the locations where only two velocity components are available (black markers in Figure 10), the turbulence kinetic energy is obtained by:

$$k = \frac{1}{2}\left(\langle u' \rangle_{RMS} + 2\langle v' \rangle_{RMS}\right) \qquad (26)$$

The mean velocity profile obtained from the LDA measurements at the inlet of the CFD domain is presented in Figure 11. This figure also shows the location of the measuring points. Points located at the walls were assigned with null values.

Figure 11. LDA mean velocity profiles at the inlet of the CFD domain (50 mm behind the tip of the splitter plate)

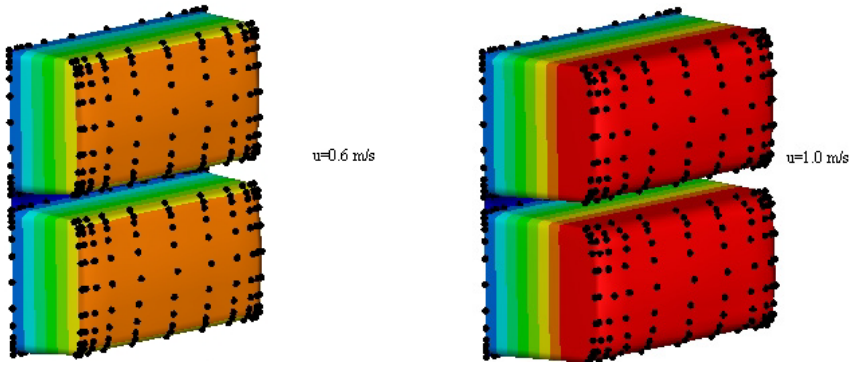

Because the Reynolds number was the same for $\Delta\rho = 0\%$ and $\Delta\rho = 1\%$, the velocity profiles and turbulence quantities are assumed to be equal for these two cases.

9. GENERAL INFORMATION ABOUT THE SUBMISSIONS

9.1. Registered participants

There were a total of 21 registered participants from 13 countries (Table 5). All participants received the specifications and the experimental data files to performed their UQ analyses. However, only 13 participants from 9 countries completed the task.

Table 5. List of participants by country and their submission status

Country	Status
France	OK
France	OK
France	OK
France	OK
Hungary	No results
Italy	No results
Korea	OK
Korea	No results
Netherlands	OK
Poland	OK
Russia	OK
Russia	No results
Russia	No results
Slovenia	No results (work done, but not delivered)
Spain	OK
Sweden	OK
Switzerland	No results
United Kingdom	OK
United States	OK
United States	OK
United States	No results

10. ABOUT THE SUBMISSIONS

In Table 6, we summarise the most important information about each individual submission. One can see that the number of simulations required to perform the UQCFD analysis varied over a broad spectrum. For example, user-11 required only 4 simulations, while user-03 needed a staggering total of 836 runs to complete the analysis. Regarding turbulence models, the most employed model was $k-\varepsilon$ (including all its variants) with 5 submissions, followed by $k-\omega$ with 4, large eddy simulation (LES) with 2, and root mean square (RMS) with 1. It is noteworthy to mention the incredible effort made by user-18, who used LES and needed a total of 22 simulations to obtain the UQCFD results. In terms of software usage, the commercial packages developed by ANSYS (fluent + CFX) were used 5 times, followed by Star-CCM+ with 2. The rest of the participants used either open source or in-house codes. Code_Saturne had the highest number of users (2), followed by CUPID, TrioCFD, P2REMICS and OpenFOAM having each of them only 1 user. For the UQ methodology, 10 users considered only a propagation step and 3 users propagation + extrapolation. Among the most used propagation methods was Polynomial Chaos Expansions with 4 users, followed by Monte Carlo (2) and Deterministic Sampling (2). All the other methods were used only once. For additional information on each method, the reader is referred to the Appendix B and the references therein.

Table 6. Additional details of the individual submissions

USER-ID	UQ method	CFD CODE	# of Simulations	Turbulence model	Wall treatment	Mesh size
user-01	PERCEIVE (Propagation + Extrapolation)	Code_Saturne 4.2	6	EBRSM and kw	Wall-resolved	652320
user-02	anchored-ANOVA + POD-Kriging (Sensitivity analysis + propagation)	P2REMICS V0	26	k-omega SST	Wall-resolved	712704
user-03	EDF WAVE Method (Propagation + Extrapolation)	ANSYS CFX 15.0.7	836	standard k-e	scalable wall-function	813276
user-04	Uncertainty Quantification and Sensitivity Analysis in CFD based on Distinction between Categorical and Continuous Variables	TrioCFD, V1.7.2	220	standard k-e	standard wall function	59850
user-07	PCE	CUPID 1.9	103	standard k-e	standard wall function	156260
user-09	ASME V&V 20-2009	ANSYS Fluent, V14.0	24	low Re Abid k-eps	damping functions	62418
user-10	Monte Carlo	ANSYS Fluent, V16.1.0	144	standard k-e	scalable wall function	3696000
user-11	Deterministic Sampling	ANSYS CFX, V14.5.7	4	Zonal LES Model (Beta)	Wall-resolved	3596992
user-15	PCE	ANSYS CFX 17.0	16	k-w SST	Scalable wall function	300000
user-16	Unscented Transform Deterministic Sampling	OpenFOAM 2.4.0	8	K-epsilon	Standard wall function	675168
user-18	PCE	Code_Saturne 4.0.4	22	LES (Smagorinsky)	Wall resolved	20644596
user-19	Root Sum Square of individual Uncertainties + GCI	STAR-CCM+ 10.06.010	15	Elliptic Blending K-Epsilon	standard wall functions	1637784
user-20	Monte Carlo	Star-CCM+ Version 10.06	40	k-w	y+ wall treatment	5753458

11. RANKING THE SUBMISSIONS ACCORDING TO SPECIFIC MEASURES

To generate a ranking for the submissions, it was necessary to establish a measure that account for: the difference between calculated and experimental mean values, uncertainty level of the CFD simulations, and the proper shape of the required profiles. These constrains impede the use of a linear measure, such as the one used in the previous OECD-PANDA benchmark, which is given by

$$M = \frac{1}{N_{data}} \sum_{i=1}^{N_{data}} |S_i - E_i| \qquad (27)$$

where S_i and E_i represent the simulated and experimental values respectively, and N_{data} the total number of data points used in the analysis. If we take for example the velocity profile shown in Figure 12, it is seen that the flat uniform velocity profile (blue line) would lead to a lower value for M compared to the red profile. However, the red velocity profile is of a higher physical significance than the uniform profile. Another important issue to note is that in this benchmark exercise, the comparison between simulations and experiments must also account for uncertainty bands.

Figure 12. Schematic comparison between two simulated velocity profiles (continuous lines) and experiments (symbols)

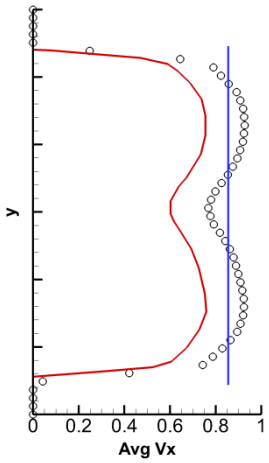

Depending on the type of UQ method used by each participant, the uncertainty band could be related to a certain quantile of a probability density function, to an interval (min, max) or to a member function (fuzzy variable). Therefore, a standardised measure that accounts for all these possibilities becomes highly complex. To simplify the analysis, a unique measure –based on a Gaussian distribution– is proposed. Let us imagine that the experimental and simulated values are represented by two Gaussian distributions –each characterised by a mean and standard deviation– then a normalised measure of the overlap between the two distributions would indicate how close the simulations and experiments are.

Figure 13. Schematic representation of the overlapping degree density (fidelity density) between two Gaussian distributions (filled blue)

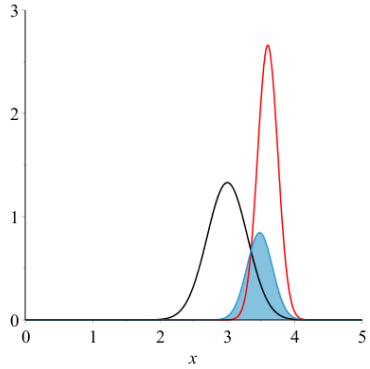

We define then the degree of overlap or fidelity of the numerical simulations by:

$$\Omega = \int_{-\infty}^{\infty} \omega(x)dx \tag{28}$$

$$\omega(x) = \frac{1}{2\sigma_{sim}\sqrt{\pi}} \exp\left\{-\frac{1}{4}\left[\left(\frac{x-\mu_{\exp}}{\sigma_{\exp}}\right)^2 + \left(\frac{x-\mu_{sim}}{\sigma_{sim}}\right)^2\right]\right\} \tag{29}$$

where the $\omega(x)$ is the fidelity density (overlap degree), and the subscripts *sim* and *exp* stand for simulation and experiment. Equation (28) can clearly be written as a convolution of two normal distributions, that is:

$$\Omega(x) = \left(\frac{\sigma_{exp}}{2\sigma_{sim}} N(x, \mu_{exp}, \sigma_{exp}) * N(x, \mu_{sim}, \sigma_{sim})\right)^{1/2} \tag{30}$$

This allows us to find a simple analytical solution for the fidelity, avoiding the need to calculate explicitly the integral in Eq. (28). Thus, the fidelity is expressed as:

$$\Omega(x) = \beta(x)^{-1/2} exp\left(-\frac{\alpha(x)}{4\beta(x)}\right) \tag{31}$$

With $\alpha(x) = \left[\left(\mu_{exp} - \mu_{sim}\right)/\sigma_{exp}\right]^2$ and $\beta(x) = 1 + \left(\sigma_{sim}/\sigma_{exp}\right)^2$. The coefficient α is a measure of the error (or bias) between the experiments and simulations, and beta is a measure of how informative a simulation is – large values indicate a very uninformative simulation. The fidelity Ω will reach a maximum value – equal to 1 – when the mean values of the two distributions coincide and the standard deviation of the simulations goes to zero (Figure 15c). Thus, the maximum value will be reached only when the uncertainty in the simulations is zero and the simulations coincide exactly with experimental points (mean values). Increasing the uncertainty in the simulations or having a large difference between experimental and simulated mean values, will lead to a fidelity value lower than one. This implies that Ω is bounded to the interval $\Omega \in [0,1]$. Figure 14 shows a three-dimensional plot of Ω, where iso-level for the fidelity can be attained for different combinations for α and β. When using a measure such as the one defined in Eq. (30), a simulation with mean values close to the experimental ones and a narrow uncertainty band, can have a fidelity Ω higher than that of a simulation with a broader uncertainty band and mean values coinciding exactly with the experimental ones (see Figure 15). Hence, simulations with large uncertainty bands or with mean values far from the experimental one will be penalised naturally in the calculation of Ω. This characteristic is quite relevant for any multivariate measure used in the

assessment of UQ methods. For instance, a simulation matching exactly the experimental points, but with a very large uncertainty band become meaningless in the context of nuclear reactor safety (there is no reliability in the results). This is the main difference between the assessment of conventional CFD simulations and UQCFD, which might not be completely clear to CFD practitioners entering the UQ field.

The concept of fidelity presented in this report has undoubtedly some issues. For example, it is assumed that the probability density function of both the experimental and CFD results is a Gaussian distribution. Although outputs PDFs are most certainly not conforming exactly to normal distributions, their mapping onto a known distribution –such as the normal– seems unavoidable. If every user, for instance, had provided us with the exact output PDF, we could calculate the fidelity by directly using the convolution of the two distributions (plus a normalisation coefficient). However, how could we compare two submissions –based on the fidelity concept– if the outputs PDFs of the participants are not the same? Thus, it seems imperative to establish a standard procedure to compare the fidelity (or any other measure for that matter) for several submissions. Therefore, we chose to map the experimental and simulation PDFs onto normal distributions, which allows us to obtain the fidelity value from an analytical solution.

Figure 14. fidelity as a function of α and β

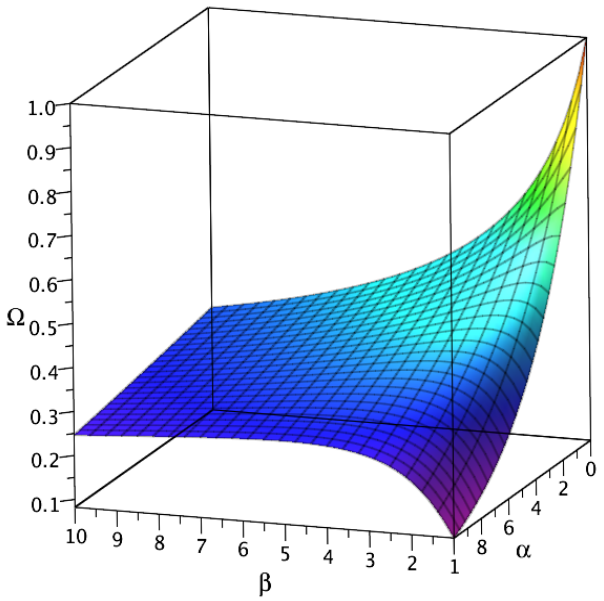

To standardise the procedure for calculating the fidelity, the uncertainty bands provided by the participants were associated to $\pm 2\sigma_{sim}$ in the Gaussian distribution representing the CFD results. When the CFD uncertainty bands are not symmetric respect to the mean value, half of the difference between the upper and lower bands are used to calculate the standard deviation of the simulations, that is:

$$2\sigma_{sim} = \frac{(Upper - Lower)}{2} \tag{32}$$

Figure 15. Overlapping degree between simulations (continuous red) and experiments (continuous black)

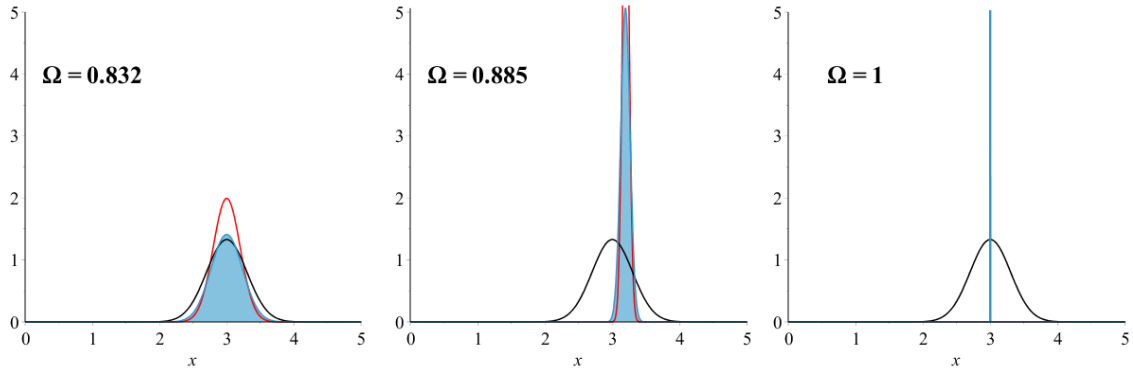

(a) The mean value of the simulations coincides with the experimental one and the CFD uncertainty band is slightly narrower than that of the experiment.
(b) The mean value of the simulations is slightly different than the experimental one, but the CFD uncertainty is much less than the one observed in the experiments.
(c) The CFD uncertainty is zero and the simulated variable coincides with the mean value from the experiment.

The mean value μ_{sim} is the one provided by the participants. The fidelity Ω is then calculated at each grid point along all profiles for concentration, velocity and turbulence kinetic energy (see Figure 4) for the location of the profiles). To evaluate the correctness of the shape of the profiles, we fit a piecewise third order spline to the experimental and simulated results (mean values), and calculated the profiles derivatives at each grid point from the fitting curve *f*. Thus, at each grid point we evaluate the correctness of the profiles' shape based on the relative error between the derivatives calculated from CFD and experimental results:

$$\mathrm{E} = \left| 1 - \frac{df_{sim}}{dy} \Big/ \frac{df_{\exp}}{dy} \right| \tag{33}$$

11.1. Figure of merit

To generate a ranking table, it is necessary to account for both the fidelity and the correctness of the profiles in a single measure. It was initially proposed to use a simple combination of the averaged $\overline{\Omega}$ and $\overline{\mathrm{E}}$ in the form of:

$$M = \theta_1 \left[1 - \frac{1}{N_{data}} \sum_{i=1}^{N_{data}} \Omega_i \right] + \theta_2 \left[\frac{1}{N_{data}} \sum_{i=1}^{N_{data}} \mathrm{E}_i \right] \tag{34}$$

where θ_1 and θ_2 are coefficients between 0 and 1. However, and due to the high nonlinearity of the fidelity, a different figure of merit (FoM) had to be defined. To define the FoM used in this benchmark, we elaborated ranking tables for each grid point based independently on Ω and E, where the rank for each participant varied from 1 (highest) to $N_{participants}$ (lowest). The FoM based on individual rankings of $R_{\Omega,i}$ and $R_{\mathrm{E},i}$ is given by

$$FoM = \frac{1}{N_{data}} \sum_{i=1}^{N_{data}} \frac{1}{2} \left(R_{\Omega,i} + R_{\mathrm{E},i} \right) \tag{35}$$

where the subscript *i* refers to i-th experimental point and N_{data} to the total number of data points used in the analysis. Hence, the FoM represents an average of individual rankings. The final ranking tables for

velocity, turbulence kinetic energy and concentration, were generated based on the measure defined in Eq. (35).

Since the transport of a scalar field (i.e. temperature and/or concentration) in turbulent mixing is the most important physical phenomenon from a safety point of view, an additional measure is established to evaluate the accuracy of the simulations in predicting the concentration field. From the five concentration profiles submitted by the participants, we extracted –in an automated manner– the thickness of the mixing layer and compared it with the experimental values. To extract the mixing layer thickness $\delta(x)$, we fitted an error function to the experimental and simulated data points,

$$c(x) = \frac{1}{2}\left(1 + erf\left[\frac{y-y_0}{\delta(x)/2}\right]\right) \qquad (36)$$

Then, the measure used to generate the ranking tables was the average of the absolute difference between the mixing layer thickness obtained from the simulations and experimental data points.

$$M_C = \frac{1}{5}\sum_{i=1}^{5}\left|\delta_i^{\exp} - \delta_i^{sim}\right| \qquad (37)$$

12. EXPERIMENTAL RESULTS

In this benchmark, only mean velocity, turbulence kinetic energy and mean concentration were used to assess the uncertainty quantification (UQ) methodologies. Five profiles along the mixing section were provided.

12.1. Mean velocity profile

The mean velocity profiles for all experiments (including the blind case) are presented in Figure 16. It is seen that a small density difference of 1% between the upper and lower streams, has a negligible effect on the mean velocity profiles. Only near the tip of the splitter plate (x = 50mm), a mild difference is observed within the mixing layer, which is consistent with the higher kinetic energy measured within the mixing layer.

Figure 16. Mean velocity profiles at five selected location along the mixing section

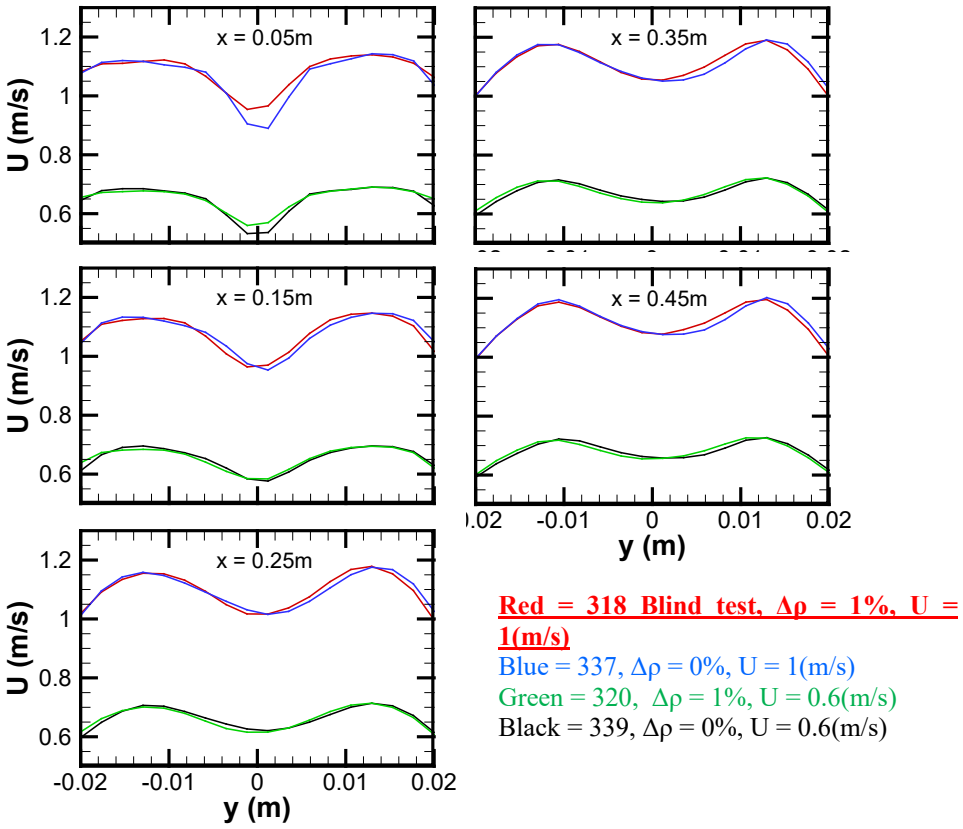

12.2. Turbulence kinetic energy

Profiles for the turbulence kinetic energy are shown in Figure 17 for five different locations along the mixing section. As seen in the figures, the turbulence kinetic energy is always higher – within the mixing layer – for the cases with a mild density difference. As discussed in the section for experimental uncertainties, we believe that the higher values for this variable obey an experimental bias. However, if higher values of the turbulence kinetic energy are indeed an artefact arising from an inhomogeneous refraction index, we would expect the bias to be the same for both experiments with density difference (experiments 318 and 320). The concentration profiles show that the thickness of the mixing layer is almost identical for the four experiments and, thus, the bending experienced by a beam of light crossing the inhomogeneous mixing layer would be the same or at least similar. Nonetheless, the turbulence kinetic energy is much larger for the experiment 318, which is consistent with a higher Reynolds number. Outside the mixing layer, the measurements agree well for experiments with the same Reynolds number.

Figure 17. Turbulence kinetic energy at five different locations along the mixing section

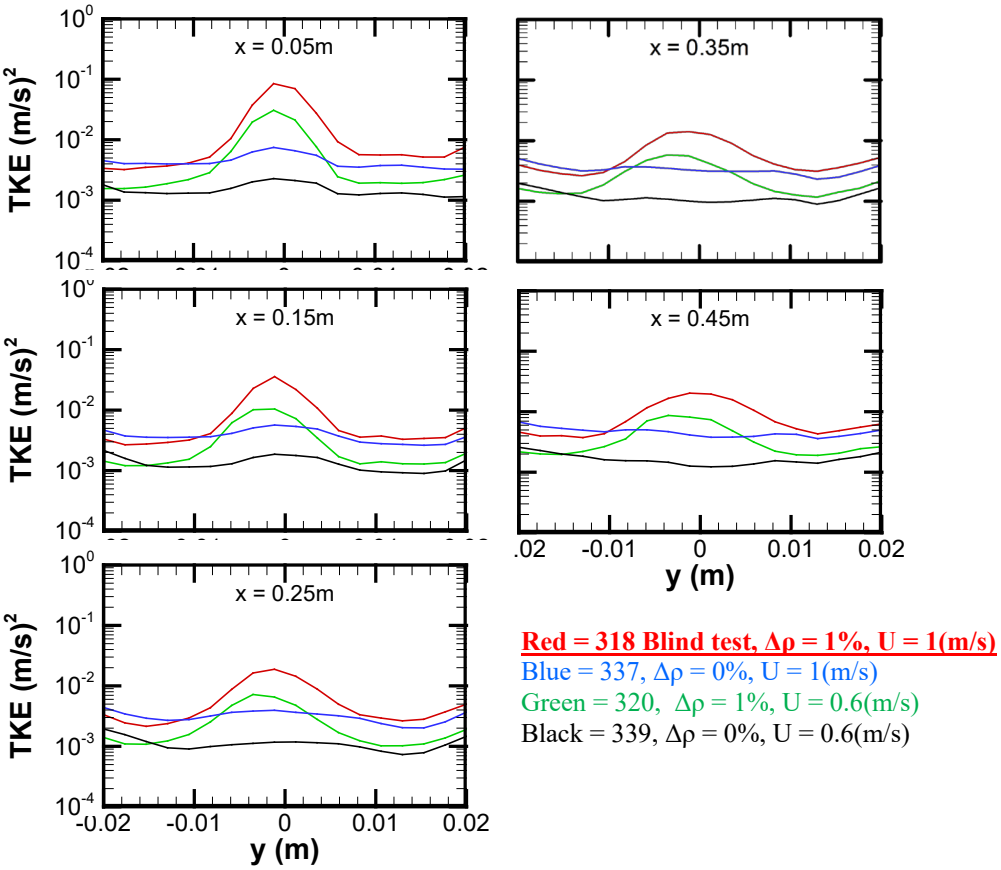

It is also interesting to see that when the axis of the turbulence kinetic energy is in logarithmic scale, the profiles between experiments 318 and 320 are parallel, just like for the two experiments without density difference. Again, this behaviour does not appear to be possible if the bias for all the experiments with a density difference is the same. Another point that is worth mentioning is that in particle image velocimetry (PIV) measurements, the time delay between the two laser pulses (to obtain the pair of images used in the calculation of the instantaneous velocity field), is of the order of microsecond and,

therefore, a beam of light would cross a concentration field that is virtually frozen. Although an inhomogeneous refraction index introduces a small bending of the beam light, the bending would be almost identical for the two consecutives images. This also contributes to the unknowns in the uncertainties in the PIV measurements of the turbulence kinetic energy. One way to test the influence of the light bending (or the inhomogeneity of the refraction index), would be to run the same experiment with different time delay between the pair of images. By increasing the time delay, we would expect an increase in the turbulence kinetic energy if the bending of the light beam is truly causing a relevant experimental bias. Another more convincing alternative, would be to run a mixing experiment with two fluids with the same density and viscosity, but with a different refraction index. Unfortunately, and to the best of our knowledge, there are no fluids that comply strictly to these constrains.

12.3. Mean concentration profiles

The mean concentration profiles obtained by laser-induced fluorescence (LIF) (Figure 18) also show a remarkable result. Profiles are almost identical (within the experimental uncertainties) for all the experiments, irrespective of the Reynolds number. Initially this appeared to be quite suspicious, but after a deeper analysis of the results, they make perfect sense. Despite the fact that mixing is stronger for the experiments with higher velocity fluctuations, the mean velocity is higher and the residence time inside the mixing section is lower. This means that as the mixing layer spreads faster for higher Reynolds numbers, it also gets advected faster which compensates for the stronger mixing. Thus, the mean concentration profiles display a self-similar behavior in terms of the Reynolds number. It is precisely this self-similarity what make us strongly believe that the higher value for the turbulence kinetic energy for the case with a mild density difference, is the result of an experimental bias. If the turbulence kinetic energy is truly higher for experiment 318, then the mean concentration profiles should look different for experiments 318 and 337. Nonetheless, this is just a conjecture that cannot be proved with the available data.

Figure 18. Concentration profiles.

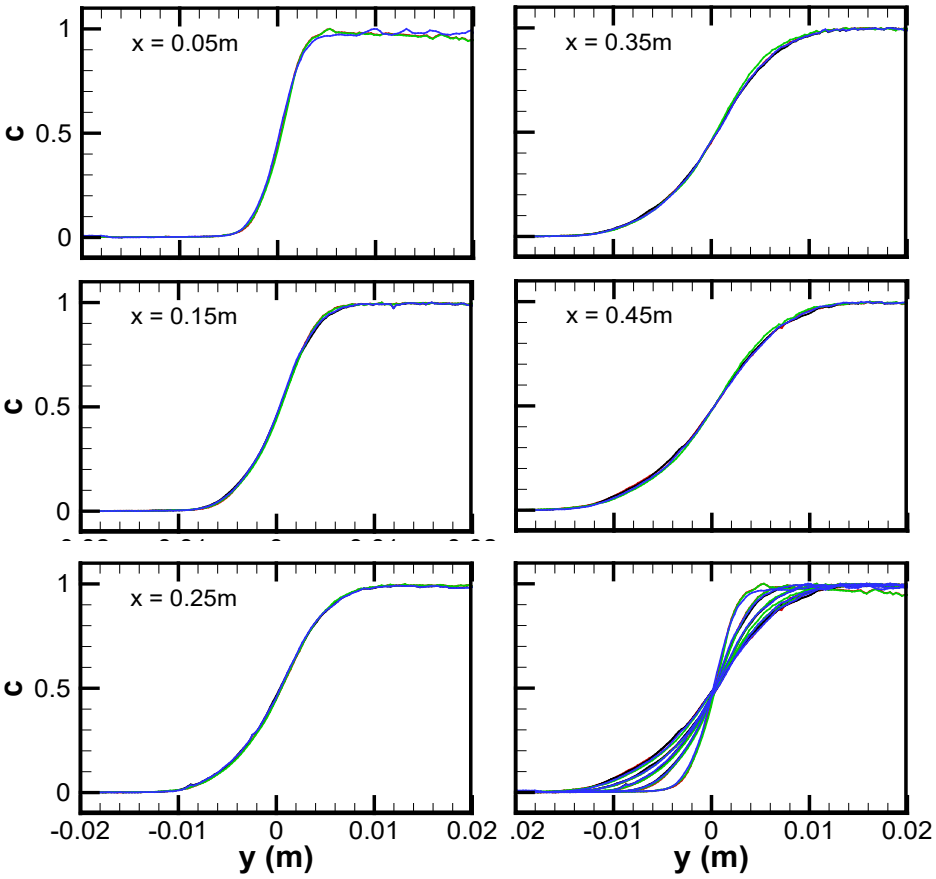

Red = 318 Blind test, Δρ = 1%, U = 1(m/s)
Blue = 337, Δρ = 0%, U = 1(m/s)
Green = 320, Δρ = 1%, U = 0.6(m/s)
Black = 339, Δρ = 0%, U = 0.6(m/s)

13. UQCFD RESULTS AND FINAL RANKING TABLE

The results provided by the participants are very encouraging, because, this being the first benchmark exercise on uncertainty quantification in computational fluid dynamic (UQCFD) worldwide, we expected a broader scatter of the results, which was not the case. Although the problem of turbulence mixing in a square channel may have appeared to be a simple one at first glance, the reality is quite different. For instance, the simple geometry of the mixing GEMIX facility led two of the participants to use 2D simulations, despite that the velocity profile inside the mixing section is fully three-dimensional. When using the experimental inlet velocity profile provided in this benchmark for two-dimensional simulations, the mass flow rate cannot be captured properly due to the three-dimensionality of the inlet velocity profile. In addition, the development of the velocity field along the mixing section is affected by all the walls, not only the upper and lower walls as in a two-dimensional case. Despite the difficulties related to turbulent mixing, some of the participants obtained astonishing good results. Users 01, 03 and 19 stand out from the rest of the submissions. For example, user-19 bounded the experimental velocity profiles perfectly with the UQCFD uncertainty bands, without using an extrapolation step as done by users-01 and -03. Table 7 presents the final raking table for the present benchmark exercise. In red bold symbols, are the submissions that obtained a place in the top 3. As mentioned earlier, the results for the turbulence kinetic energy must be considered with precaution, due to the unknown experimental uncertainties in this variable.

Table 7. Final ranking table

user	Rank. U	Rank. TKE*	Rank. C	Rank. δ	UQ (# sim)	Tub. model
1	**3**	**2**	**1**	**2**	PERCEIVE (6)	EBRSM and k-w
2	5	6	5	7	Kriging (26)	k-w SST
3	**2**	**1**	4	**1**	WAVE (836)	Standard *k-ε*
4	10	7	12	13	PCE (220)	Standard *k-ε*
7	11	4	9	6	PCE (103)	Standard *k-ε*
9	4	5	**3**	5	ASME V&V 20-2009 (24)	Low Re Abid *k-ε*
10	7	12	6	4	Monte Carlo (144)	Standard *k-ε*
11	9	13	10	11	Deterministic Sampling (4)	Zonal LES Model
15	6	8	8	8	PCE (16)	k-w SST
16	12	**3**	7	10	Deterministic Sampling (8)	Standard *k-ε*
18	13	11	13	12	PCE (22)	LES (Smagorinsky)
19	**1**	9	**2**	**3**	Root Sum Square Ind. Uncert. + GCI (15)	Ellip. Blending *k-ε*
20	8	10	11	9	Monte Carlo (40)	k-w

As seen in previous benchmarks (e.g. PANDA benchmark), large eddy simulation (LES) did not provide an advantage against conventional Reynolds Averaged Navier Stokes (RANS) models (i.e. users-11 and -18). We are all aware of the capabilities of LES for simulating turbulent flows, but as with any other simulation technique, we must also be aware of its limitations. For instance, when the aspect ratio of the numerical cell is too large (elongated cells in the axial direction), we might be resolving properly the turbulent scales in the spanwise direction, but not in the stream-wise direction. LES considers subgrid scales models that assume isotropy, but elongated cells introduce a fair amount of anisotropy in the Reynolds stresses, due to the disparity of wavelengths that are being resolved in each direction. Detached eddy simulations (DES or Zonal LES), attempt to mitigate this issue near walls –where cells usually possess a large aspect ratio– by switching to a RANS model. However, if the aspect ratio is still high in the core region, the eddy viscosity will be artificially higher than the one predicted with a uniform mesh with a grid spacing corresponding to the smallest size of an elongated cell. Calculating the filter size by using the cubic root of the cell volume, works for aspect ratios close to 1. For aspect ratios higher than 2, the use of LES models may require some compensating terms in the subgrid scale models. For high aspect ratios, LES equations lose their accuracy in representing properly a turbulent flow. The main idea in LES is very basic: we must resolve most the energetic scales, while the rest (including the dissipative ones) are approximated by the subgrid scale models. Celik et. al. [6] proposed that for reliable LES results, we must resolve 80% of the kinetic energy of the flow. To evaluate if a simulation fulfils this requirement, we can compare directly the ratio between the kinetic energy from the subgrid scale model and the total kinetic energy (kinetic energy predicted by LES + kinetic energy from the subgrid scale model). This criterion, which seems very appropriate, is seldom applied. Although DES provides a good alternative for the demanding requirements for the cell size near the wall, DES does not always solve the problem in this region, as seen in the velocity profiles of user-11. If we look closely to these results, we can see that the shape of the mean velocity profile near the wall is not correct, which indicates poorly resolved wall stresses.

Another important issue observed in the present benchmark, is the use of two-dimensional simulations to reproduce a fully three-dimensional problem. For example, we believe that the use of two-dimensional simulations had an important impact on the results of user-04, where velocity and concentration profiles were not well reproduced. However, and despite of using two-dimensional simulations, user-09 obtained good scores in all the variables. These two users employed the $k-\varepsilon$ model, but user-09 used a variant for low Reynolds number. This choice seems strange to us, because the problem under study is fully turbulent (Re = 50 000 in the mixing section) and low Reynolds number models are reserved mostly for transitional regimes. Since these models are less diffusive, the velocity profile calculated by user-09 is less flattened than the one obtained by user-04 at x = 450 mm. This is confirmed by the lower values of turbulence kinetic energy from user-09. It might be possible that the physical errors derived from using a low Reynolds number model for a fully turbulent flow, are somehow absorbed by the UQ analysis when the uncertainties associated to the turbulence model are properly treated.

The measures used to assess the capability of the UQCFD analyses in reproducing the concentration file show interesting results. The measure for the mixing layer thickness is linear (Eq. 37) and only considers the mean concentration profiles (without the uncertainty band). The second measure contains the UQ results through the non-linear concept of fidelity plus the correctness of the mean concentration profile. We see that there is a slight change in the ranking between 0 and 3. One of the critical cases is user-03, who ranked 4th for the concentration profile, but 1st for the mixing layer thickness. To us, the ranking evaluating the concentration profile is more significant than the one assessing the mixing layer thickness. The main reason for this is that when assessing the thickness of the mixing layer, the uncertainty bands are not accounted for. User-04 provides one of the most accurate results for the mean experimental values; however, the uncertainty bands are rather large making the results less reliable. This is an interesting property of the measure proposed in this benchmark, because it shows clearly that reproducing mean profiles is not enough to have a high score.

The number of CFD simulations required by each participant to obtain the uncertainty bands varied broadly from 4 to 836. However, and as seen in the final ranking table, an elevated number of CFD runs does not guarantee a high score. For instance, users-01 and -19 required 6 and 15 simulations respectively, to achieve excellent scores for all the measures. The combination of propagation and extrapolation (e.g. users-01, -03) did no present a clear advantage against a purely propagating method (user-19). Nonetheless, these three users used the open test cases in one way or another to improve their results. For instance, user-19 calibrated their CFD model (mesh, turbulence model, etc.) with the open tests. Users-01 and -03 used the open tests to calculate the bias in the CFD results, which was then extrapolated to the blind test case. This extrapolation meant basically correcting the raw numerical results by the extrapolated bias obtained with the open tests. The extrapolation step is the main reason why these two users could get a close agreement for the turbulence kinetic energy within the mixing layer, and predicted the decrease of the concentration profile from the mixing layer towardss the wall. Unfortunately, the test matrix in the present benchmark exercise was essentially linear with respect to the Froude and Reynolds numbers, which makes an extrapolation step the perfect choice for calculating the bias in the CFD models. This means that for a system with almost a linear response to the relevant parameters (e.g. Froude and Reynolds number), whatever error is made in the CFD calculations, can be corrected (almost to perfection) with the extrapolation step. This will not be the case, for instance, when the bias in the numerical simulations is obtained from integral effect tests (IETs) and then extrapolated to a real reactor scenario.

It is worth mentioning the low number of simulations required by the Deterministic Sampling method. Even though the two users employing this method (11 and 16) obtained relatively low scores, only a few simulations were needed to obtain the uncertainty bands. This is highly desirable in a method that could potentially be applied to a real reactor calculation. The main strength of Deterministic Sampling is the direct propagation of the moments from input parameters to the final solution. Thus, the number of simulations will increase with the number of input parameters and for the propagation of higher order moments. This simple observation opens the door to a difficult question. How to assess the quality of the UQ method when so many variables can play a key role in the final UQCFD solution? We have the user effect, mesh, turbulence model and UQ methodology that affect greatly the results. For example, Monte Carlo is the prime method when it comes to propagation of uncertainties. However, we see that users working with Monte Carlo did not obtain the highest scores. The low number of samples from user-20 might have an impact on the accuracy of the uncertainty propagation, but even with 40 samples, a reasonable estimation of the standard of the output should be made. From the scores of user-10, it may seem that increasing the number of samples in the Monte Carlo (MC) propagation, increases also the quality of the results. But these two users also used different turbulence models, mesh and software, which makes the assessment of the UQ methodology difficult. Polynomial Chaos Expansions (PCE) is another propagation method that did not perform well in the present benchmark (users-04, -07, -15, -18). Nevertheless, PCE as well as MC are methods supported by very well-known mathematical theories and used successfully in countless cases.

For the reasons here exposed, we believe that from the current results, it is almost impossible to decide which UQ methodology is the best. This is the main reason for proposing –at the beginning of the benchmark– to fix the mesh, turbulence model and numerics (e.g. advection scheme, convergence criteria, etc.) to focus only on the UQ methodology. Thus, the scores obtained in the present benchmark cannot be used reliably in assessing the quality and capabilities of the UQ methods. We believe that for future benchmarks on this area (if any), these considerations must be discussed carefully when deciding the aim of the benchmark. In uncertainty quantification, one of the most difficult parts is the determination of the input parameters and their associated uncertainties. A robust UQ methodology must include a clear and structured procedure (e.g. Phenomena identification and ranking table – PIRT) to determine all the input uncertainties and decide which are the dominant parameters that should be

considered in the propagation step. Fixing the conditions for the CFD models (mesh, turbulence model, etc.), would have helped us in assessing the robustness, efficiency and accuracy of the UQ methodology.

Finally, we must note that the uncertainty bands obtained in the present benchmark (+/- 2 std), do not conform to the standards in the context of nuclear reactor safety, where uncertainty bands are constructed from tolerance intervals. When the output probability density function of the UQCFD analysis is different than a normal distribution, the interval constructed from +/- 2 std does not correspond to the tolerance interval (5%, 95%) usually used in the calculation of uncertainties in nuclear reactor safety. Enforcing the generation of uncertainty bands from a tolerance interval, introduces additional difficulties in UQCFD. For instance, when using Polynomial Chaos, the standard deviation from inputs can be propagated easily to the output. However, when the uncertainty bands must correspond to a tolerance interval, additional simulations are required to calculate higher order moments (needed for the calculation of the tolerance interval), or Monte Carlo simulations must be used in the response surface to obtain the appropriate output probability density function.

Figure 19. Concentration at x = 50mm

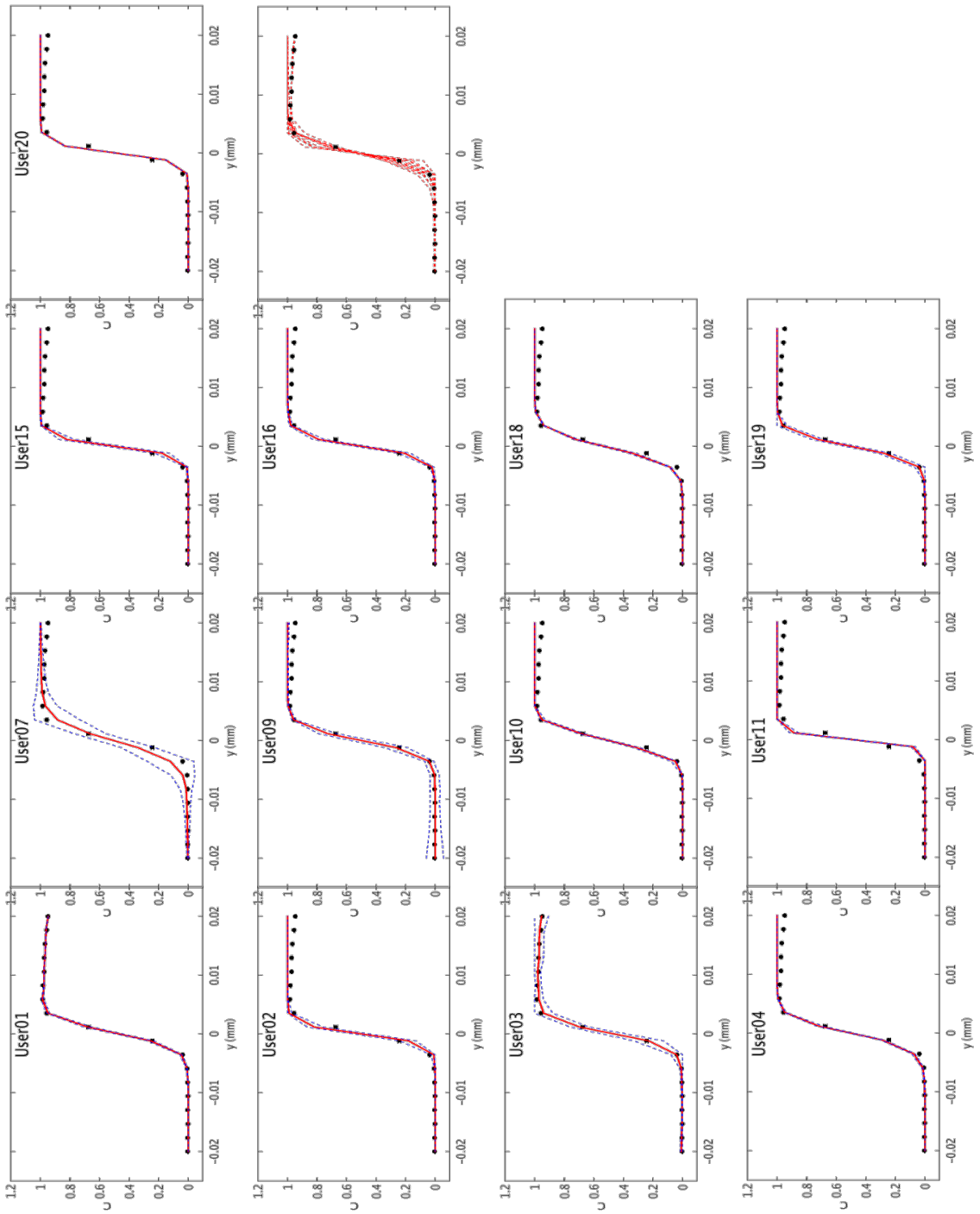

Figure 20. Concentration at x = 150mm

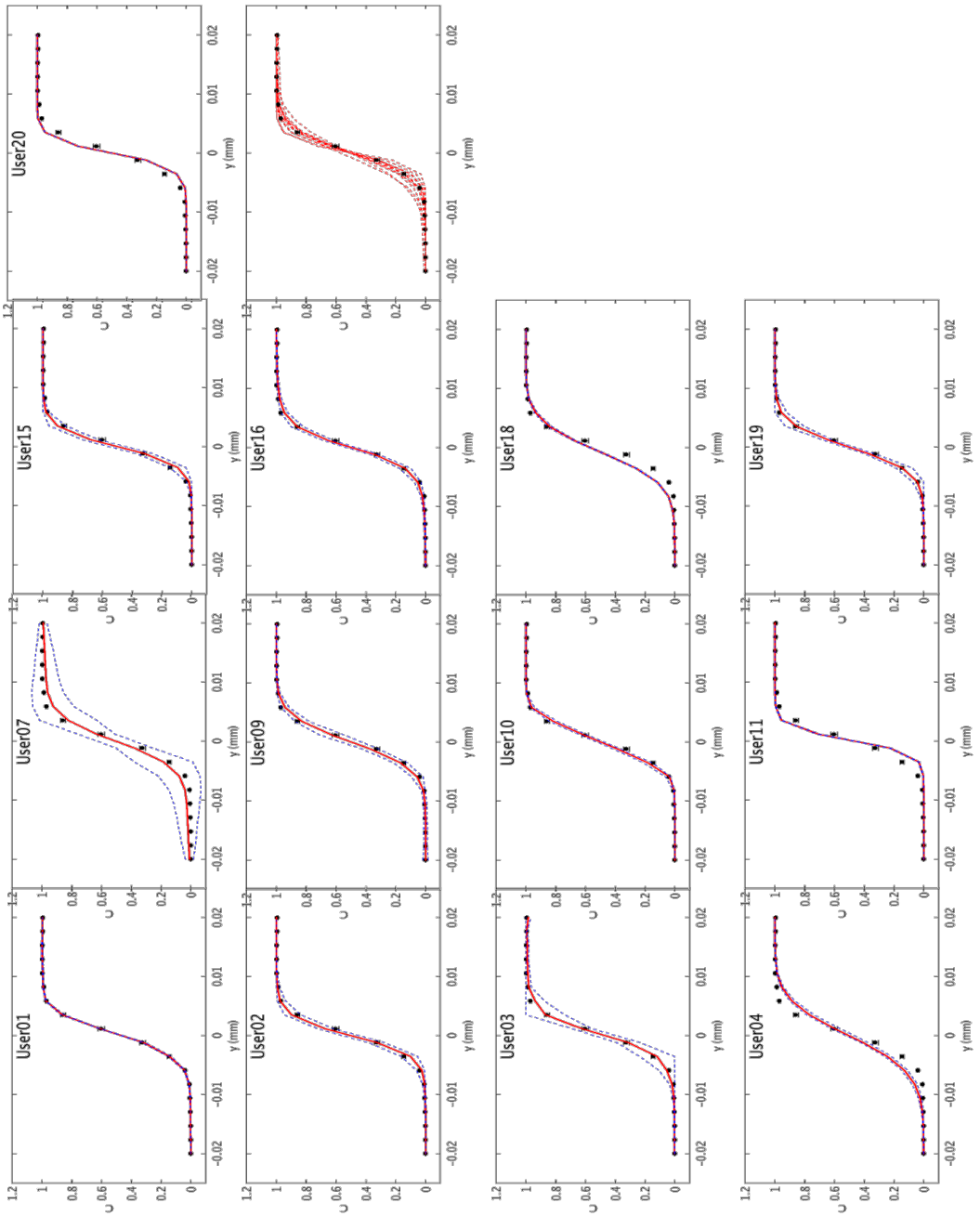

Figure 21. Concentration at x = 250mm

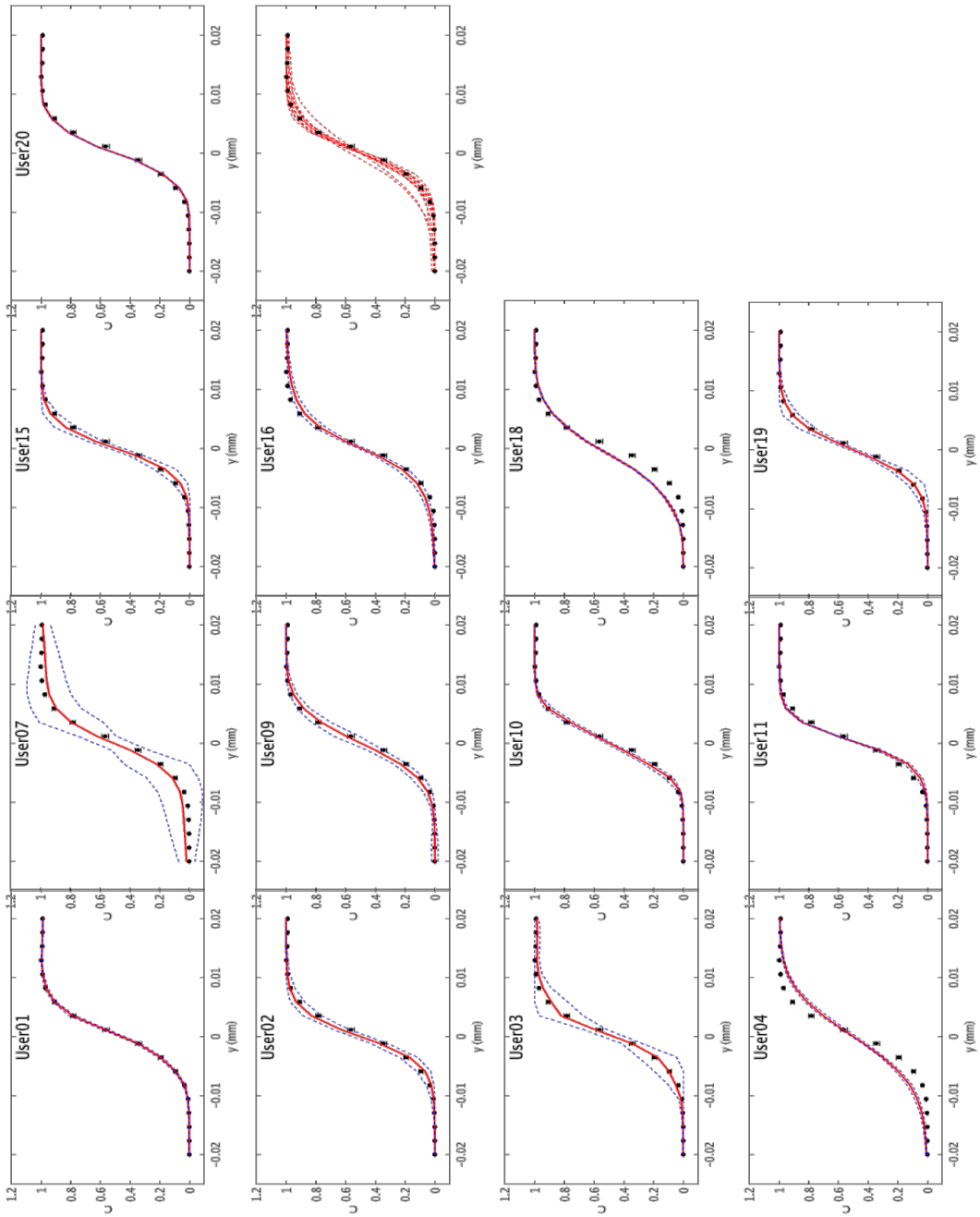

Figure 22. Concentration at x = 350mm

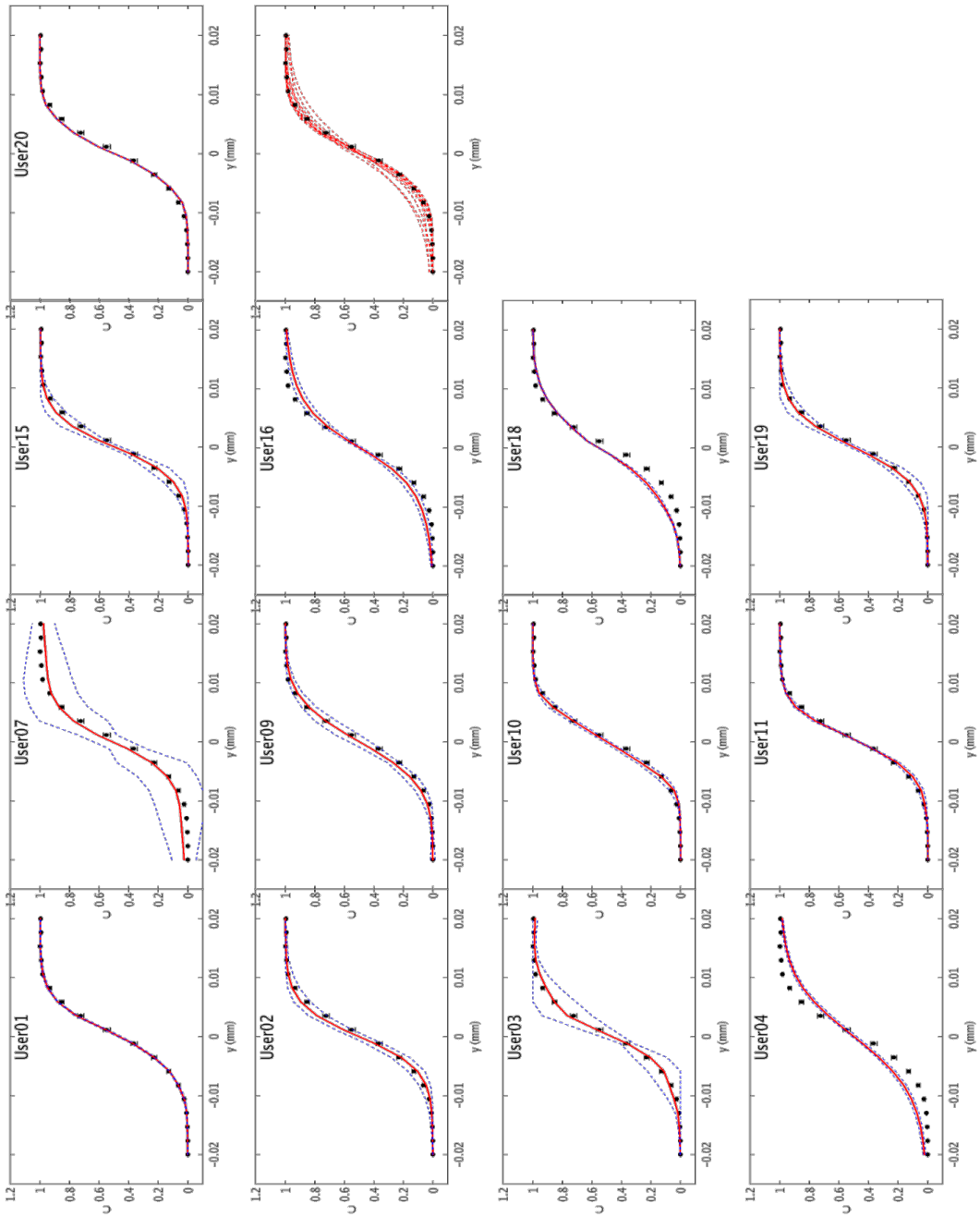

Figure 23. Concentration at 450

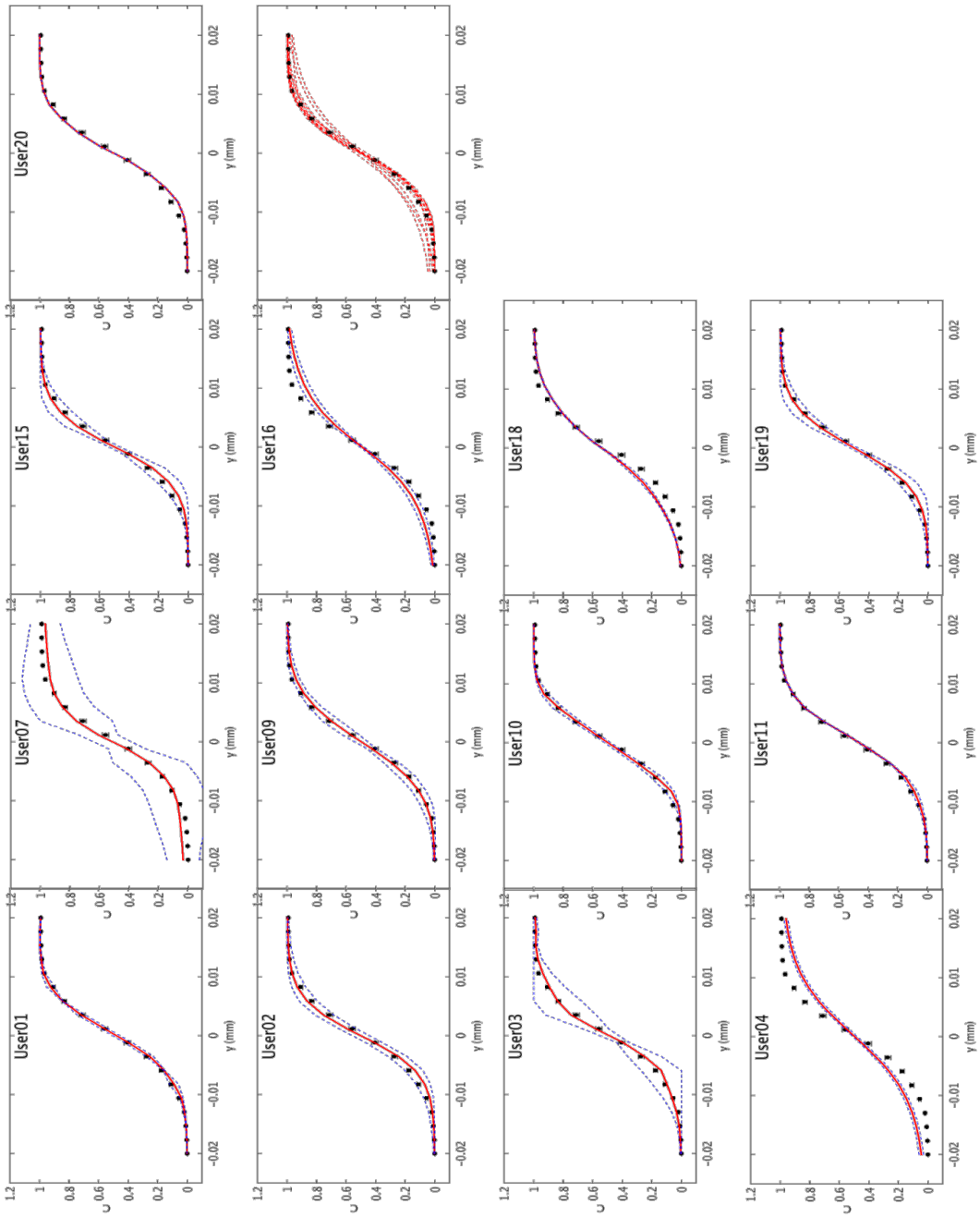

Figure 24. Mean velocity profiles at x = 50mm

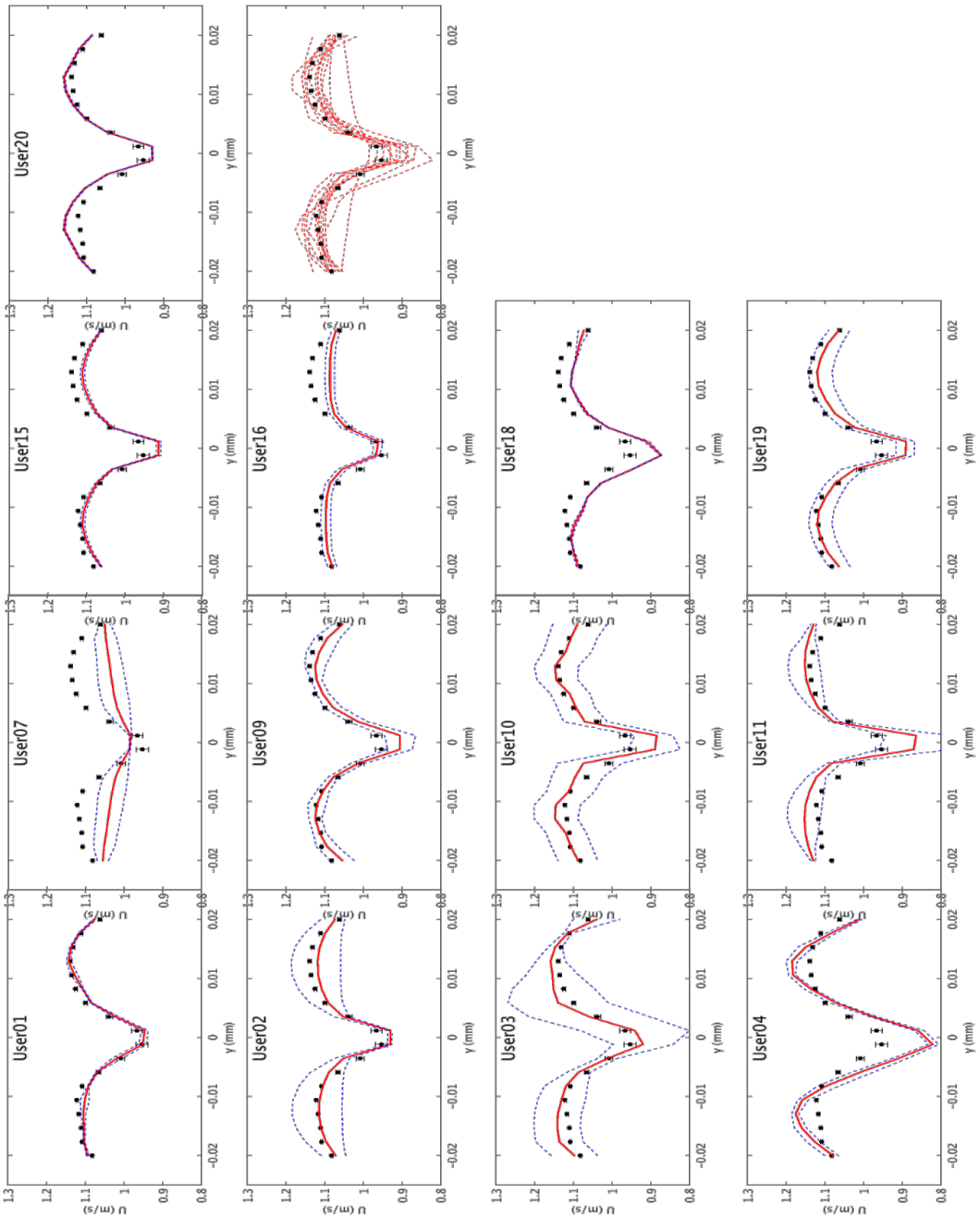

Figure 25. Mean velocities at x = 150mm

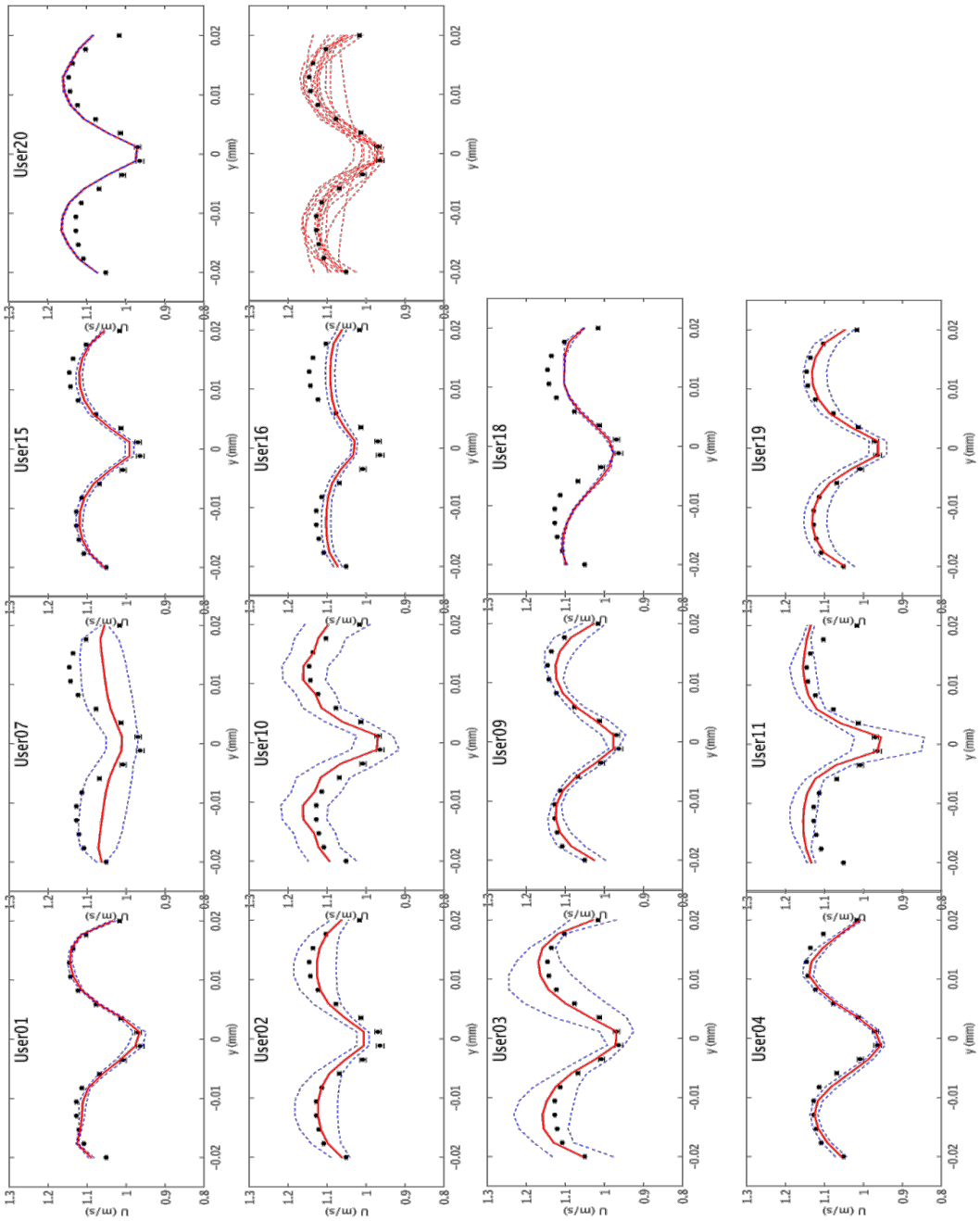

Figure 26. Mean velocity at x = 250mm

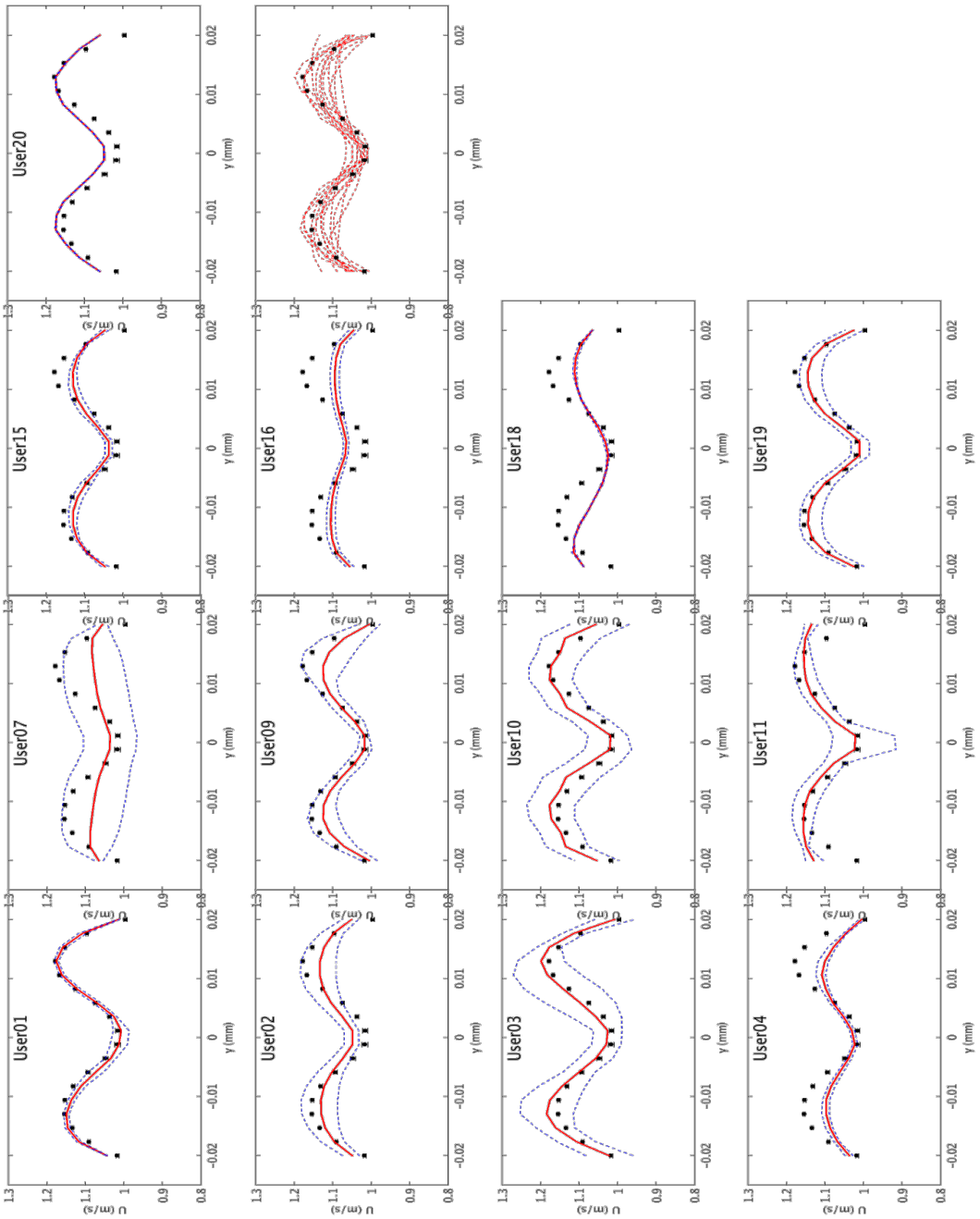

Figure 27. Mean velocity at x = 350mm

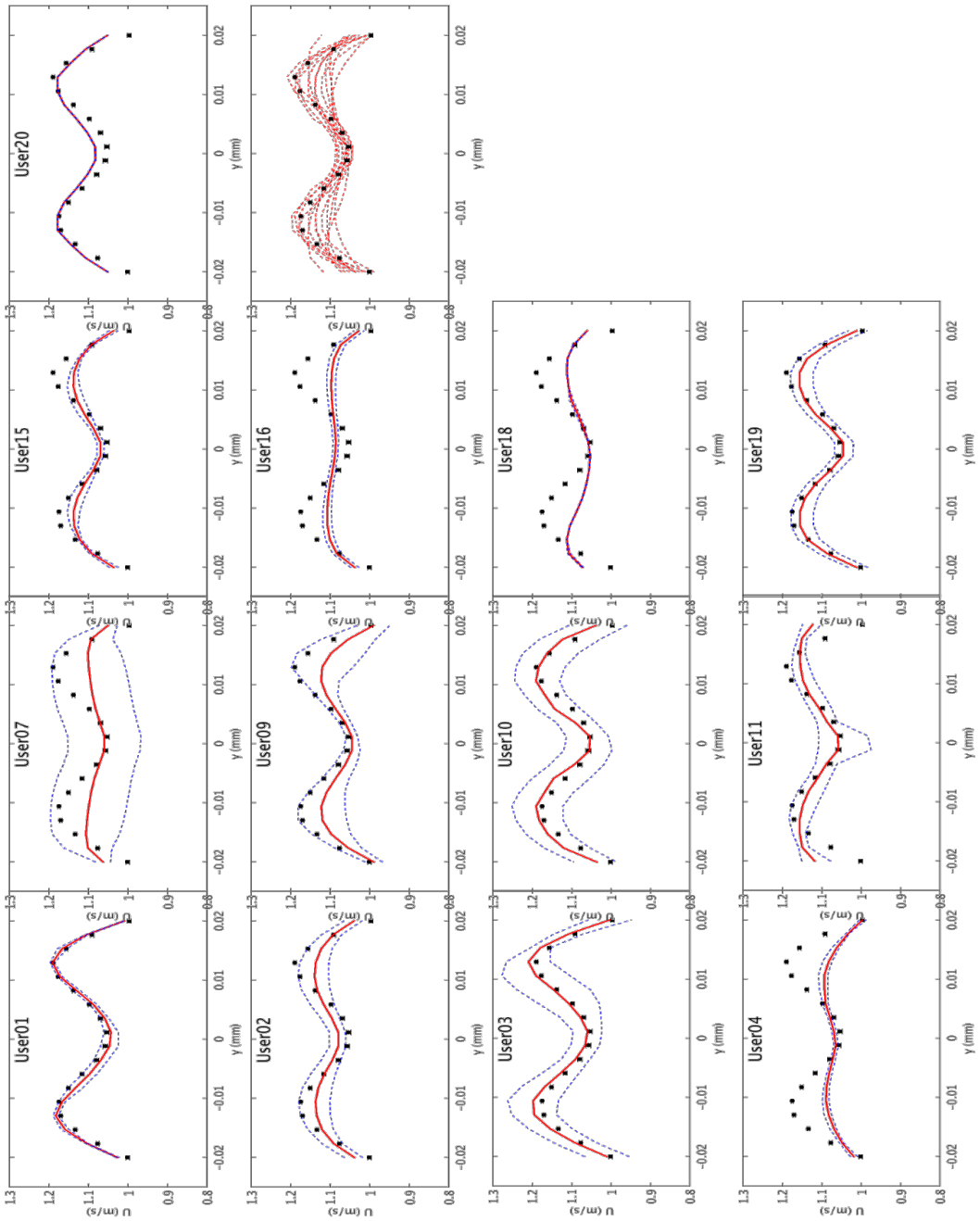

Figure 28. Mean velocity profile at x = 450

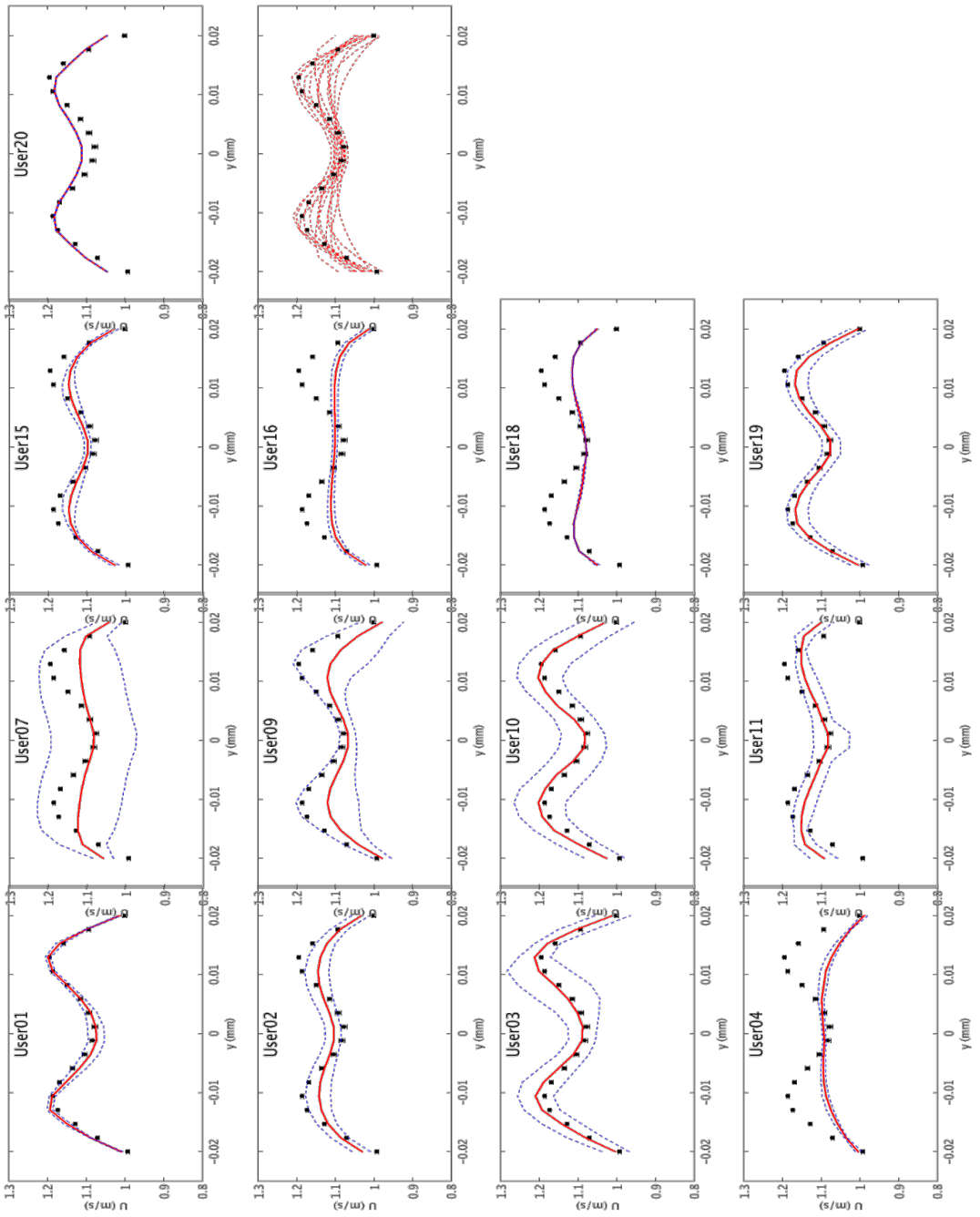

Figure 29. Turbulence kinetic energy at x = 50

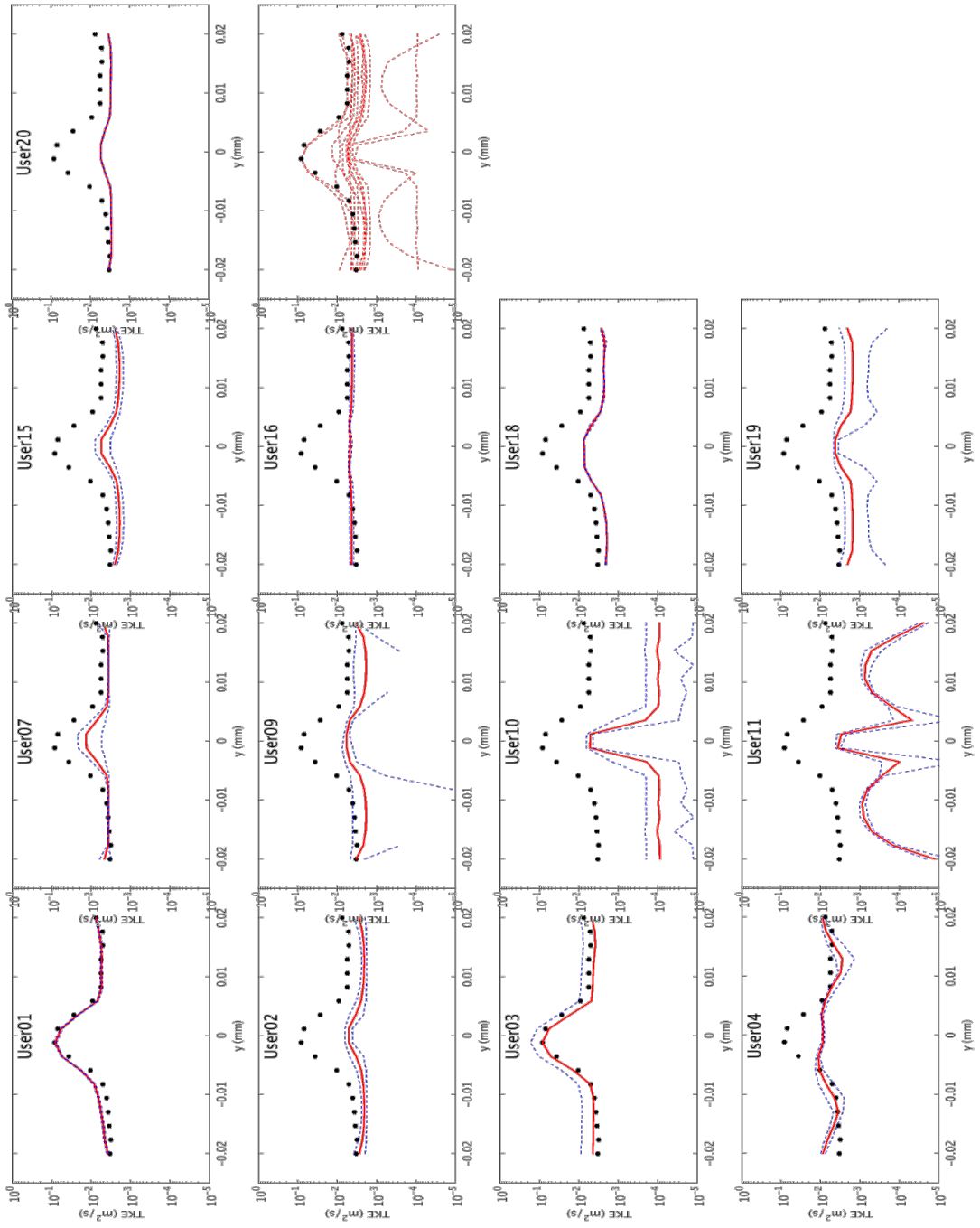

Figure 30. Kinetic energy at x = 150mm

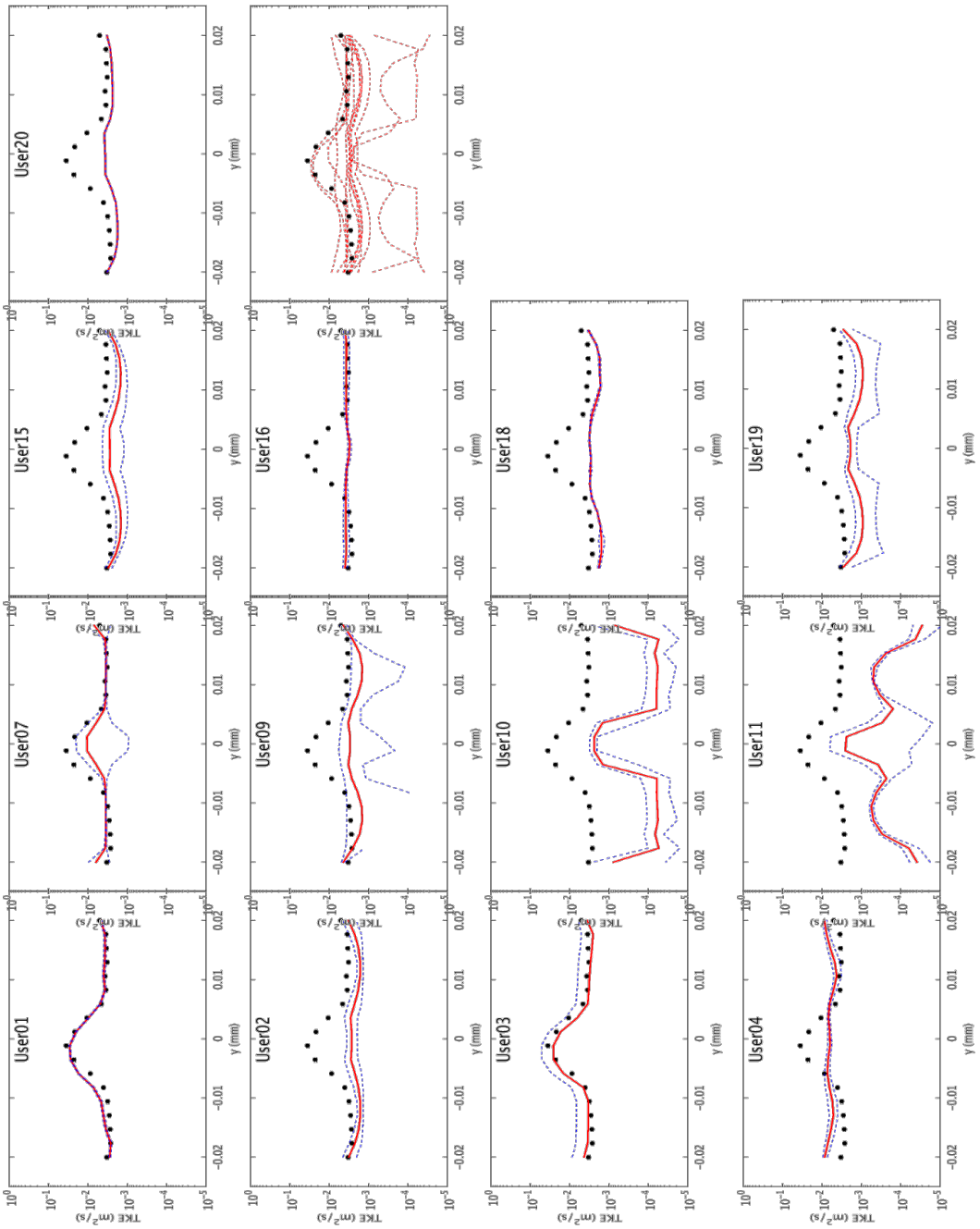

Figure 31. Kinetic energy at x = 250mm

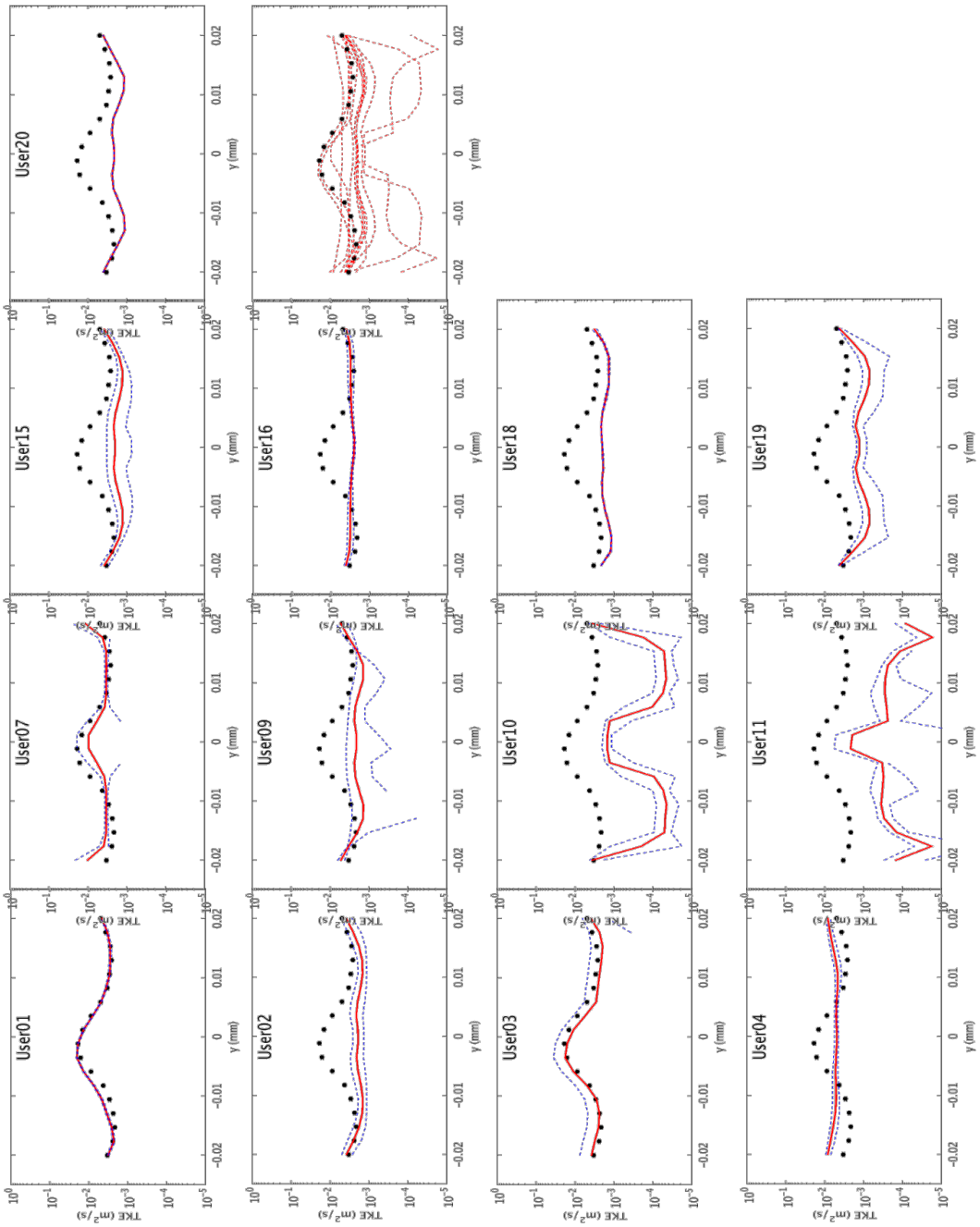

Figure 32. Kinetic energy at x = 350mm

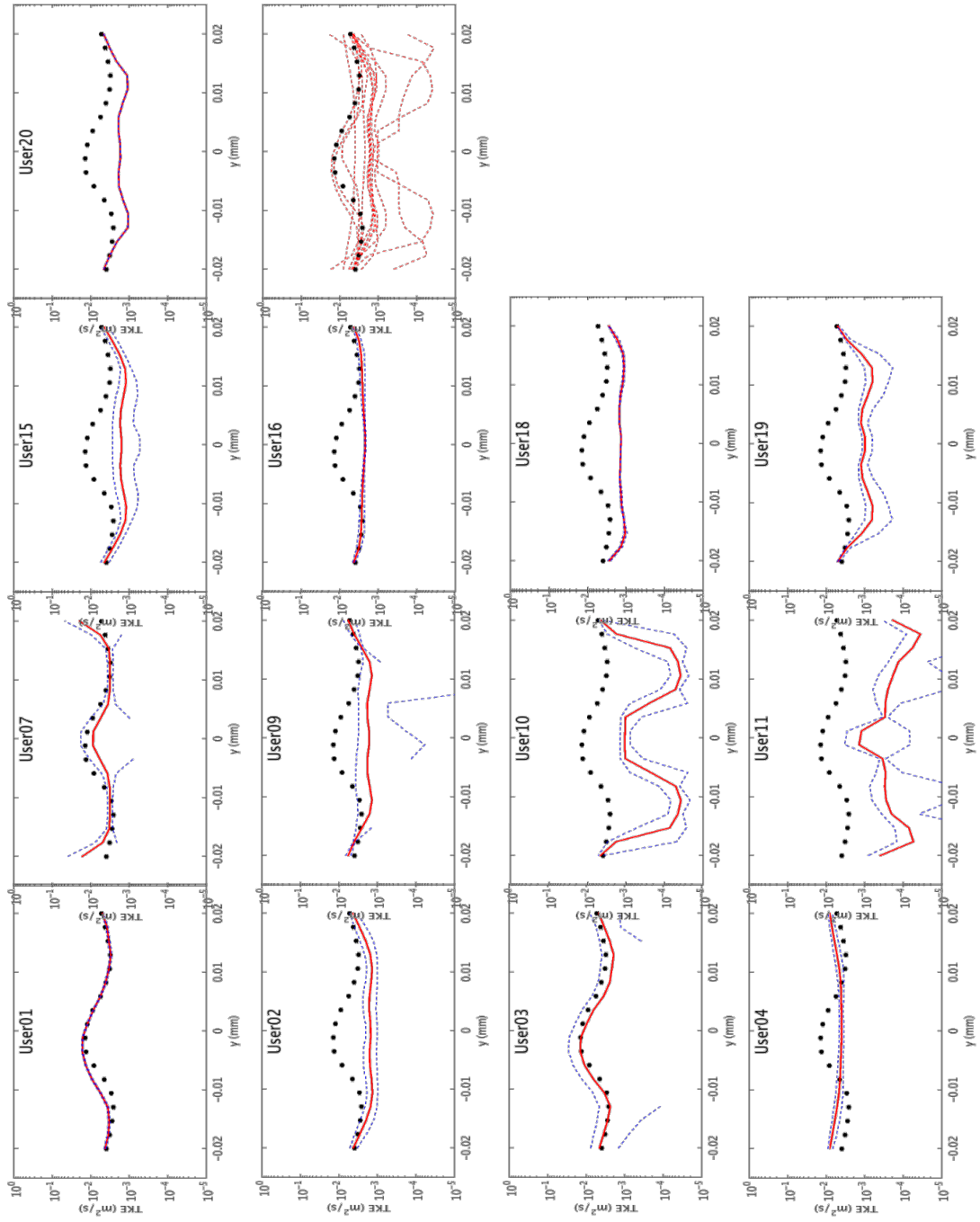

Figure 33. Mixing layer thickness

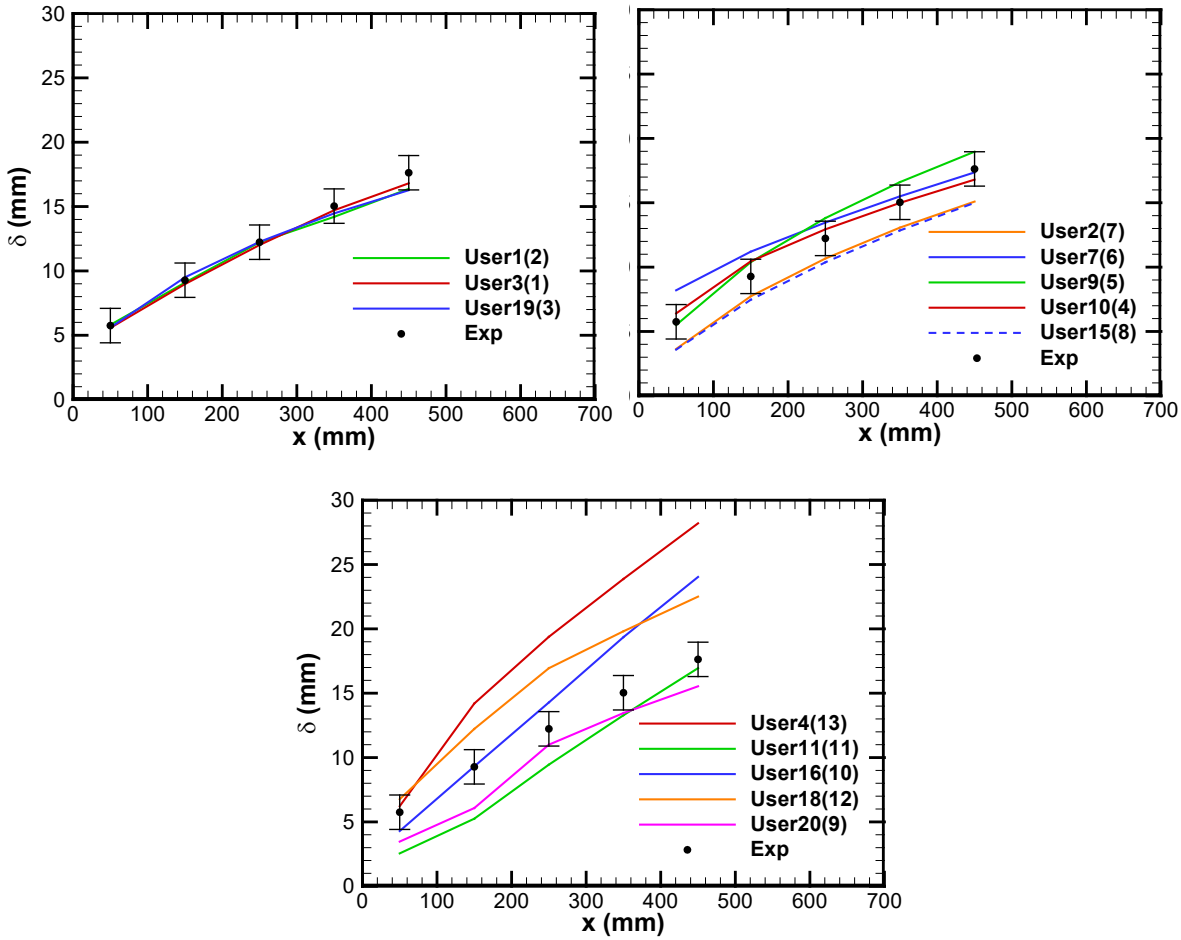

The results were separated in three groups (images): On the left image, we put the top three submissions; on the right image, we included the submissions that predicted the growth rate of thickness of the mixing layer, reasonably well. On the bottom figure are the submissions with the lowest scores. We have included the ranking of each participant in parenthesis.

14. CONCLUDING REMARKS AND COMMENTS

As the first benchmark exercise of its kind worldwide, participants and the organising team were faced with several problems along the way, not only from the experimental point of view but also on assessment of the uncertainty quantification in computational fluid dynamic (UQCFD) data, making it a very challenging benchmark. In the GEMIX facility, the measurement of the inlet boundary condition was not considered in the design of the experiment and, therefore, a substantial additional effort was made at PSI to provide all the required data. Despite the geometrical simplicity of the mixing section in the GEMIX facility, it was determined that even using advanced experimental techniques such as particle image velocimetry (PIV), laser Doppler anemometry (LDA), laser-induced fluorescence (LIF) and wire mesh sensor (WMS), it was still challenging to obtain UQCFD grade data, with the appropriate estimation of the experimental uncertainties. While the difficulties in determining experimental uncertainties were evident, without a comprehensive evaluation of them, the comparison between simulations and experiments becomes less reliable. For a conventional assessment of CFD simulations, uncertainty bands are not considered (only mean values), but in the present benchmark, the fidelity parameter depended strongly on the experimental and numerical uncertainties and, thus, unreliable experimental uncertainties lead to an unreliable fidelity and ranking scores.

Despite the difficult problems encountered during this benchmark, the overall results are truly encouraging. For many users, this was perhaps the first encounter with uncertainty quantification. However, the spread in the results was less than expected. For instance, the mean velocity profiles provided by the participants are within a narrow band (+/- 7%) from the experimental values. The concentration profiles were also reasonably well predicted by most of the participants, which is also the case for the thickness of the mixing layer. Another quite positive aspect of this benchmark was the proposal of a multivariate measure, namely the fidelity, that seems to be a good candidate for this type of analysis. Although there are still issues with, such as the assumption that the output probabilities of the simulations and experiments are Gaussian, its analytical form makes the evaluation of this measure very simple. Since the fidelity is basically a rescaled convolution between two probability density functions, the same concept could be used for any other distributions if they are known. However, the experimental uncertainties are seldom (or never) provided in the form of a probability distribution and, thus, a fidelity measure based on other distributions seems unnecessary.

After a careful analysis of the results and methods employed by the participants, it was concluded that a general UQCFD methodology for nuclear reactor safety should contain (whenever possible) four steps: uncertainty identification, calibration, extrapolation, and propagation (UNICEP). These four fundamental steps appear to contain all the ingredients for a robust UQCFD methodology. Even though CFD simulations can be very accurate when the main characteristics of the flow are well resolved by the mesh, for nuclear applications, that level of accuracy can seldom be achieved, and thus it is important to do the best with the computational resources at one's disposal. This is where the calibration and extrapolation steps play a fundamental role. Even if mesh cannot resolve the flow structure, the models (boundary conditions, mesh, turbulence model coefficients, etc.) can be calibrated on open tests to improve the CFD results and then perform the simulations at the reactor scale with extrapolated errors. However, this is still a challenging task, which requires high quality experimental data.

The mathematical bases of all the propagation methods used in this benchmark have several things in common and, thus, the propagation method itself seems to have a minor effect on the final quantification of uncertainties. For instance, if the same mathematical model with the same uncertainty sources is considered when using Monte Carlo or Polynomial Chaos to propagate the uncertainties, the output probability density function will be the same if the number of sampling point is large and the polynomial degree is high enough. It might be that Polynomial Chaos converges faster for a small number of input parameters, but for a large number of random inputs, Monte Carlo might take the lead on efficiency. Assuming that all propagation methods yield similar output probability density functions, the selection of the method should be based on what is needed from the output (level of accuracy, tolerance interval, etc.) and the computational resources at one's disposal. If the only interest is on propagating the second moment (variance) of an input probability density function, then deterministic sampling might be the best option. If the output probability distribution function (PDF) is important, the response surface from polynomial chaos as a meta-model and Monte Carlo could be used to obtain the output probability response. In addition, polynomial chaos allows one to perform a sensitivity analysis on the response surface and obtain the Sobol indices at no extra cost. If the uncertainties are not random, but categorical variables, then the propagation method must be selected accordingly and based on our interpretation of those categorical variables.

The main conclusions of this benchmark are summarised in the following.

14.1. Background

The main objectives of the current activity are the promotion, test and evaluation of various methodologies for UQCFD for nuclear reactor safety (NRS) applications. The assessment of the UQ methodologies was based on a blind test case from GEMIX with a density gradient, which is of practical interest to NRS. The product is a synthesis report presenting a detailed assessment of numerical predictions – including the uncertainty bands – with measured data. This report was presented at the CFD4NRS-6 Workshop held in Boston in 2016.

The numerical benchmark exercise is restricted to single-phase flow, with turbulent mixing in the presence of density gradients, which is a typical situation encountered in many reactor issues, where CFD is currently used. The exercise was based on the GEMIX experiment, which was carried out at the Paul Scherrer Institute in Switzerland. Participants submitted a calculation for the blind test case, where they presented their predictions for mean velocity, turbulence kinetic energy and concentration profiles. All the results included uncertainty bands. Since some methodologies for UQCFD use data from a validation step (for the definition of the model, its calibration and/or extrapolation of errors), three open tests cases were provided to the participants. It is noteworthy to mention that for the blind test, the density ratio between the two mixing streams was 1%, which is much lower than the values encountered, for example, in pressured thermal shocks.

In recent years, the use of CFD to address issues related to NRS has become very popular due to its higher (temporal and spatial) resolution compared to system codes. Reactor components where inherent three-dimensional phenomena taking place are particularly suited for these computational tools. For instance, the junction of the cold leg (CL) with the reactor pressure vessel (RPV) may be subjected to thermal stresses in pressurised thermal shock (PTS) scenarios. Accurately predicting three-dimensional (3D) flows with a sufficiently fine resolution cannot be handled by lump parameter codes nor by system codes, which makes CFD the only option.

Despite the enormous advances in conventional CFD (which involves single-phase turbulent flows) there are still questions about the level of accuracy of these simulations, which acquire a special relevance for licensing purposes. Although in CFD simulations, the number of parameters is much lower than that of system codes, the uncertainties associated with the mesh resolution, turbulence models,

boundary conditions and numerical schemes still renders the use of these advanced tools, to mere "demonstrations" in the context of NRS.

There are several methodologies available nowadays for UQCFD, and most of them involve sampling the parameter space. Compared to system code, each CFD realisation might be orders of magnitude more expensive, and thus efficient methods, which can obtain a good estimation of the uncertainties with few samples, are needed. Therefore, the GEMIX benchmark exercise presents a unique opportunity to investigate the advantages and disadvantages of each method, which can provide valuable information when selecting a UQCFD for NRS applications.

Methods to assess model uncertainties can be divided into two classes: propagation methods and extrapolation methods. Propagation of uncertainty methods requires several steps:

- identification of all uncertain input parameters;
- determination of the uncertainty of all uncertain input parameters;
- calculating a number of runs with each uncertain parameter being sampled according to the established PDF;
- from the runs, determination of the PDF of the figure(s) of merit (FoM) or of any code response.

Various propagation methods may differ by the use of random sampling or deterministic sampling, and by a possible use of meta-models (e.g. polynomial chaos expansion).

Extrapolation methods measure the accuracy of predictions on some experiments (here on open GEMIX tests) and extrapolate the accuracy to the blind problem.

There are also methods combining extrapolation for some sources of uncertainty (e.g. uncertainty due to physical model) with propagation of uncertainty for other sources of uncertainty (e.g. initial and boundary conditions). Extrapolation methods may also use some meta-models.

Extrapolation methods may need a lower number of runs than propagation methods. Propagation methods may reduce the number of runs by using deterministic sampling rather than random sampling. The use of meta-models may reduce the number of runs if the number of uncertain parameters is not too high.

14.2. Deliverables, expected results and users

- Mean velocity, turbulence kinetic energy, and concentration profiles were predicted and compared to experimental values (GEMIX).
- A synthesis was presented at the CFD4NRS-6 Workshop held in September 2016 and a detailed synthesis report on comparisons between numerical and measured data was produced.
- Users are all actors in safety analysis and in nuclear fuel design.

The exercise complements ongoing national programmes for the study of nuclear safety, and European initiatives, such as NURESAFE (7^{th} EU - FP).

14.3. Safety significance of the current results

The absence of UQCFD application to nuclear safety is a major limitation in the use of mature single-phase CFD tools in safety demonstrations for licensing.

Most single-phase issues – for which it was recognised that CFD may bring benefits – are mixing problems with or without density effects (buoyancy/stratification). The proposed activity addresses UQ for mixing problems in the presence of such effects, though with a limited density ratio and some incomplete experimental uncertainties.

14.4. Main conclusions

- Actors should be aware of the limitations of PIV when working with slightly inhomogeneous fluids. In this benchmark, we could not prove if the high values for the turbulence kinetic energy in the mixing layer, for a slightly inhomogeneous medium, is physical or not, but there is a suspicion of a measuring artefact. The turbulence kinetic energy was therefore not considered in the evaluation and ranking of code predictions and of uncertainty quantifications.
- A new measure (fidelity) has been proposed to assess UQCFD results. It is given by the convolution of the probability distributions of a predicted value and the corresponding experimental value, both assumed to be Gaussian.
- The scatter in the results is less than expected given the complexity of the problem. For example, velocity profiles from all participants fall within a narrow band (±7%), close to experimental values.
- Although the shape of concentration profiles was in general well predicted, a larger scatter was observed for the thickness of the mixing layer, indicating some problems when selecting the turbulent Schmidt number. Since the spreading of the mixing layer is primarily controlled by the turbulent Schmidt number, it seems logical to include this parameter as a source of uncertainty in future UQCFD analyses.
- Very good results could be obtained with both uncertainty propagation method and combined accuracy extrapolation and uncertainty propagation methods. The top 3 users needed 6, 15 and 836 simulations of the blind test showing that some methods may be used successfully with a low number of calculations at least in this rather simple case. Extrapolation methods may need a lower number of runs than propagation methods and propagation methods may reduce the number of runs by using meta-models, provided that the number of uncertain parameters is not too high. Such low numbers of runs may thus not be generalisable to other more complex problems, with more challenging geometries and boundary conditions. In addition, many preliminary calculations of open tests may have been necessary when using extrapolation methods, before the application to the blind test.
- The participants using a combined method (propagation and extrapolation) obtained the best agreement with the blind data. However, this should be analysed with care, because if the experimental results – on which the extrapolated errors are based – have a large bias, the numerical results will reflect that, as seen with the (most likely) unphysical value for the turbulence kinetic energy.
- Some methods give a very narrow band of uncertainties, while some others give a rather wide band of uncertainties. It may be linked to the input uncertainties taken into account, but possibly also to the characteristics of the methods themselves. The applicability of these methods, in the field of nuclear safety assessment, still raises questions to be further discussed and requires at least further testing and benchmarking.
- The most important step in the UQCFD analysis is the proper characterisation of the input uncertainties. When analysing the scattering in the rankings from users employing the same turbulence model (e.g. k-$\mathcal{E}$), it is clear that the turbulence model alone cannot be responsible for

such variability in the results. As explained in the text, if we focus only on propagating a PDF through a mathematical model, the output PDF should be independent of the propagation method. The propagation method and turbulence model therefore must have a marginal influence in the present exercise. Since the users' results were not used to perform a sensitivity analysis to determine the most influential variables, the last statement should be taken with precaution, as there is no definitive scientific proof to support it.

- In the present exercise, the results of some participants give confidence in the applicability of UQCFD, for more realistic scenarios relevant for NRS.
- As a result of small density effects in the benchmark and small differences between open and blind tests, the extrapolation from open tests made the benchmark somewhat easier. Future benchmarks should investigate situations with stronger density effects and with more different conditions between open and blind tests.

15. REFERENCES

[1] Henning Wolf, “Determination of water density: limitations at the uncertainty”, Accred. Qual. Assur, Vol. 13, pp. 587–591, 2008.

[2] A. Nagashima. "Viscosity of water substance—new international formulation and its background”, J. of Physical and Chemical Reference Data, Vol. 6, pp. 1133, 1977.

[3] Review of Uncertainty Methods for Computational Fluid Dynamics Application to Nuclear Reactor Thermal Hydraulics. Nuclear Safety NEA/CSNI/R(2016)4. www.oecd-nea.org/

[4] J. Fokken, “Velocity and Concentration Field Measurements of Unratified and Stably Stratified Confined Wake Flows Past a Plate”. Ph.D. thesis, ETHZ, 2015.

[5] P. Piwnicki, “Geometrical approach to light in inhomogeneous media”, Int. J. Mod. Phys. A Vol. 17, pp. 1543-1558, 2002.

[6] Celik et. al. “Index of resolution quality for large eddy simulations”. Journal of Fluids Engineering, Vol. 127, pp. 949–958, 2005.

APPENDIX A: FILTERED NAVIER-STOKES EQUATIONS

When filtering the Navier-Stokes equations, we can make use of the Reynolds decomposition, but the precaution that successive filtering operations, denoted by $\langle\cdot\rangle$, lead to time dependent smoother fields. Expressing the velocity in terms of the first filtered field $\bar{\mathbf{u}}$ and its fluctuating part $\mathbf{u}'$, we can express the mass conservation equation as:

$$\langle \nabla \cdot [\bar{\mathbf{u}} + \mathbf{u}'] \rangle = 0 \qquad (A.1)$$

or

$$\nabla \cdot \bar{\bar{\mathbf{u}}} + \nabla \cdot \langle \mathbf{u}' \rangle = 0 \qquad (A.2)$$

where $\bar{\bar{\mathbf{u}}} \equiv \langle \bar{\mathbf{u}} \rangle$. If we define a second fluctuating field in terms of a second filtering operation, we have $\bar{\mathbf{u}} = \bar{\bar{\mathbf{u}}} + \mathbf{u}''$. Thus, mass conservation expressed in terms of the first filtered field is written as:

$$\nabla \cdot \bar{\mathbf{u}} = -\nabla \cdot \langle \mathbf{u}' - \mathbf{u}'' \rangle \qquad (A.3)$$

Similarly, we can rewrite the momentum equation in terms of the first filtered velocity field as:

$$\frac{\partial \bar{\mathbf{u}}}{\partial t} + \nabla \cdot (\bar{\mathbf{u}}\bar{\mathbf{u}}) + \nabla \cdot \langle \mathbf{u}'\mathbf{u}' \rangle = -\frac{1}{\rho}\nabla \bar{\mathrm{P}} + \nabla \cdot (\nu \nabla \bar{\mathbf{u}} + \nu \nabla \bar{\mathbf{u}}^T) + \frac{1}{\rho}\bar{\mathbf{f}} - \boldsymbol{f}_{correction} \qquad (A.3)$$

with the correcting force defined by:

$$\boldsymbol{f}_{correction} = \frac{\partial \langle \mathbf{u}' - \mathbf{u}'' \rangle}{\partial t} + 2\nabla \cdot \langle \bar{\mathbf{u}}\mathbf{u}' \rangle + \nabla \cdot (\langle \bar{\mathbf{u}}\bar{\mathbf{u}} \rangle - \bar{\mathbf{u}}\bar{\mathbf{u}}) \qquad (A.4)$$

When the filtering operation corresponds to the time average, then the correcting force and the time derivatives are null. Most CFD researchers neglect the contribution from the correcting force and focus only on the Reynolds stresses. This is the first source of uncertainty in subgrid (space/time) scale models. The second, and arguably the most important source of uncertainty, arises from the approximation of the Reynolds stresses.

APPENDIX B: SHORT DESCRIPTION OF THE UQ METHOD

(non-edited documents prepared by each participant)

User-02

1. Selection of the uncertainty sources and method for mapping the experimental inlet boundary conditions

In order to deal with some uncertainties on flow conditions at the inlet sections, the velocity profile was varied between a uniform and a fully developed profile according to the relationship:

$$u(y,z,\alpha) = \left(\frac{\alpha}{u_d(y,z)} + \frac{1-\alpha}{u_u}\right)^{-1} \quad (1)$$

where $u_d(y,z)$ corresponds to the fully developed profile and u_u denotes the uniform profile.

The fully developed profile is obtained from a precursor calculation in a small portion of the upper leg using the same mesh and periodic boundary conditions in the stream-wise direction, a mean pressure gradient is added that corresponds to the prescribed mass flow rate. In this way, the velocity profile $u(y,z,\alpha)$ leads also the same prescribed mass flow rate. Then, another precursor calculation is performed, again in a small portion of the upper leg and using the same mesh but by imposing the computed profile $u(y,z,\alpha)$ at the inlet and by specifying the turbulent kinetic energy k as:

$$k = \frac{3}{2}\,(i\,u(y,z,\alpha))^2 \quad (2)$$

where i denotes the turbulent intensity.

The final profiles for both the inlet velocity and the turbulent quantities (namely here for the k-ω SST model, the inlet turbulent kinetic energy k and the specific dissipation ω) are then derived from this second precursor calculation at a stream-wise distance x_c from the inlet plane. Several precursor calculations have been performed to select a value for (i, x_c) at $\alpha = 0.5$ that best fit the experimental profiles for the velocity and the turbulent kinetic energy. In practice, the velocity profile appears almost identically along the streamwise direction whereas the best fit for the turbulent kinetic energy is found at $x_c = 0.015$ m, together with an inlet turbulent intensity $i = 0.042$. Keeping $(i, x_c) = (0.042, 0.015)$ and varying α, it should be pointed out that the numerical results at x_c embrace the experimental profiles well.

Then, the uncertainty source α was varied in each leg, possibly with different values at the upper and the lower leg, between 0.1 and 0.9 keeping fixed $(i, x_c) = (0.042, 0.015)$. In addition, the turbulent Schmidt number S_c was also varied between 0.5 and 1.3. A uniform probability density distribution was assigned to the random variables α and S_c.

2. The c-ANOVA-POD-Kriging method for uncertainty quantification

The c-APK method [1] relies on the merging of the c-ANOVA method for sensitivity analysis [2] and the POD/Kriging method for meta-modelling [3]. This approach aims to improve the domain exploration of Kriging-based methods known as the curse of dimensionality of the existing UQ strategies when dealing

with highly expensive simulations to extend them from low to medium dimension spaces. This is done by using the anchored-ANOVA decomposition to reduce the N-dimensional uncertain space to the sum of usually mono-dimensional and bi-dimensional UQ parameter spaces plus a residual term. The Kriging-based meta-modelling is applied to each sub-space and the full response surface can then be reconstructed just by summing all the sub-meta-models.

2.1 The c-ANOVA decomposition

We first recall the ANOVA decomposition equation:

$$X(\omega) = X_0 + \sum_{1\le j_1\le N} X_{j_1}(\omega_{j_1}) + \sum_{1\le j_1\le j_2\le N} X_{j_1,j_2}(\omega_{j_1},\omega_{j_2}) + \cdots + X_{1,2,\dots,N}(\omega_1,\omega_2,\dots,\omega_N) \quad (3)$$

where $X(\omega)$ is a generic output of the UQ method (when the quantity of interest is a field $X(\Omega, D)$, the decomposition apply to each grid point in the domain of interest D), which is function of a set of N input parameters $\omega = (\omega_1, \omega_2, \dots, \omega_N)$ and X_0, $X_{j_1}(\omega_{j_1})$,… , $X_{1,2,\dots,N}(\omega_1, \omega_2, \dots, \omega_N)$ are the ANOVA decomposition terms, where X_0 is a constant computed as follows:

$$X_0 = \int_\Omega X(\omega)\, d\mu(\omega) \quad (4)$$

i.e. it is the ensemble average of the dependent variable X against the Lebesgue measure $\mu(\omega)$ of the random space $\Omega = [0,1]^N$. Considering the following properties of the ANOVA decomposition:

$$\int X_{j_1,\dots,j_s}\, d\mu(\omega_{j_k}) = 0 \;\; 1 \le k \le \mathrm{s} \quad (5)$$

and

$$\int_\Omega X_{j_1,\dots,j_s} X_{k_1,\dots,k_m}\, d\mu(\omega) = 0 \quad \forall\, (j_1,\dots,j_s) \ne (k_1,\dots,k_m) \quad (6)$$

the higher order terms can be obtained through the following recurrence formula:

$$X_{j_1,j_2,\dots,j_s}(\omega_{j_1},\omega_{j_2},\dots,\omega_{j_s}) = \int \dots \int X(\omega)\, d\mu(\omega_{j_{s+1}}) \dots d\mu(\omega_{j_N}) - \sum_{j_m,\dots,j_n} X_{j_m,\dots,j_n}(\omega_{j_m},\dots,\omega_{j_n}) \quad (7)$$

with:

$$j_m,\dots,j_n \subset j_1,\dots,j_s \quad (8)$$

The dimensionality of each term is denoted ν so that $\nu = 1$ is related to the mono-dimensional terms, i.e. single effects components. We truncate the ANOVA decomposition to $\nu = 2$, discarding from the beginning any higher order interaction between input parameters than simple effects and two-by-two couplings.

At this step, a generic output variable $X(\omega)$ can be approximated as a fixed order $\nu = 2$ ANOVA decomposition:

$$X(\omega) = X_0 + \sum_{1\le j_1\le N} X_{j_1}(\omega_{j_1}) + \sum_{1\le j_1\le j_2\le N} X_{j_1,j_2}(\omega_{j_1},\omega_{j_2}) + \epsilon_T \quad (9)$$

Where ϵ_T is the ANOVA truncation error.

The computation of each ANOVA term requires the evaluation of a number of high-dimensional integrals. A possible solution is to switch to the anchored-ANOVA in order to compute the terms of the decomposition [2,4].The main concept of the anchored-ANOVA decomposition is to adopt a Dirac measure instead of the standard Lebesgue one, so that:

$$d\mu(\omega) = \delta(\omega - c)d\omega \quad (10)$$

Where $d\mu(\omega)$ is the Lebesgue measure, $\delta(x)$is the Dirac function and $c = (c_1, c_2, \dots, c_N)$ is the anchor point. Recalling that a good choice for the anchor point $c = (c_1, c_2, \dots, c_N)$ is the centroid (centre of gravity weighted with the input parameter distributions) of the uncertain space [5], one can write:

$$X_0 = X(c_1, c_2, \dots, c_N) \quad (11)$$

$$X_{j_1}(\omega_{j_1}) = X(c_1, c_2, \dots, \omega_{j_1}, \dots, c_N) - X_0 \quad (12)$$

$$X_{j_1,j_2}(\omega_{j_1}, \omega_{j_2}) = X(c_1, c_2, \dots, \omega_{j_1}, \dots, \omega_{j_2} \dots, c_N) - X_{j_1}(\omega_{j_1}) - X_{j_2}(\omega_{j_2}) - X_0 \quad (13)$$

Convergence in the dimensionality ν is assured by monitoring the c-ANOVA dimension truncation error, which can be seen as a $X_T = X_{1,2,\dots,N}(\omega_1, \omega_2, \dots, \omega_N)$ term where all terms of order higher than $\nu = 2$ are merged. The method will be efficient if ϵ_T is low and this must be evaluated from the beginning and monitored all along the UQ analysis.

2.2 The POD/Kriging sub-meta-models

In order to build the full response surface, each term of the anchored-ANOVA decomposition is interpolated, which can be done applying Ordinary Kriging directly if $X(\omega)$ is a scalar or using a POD/Kriging-based approach, as illustrated in Bracconier et al. [3], in the more general case where $X(\omega)$ is a long vector containing all the investigated information for a single simulation. As in this benchmark we performed RANS simulations, the POD step is skipped.

In the Ordinary Kriging, a covariance parameter of $\theta = 0.1$ is used in the efficient polynomial cubic splines covariance function:

$$Cov(x) = \begin{cases} 1 - 6(x\theta)^2 + 6(x\theta)^3, x < \frac{1}{2\theta} \\ 2(1 - x\theta)^3, \ \frac{1}{2\theta} \leq x < \frac{1}{\theta} \\ 0, \ x \geq \frac{1}{\theta} \end{cases} \quad (14)$$

An adaptive strategy to feed the sub-meta-model approximation is adopted in order to minimise the number of function calls by optimising their repartition. As for the POD/Kriging-based method in Bracconier et al. [3], the leave-one-out method is used to cross-validate the response surface.

2.3 Main statistics estimators and sensitivity analysis from the c-APK surrogate model

In the c-APK method the output statistics are calculated from the full response surface by quasi-Monte Carlo (quasi-MC) integration. Sobol sequences are used to generate the quasi Monte Carlo samples.

The main statistics are obtained through quasi Monte Carlo (Sobol sequences) estimators [6]. The mean estimate $\mu(X)$ is calculated as:

$$\mu(X) = \frac{1}{q_{MC}} \sum_{i=1}^{q_{MC}} X_i \quad (15)$$

where q_{MC} is the number of quasi Monte Carlo samples X_i of the c-APK surrogate model of $X(\Omega)$.

The variance $\sigma^2(X)$ is calculated as:

$$\sigma^2(X) = \frac{1}{q_{MC}} \sum_{i=1}^{q_{MC}} (X_i - \mu(X))^2 \quad (16)$$

First order Sobol' variance-based sensitivity indexes [7] are directly obtained from the c-ANOVA decomposition (note that Dirac Sobol' variance-based indexes are not the same as the Lebesgue one as the covariance between c-ANOVA terms is not null [8]). NaN values in the provided files correspond to zero-variance values of the quantity of interest at grid points.

It should be noticed that the additional files including the results of the sensitivity analysis have been written for each output variable, namely the concentration (files User02-SA-C_*.dat), the velocity (files User02-SA-U_*.dat) and the turbulent kinetic energy (files User02-SA-K_*.dat).

REFERENCES

[1] L. Margheri and P. Sagaut, A hybrid anchored-ANOVA - POD/Kriging method for Uncertainty Quantification in unsteady high-fidelity CFD simulations, *under review for the Journal of Computational Physics*, 2016

[2] X. Yang and M. Choi and G. Lin and G.E. Karniadakis, Adaptive ANOVA decomposition of stochastic incompressible and compressible flows, *Journal of Computational Physics*, 231:1587-1614, 2012

[3] T. Bracconier and M. Ferrier and J.C. Jouhaud and M. Montagnac and P. Sagaut, Towards an adaptive POD/SVD surrogate model for aeronautic design, *Computer and Fluids*, 40:195-209, 2011

[4] X. Ma and N. Zabaras, An adaptive high-dimensional stochastic model representation technique for the solution of stochastic partial differential equations, *Journal of Computational Physics*, 229:3884-3915, 2010

[5] Z. Gao and J.S Hesthaven, On ANOVA expansions and strategies for choosing the anchor point, *Applied Mathematics and Computation*, 217:3274-3285, 2010

[6] A. Saltelli and P. Annoni and I. Azzini and F. Campolongo and M. Ratto and S. Tarantola, Variance based sensitivity analysis of model output. Design and estimator for the total sensitivity index, *Computer Physics Communications*, 181(2):259-270, 2010

[7] I. Sobol, Sensitivity estimates for non-linear mathematical models, *Mathematical Modeling and Computational Experiment*, 1(4):407-414, 1993

[8] K. Tang and P. M. Congedo and R. Abgrall, Sensitivity analysis using anchored ANOVA expansion and high-order moments computation, *International Journal for Numerical Methods in Engineering*, 2015

APPENDIX C

User-03

1. Construction of uncertainty band

1.1 EDF WAVE method

The purpose of the WAVE method [1] is to produce, for a certain quantity of interest S (S being a scalar output of the CFD calculation performed at reactor scale), a value S5/95 that is smaller (or greater, depending on what is penalising) than 95% of the possible values of S, with a confidence level of 95%. The confidence level comes from the finite number of experimental test cases at one's disposal. The method is based on a comparison between experimental results and calculation results at test case scale. It also considers a propagation of the uncertainty of input data parameters.

S is the scalar quantity of interest (example: velocity, turbulent kinetic energy, etc.). In the following, we assume that S is made non-dimensional in an appropriate way, so that values at reactor scale and at test case scale can be compared directly.

We define:

- St is the "true" (unknown) value of S;
- SCFD is the value of S calculated by the CFD model;
- "r" represents the true (unknown) conditions at reactor scale;
- "R" represents the best-estimate value of "r".

Thus, St(r) is the "true" (unknown) value of S at reactor scale; SCFD(R) is the result of the CFD calculation at reactor scale; SCFD(r) is the result a CFD calculation would give with the "true" reactor scale conditions (if these conditions were known).

Similarly, "e" represents the "true" (unknown) conditions at test case scale; "E" represents our estimation of "e". Since several experimental tests are used in the method, index "k" ($k \in [1, K]$) is used to differentiate these K tests.

We also introduce the following notations:

- mk is the "true" value of S in experimental test number k, i.e.: mk = St(ek);
- Mk is the measured value of S in experimental test number k. When measuring mk, the answer we get is Mk, because instrumentation has a limited accuracy.

The CFD result at reactor scale is considered unique. Nonetheless, different numerical parameters can vary between validation and reactor calculation (mesh, time step, numerical scheme …). These different numerical configurations induce variability in the CFD results. For practical reasons, we suggest to treat this variability at test case scale. A new notation is introduced using index "CFD" with the number "1" corresponding to test case scale simulation with numerical parameters set number "1", number "2" corresponding to another set of numerical parameters. Finally, we write that the "true" value of S can be split as follows:Figure 1

Figure 1: global equation with different uncertainties

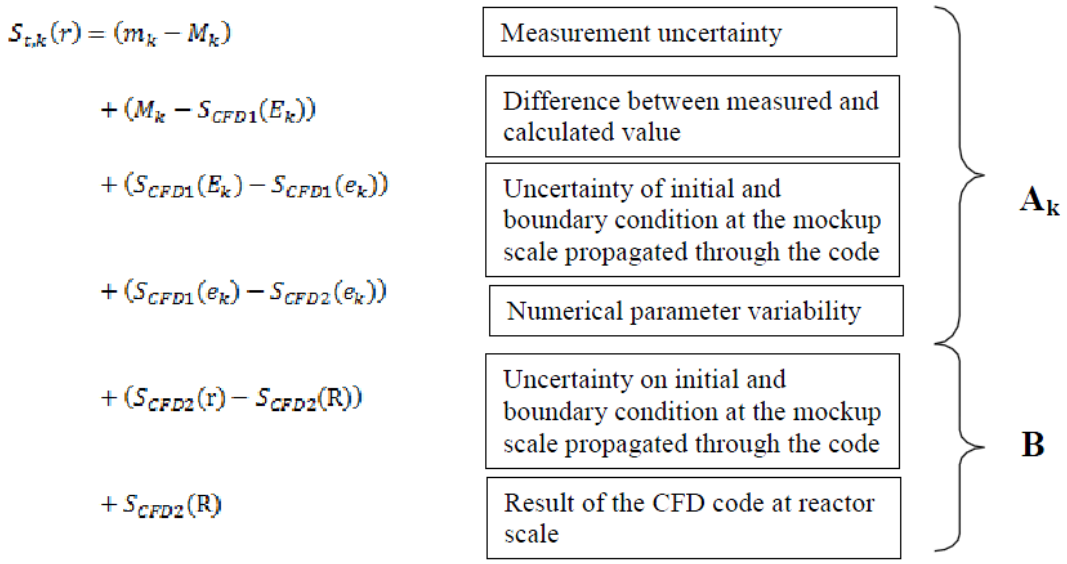

Each term is described below:

- SCFD2(R) is simply a numerical (non-random) value, the result of the CFD calculation at reactor scale for the scalar quantity S;
- The correction term (SCFD2(r) – SCFD2(R)) is treated as random; the uncertainty of reactor scale conditions is propagated through the model;
- The term (mk – Mk) represents the measurement uncertainty;
- The term (Mk – SCFD1(Ek)) is just the (non-random) difference between measured and calculated value of scalar S for test number k;
- The correction term (SCFD1(Ek) – SCFD1(ek)) is treated as random;
- The term (SCFD1(ek) – SCFD2(ek)) is treated as a random variable and takes into account the numerical parameters variability.

Since St is the sum of all terms above, by assumption it follows a normal law:

- Centred on Ek = SCFD2(R) + (Mk –SCFD1(Ek)), that is the result of the reactor scale CFD calculation, corrected by calculation-measurement difference (as seen on test number k).
- With a standard deviation σk that results from quadratic composition of the standard deviations of the Gaussian distributions corresponding respectively to: measurement uncertainty, propagated uncertainty of reactor scale conditions, propagated uncertainty of test case scale conditions and the numerical parameters variability. This expression is written:

$$\sigma_{k=}\sqrt{\sigma(m_k-M_k)^2+\sigma(S_{CFD1}(E_k)-S_{CFD1}(e_k))^2+\sigma(S_{CFD2}(r)-S_{CFD2}(R))^2+\sigma(S_{CFD1}(e_k)-S_{CFD2}(e_k))^2}$$

The S_k^5 value is the 5th percentile of the distribution of St calculated in this way. It is smaller (or greater, depending what is penalising) than 95% of the (estimated) possible values of St. This S5k value is relative to one particular test k.

$$\boldsymbol{S_k^5 = E_k - 1.645 * \sigma_k} \quad (1)$$

The distribution of the S_k^5 is considered for a series of K tests. We thus define S5/95 (with 95% confidence) as being the average of the S_k^5 corrected by a factor S^5 which multiply the standard deviation σ5 of the distribution of the K S_k^5. This factor – the Student factor 5/95 – is a function of the total number K of tests k (it is a function of a target probability, confidence level and degrees of freedom – the values are presented in the Figure 4. Student's distribution table Uncertainty Quantification and Sensitivity Analysis in CFD based on Distinction between Categorical and Continuous Variables Figure 4

$$\boldsymbol{S^{k/95} = S^5 \pm Student(5.95; n) * \sigma^5} \quad (2)$$

where « n » represents the number of experimental tests,

$$\boldsymbol{S^5 = \frac{\sum_1^n S_k^5}{n}} \text{ and } \boldsymbol{\sigma^5 = \sqrt{\frac{\sum_1^n (S_k^5 - S^5)^2}{(n-1)}}} \quad (3)$$

1.2 Method used for the benchmark

Since we want to determine an uncertainty band in this benchmark and not a penalising value, we will calculate the 2.5th and the 97.5th percentile of the experimental values, which means:

$$S_k^{2.5} = E_k - 1.645 * \sigma_k \quad (4)$$

And

$$S_k^{97.5} = E_k + 1.645 * \sigma_k \quad (5)$$

Then, the confidence level of 95% will be calculated for both percentiles previously calculated:

$$S^{k/95} = S^5 \pm Student(5.95; n) * \sigma^5 \quad (6)$$

Thus, we obtain two different interval of confidence (see the green dotted lines in Figure 2). Finally, in order to give the upper and the lower bound of the reactor case, it was decided to take the lower interval of the 2.5th percentile and the upper interval of the 97.5th percentile (see the orange line in Figure 2).

Figure 2. How our intervals are calculated

Type the subtitle here. If you do not need a subtitle, please delete this line.

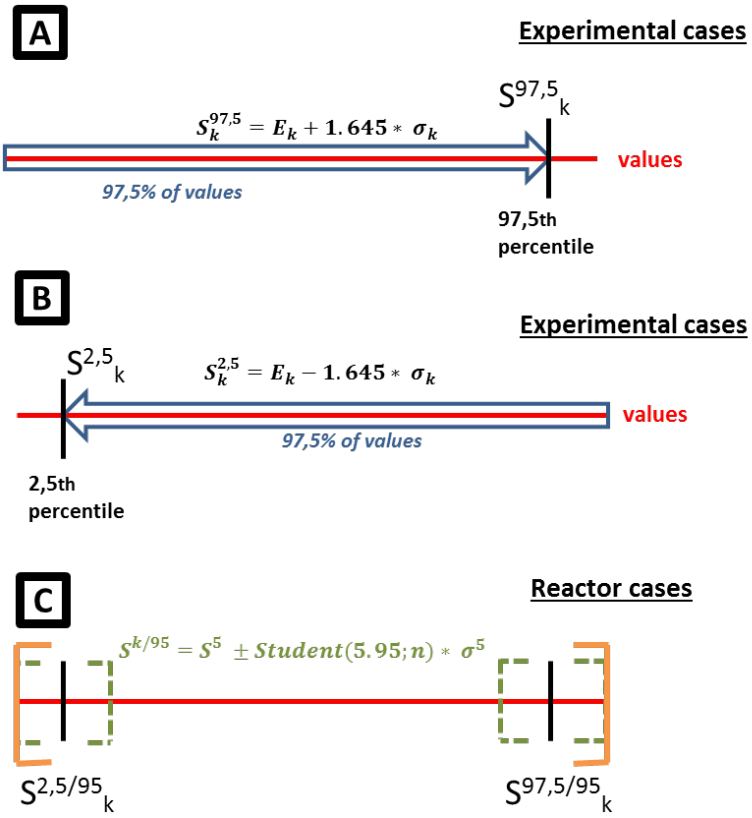

2. Selection of uncertainty sources

a. Numerical and modelling parameters

Since the k-epsilon (*k-ℰ*) model is chosen for this benchmark, the constants of this model will be varied. That means: Cμ, σk, σε, cε1 and cε2 cε2. The theoretical possible values of cε1 and cε2 were found in literature. The variations of Cμ, σk and σε were taken according to the order of variations of those constants in the *k-ℰ* RNG model. All these data are summarised in the following Table 1.

Table .1. Numerical/modelling parameters uncertainties

	Value 1	Value 2	Value 3	Sources
Cμ	0.082	0.090	0.096	Speziale, et al., 1991.
σk	0.92	1.00	1.08	Yakhot, et al., 1986.
σε	1.22	1.30	1.38	Yakhot, et al., 1986.
cε1	1.36	1.44	1.52	Launder, et al., 1970.
cε2	1.84	1.92	2.00	Launder, et al., 1970.

Just three different values were taken for the constants because of time computation restrictions. Indeed, with 3 different values for 5 different parameters, $3^5 = 243$ computations should be carried out for one experimental case.

b. Initial and boundaries conditions

It is necessary to take into account the precision of the fluid temperature measurements as uncertain parameters on boundaries conditions. We suppose that the temperature errors made by measurements are less than 2 degrees. This error is taken into account when evaluating the fluid physical properties, as shown at the Table 2.

Table .2. Uncertainties on fluid physical properties

	Value 1	Value 2	Value 3
T (°C)	18	20	22
ρ (kg/m^3)	998.7	998.0	997.8
μ (kg/m.s)	0.001054	0.001002	0.000955

For the solution containing water and sucrose, same order of variations will be taken. Thus, the values are summarised at the Table 3.

Table .3. Fluid+sucrose physical uncertainties

	Value 1	Value 2	Value 3
T (°C)	20	22.5	25
ρ (kg/m^3)	1008.7	1008.0	1007.8
μ (kg/m.s)	0.001038	0.000991	0.000944

A programme was created in order to handle the uncertainties on the velocity and kinetic energy inlet profiles. This programme draws randomly a profile around the mean inlet profiles with the same standard deviation. An example of obtained profile is shown in red in the Figure.3 (the blue one is the initial profile). Since this is a random plot, we can obtain more and less “chaotic” plots by varying a random parameter.

Figure 3. inlet (blue) and new (red) velocity profiles at the inlet

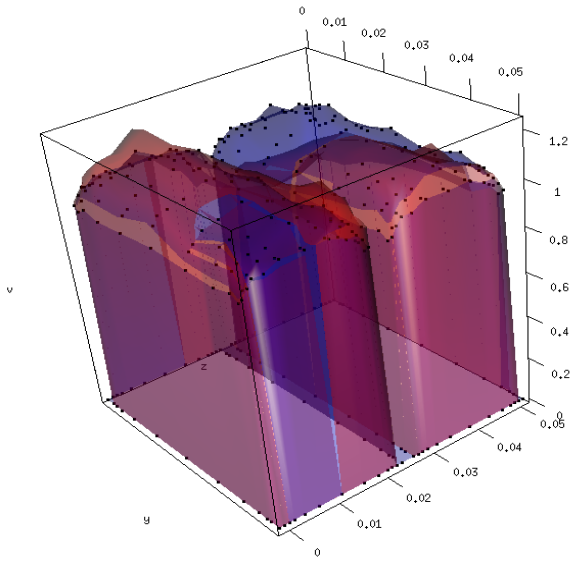

Figure 4. Student's distribution table
Uncertainty Quantification and Sensitivity Analysis in CFD based on Distinction between Categorical and Continuous Variables

Student's t Distribution Table

For example, the t value for 18 degrees of freedom is 2.101 for 95% confidence interval (**2-Tail** $\alpha = 0.05$).

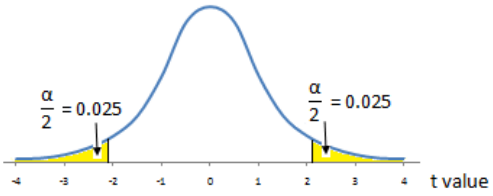

	90%	95%	97.5%	99%	99.5%	99.95%	1-Tail Confidence Level
	80%	90%	95%	98%	99%	99.9%	2-Tail Confidence Level
	0.100	0.050	0.025	0.010	0.005	0.0005	1-Tail Alpha
df	0.20	0.10	0.05	0.02	0.01	0.001	2-Tail Alpha
1	3.0777	6.3138	12.7062	31.8205	63.6567	636.6192	
2	1.8856	2.9200	4.3027	6.9646	9.9248	31.5991	
3	1.6377	2.3534	3.1824	4.5407	5.8409	12.9240	
4	1.5332	2.1318	2.7764	3.7469	4.6041	8.6103	
5	1.4759	2.0150	2.5706	3.3649	4.0321	6.8688	
6	1.4398	1.9432	2.4469	3.1427	3.7074	5.9588	
7	1.4149	1.8946	2.3646	2.9980	3.4995	5.4079	
8	1.3968	1.8595	2.3060	2.8965	3.3554	5.0413	
9	1.3830	1.8331	2.2622	2.8214	3.2498	4.7809	
10	1.3722	1.8125	2.2281	2.7638	3.1693	4.5869	
11	1.3634	1.7959	2.2010	2.7181	3.1058	4.4370	
12	1.3562	1.7823	2.1788	2.6810	3.0545	4.3178	
13	1.3502	1.7709	2.1604	2.6503	3.0123	4.2208	
14	1.3450	1.7613	2.1448	2.6245	2.9768	4.1405	
15	1.3406	1.7531	2.1314	2.6025	2.9467	4.0728	
16	1.3368	1.7459	2.1199	2.5835	2.9208	4.0150	
17	1.3334	1.7396	2.1098	2.5669	2.8982	3.9651	
18	1.3304	1.7341	2.1009	2.5524	2.8784	3.9216	
19	1.3277	1.7291	2.0930	2.5395	2.8609	3.8834	
20	1.3253	1.7247	2.0860	2.5280	2.8453	3.8495	
21	1.3232	1.7207	2.0796	2.5176	2.8314	3.8193	
22	1.3212	1.7171	2.0739	2.5083	2.8188	3.7921	
23	1.3195	1.7139	2.0687	2.4999	2.8073	3.7676	
24	1.3178	1.7109	2.0639	2.4922	2.7969	3.7454	
25	1.3163	1.7081	2.0595	2.4851	2.7874	3.7251	
26	1.3150	1.7056	2.0555	2.4786	2.7787	3.7066	
27	1.3137	1.7033	2.0518	2.4727	2.7707	3.6896	
28	1.3125	1.7011	2.0484	2.4671	2.7633	3.6739	
29	1.3114	1.6991	2.0452	2.4620	2.7564	3.6594	
30	1.3104	1.6973	2.0423	2.4573	2.7500	3.6460	

REFERENCES

[1] A. Barthet and all, ***Uncertainty quantification for a pressurized thermal shock experiment using the WAVE method***

[2] B.E. Launder and all, ***The prediction of*** laminarization with a. two-equation model of turbulence, Dept. of Mechanical Engineering Imperial College, December 1970

[3] C. G. Speziale and all**, An analysis of RNG based turbulence models for homogeneous shear flow**, NASA ICASE Report 91-37, April 1991

[4] V. Yakhot and all**, Renormalization group analysis of turbulence, Basic theory,** Journal of scientidic computing Vol. 1, No1, May 1986

User-04

Short description of the method

The main idea of this method is to make the distinction between categorical and continuous variables to propagate only uncertainties associated to continuous variables. This distinction between continuous and categorical variables is justified by the fact that we do not want to assign a probability to each level of categorical variables.

Uncertainties are propagated for given levels of the categorical variables. For the propagation step, a meta-model is built with a third degree polynomial chaos expansion. For each point of considered profiles (mean velocity, concentration, turbulent kinetic energy), uncertainties bands are determined using order statistics, and correspond to 2.5% and 97.5% percentiles.

Sensitivity analysis can then be obtained by two ways:

- In a quantitative way for a given level of a categorical variable, using Sobol indices for example to see the influence of continuous variables.
- In a qualitative way, by plotting uncertainty bands associated to a quantity of interest (for example the concentration of the fluids at a given point) for all levels of several categorical variables. By doing this we can see the influence of different levels of the categorical variables considered.

Uncertain parameters

Here are introduced the list of uncertain parameters.

To deal with the turbulence, a standard k-epsilon (k-$\mathcal{E}$) model was used. We consider that some of parameters of this model are uncertain, namely the constants $c_{1\varepsilon}$, $c_{2\varepsilon}$, $c_{3\varepsilon}$, c_{μ} and also the prandtl numbers denoted by Pr_K and Pr_{ϵ}.

Since the mixing zone length is much greater than its height as well as the density difference between the two fluids is negligible, the Boussinesq approximation was used. The concentration of fluids was obtained by considering a constituent transportation with an eddy viscosity turbulence model and a turbulent Schmidt number. A standard wall law parametrised by the same turbulent Schmidt number was used. This coefficient, denoted by Sc, controls the turbulent diffusion of the concentration between the two fluids.

Nominal values of these parameters were obtained on simple configurations and we consider that they may vary on more complex configurations. That is why it was decided to consider them as uncertain.

A last parameter was considered as uncertain, namely the α parameter associated to the so-called EF_stab convection scheme in TrioCFD[1]. The convection scheme is a mix between a centred and upwind scheme, and this relation can be expressed as: $(1-\alpha)$ centred + α upwind. This parameter was considered as uncertain since it controls the diffusivity of the scheme and its assigned value often depends on users.

When an uncertain parameter denoted by p follows a normal distribution of mean μ and standard deviation σ, then we write $p \sim \mathcal{N}(\mu, \sigma^2)$. When this parameter follows a uniform distribution between a minimal value min and a maximal value max, then we write $p \sim \mathcal{U}(min,\ max)$.

1. Formely known as Trio_U.

The distribution law of uncertain parameters is introduced below:

$c_{1\varepsilon} \sim \mathcal{N}(1.44, 0.005184)$ $\quad Pr_K \sim \mathcal{N}(1.0, 0.0025)$

$c_{2\varepsilon} \sim \mathcal{N}(1.92, 0.009216)$ $\quad Pr_\epsilon \sim \mathcal{N}(1.3, 0.004225)$

$c_{3\varepsilon} \sim \mathcal{N}(1.00, 0.0025)$ $\quad Sc \sim \mathcal{N}(0.7,\ 0.001225)$

$c_\mu \sim \mathcal{N}(0.09, 0.00002025)$ $\quad \alpha \sim \mathcal{U}(0.3\ , 0.7)$

Remarks about CFD simulations

An important fact to keep in mind is that the quality of CFD results has an important impact on the quality of uncertainty bands. Although we deal with a 3D phenomenon, we decided to start with a 2D modelling. The problem with this decision is that the velocity field is underestimated, as well as the turbulent kinetic energy.

To deal with inlet boundary conditions, a fully 3D developed profile was obtained by an independent simulation in the upper leg, considering periodic boundary conditions at the inlet and outlet. Considering a 2D slice this profile was then analytically approximated by a polynomial in order to be injected in the 2D simulation. Despite this, we miss some 3D phenomena and numerical results are impacted. That means that uncertainty bands are also impacted.

No sensitivity analysis was yet performed: neither quantitatively, nor qualitatively. We will continue the work around uncertainty quantification on Gemix, considering 3D simulations.

User-07

Item	Short description	Information
1	Method used in the quantification of uncertainties	Non-intrusive Polynomial Chaos Expansion
2	Selection of the uncertainty sources	Value of C_μ for turbulent viscosity ($C_\mu = 10^{-7} \sim 0.1$). Turbulent Schmidt number of $Sc_t = 0.1$ is chosen from the simulations for N320 case.
3	How to construct the uncertainty bands	Mean value: $< f >= \frac{1}{b-a}\int_a^b f(x)dx$ obtained from Gauss quadrature method (three points) $< f >= \frac{1}{b-a}\int_a^b f(x)dx = \frac{1}{b-a}\int_{a'}^{b'} f(r)dr$ Uncertainty band: $\sigma^2 =< f - < f >>^2 = \frac{1}{b-a}\int_a^b (f(x) - < f >)^2 dx$ obtained from Gauss quadrature method (three points)

User-09

1. Introduction

The benchmark exercise has been executed according to the ASME V&V 20-2009 standard for validation and verification and uncertainty quantification for CFD applications. An uncertainty propagation method with Latin Hypercube Sampling (LHS) is used to evaluate the uncertainty of input parameters related to material properties, initial conditions and boundary conditions. Richardson extrapolation is used to evaluate spatial discretisation uncertainty. CFD 2D steady state simulations are performed by ANSYS Fluent v14.0 with low Re Abid $k-\varepsilon$ turbulence model.

2. ASME V&V 20-2009

The ASME V&V 20-2009 standard is strongly based on the use of experimental data for V&V and consequently for UQ. With this approach, ASME makes a strong link between V&V and UQ. The global VVUQ process is given below.

Figure 1. Errors and uncertainties in the ASME V&V 20-2009 process

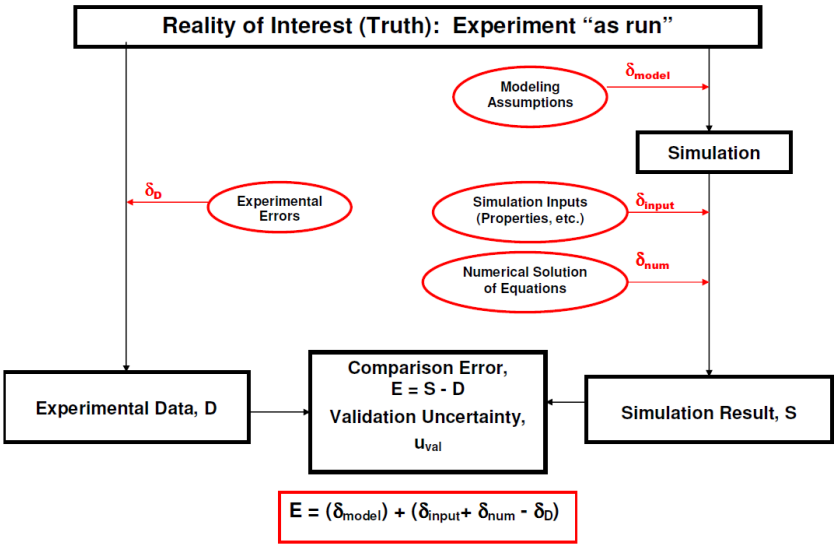

According to the standard V&V 20-2009, the comparison error E in any validation process is defined as the difference between the simulation result, denoted by S, and the experimental value D and if we denote T as the true value, then the comparison error can be split into the following:

$$E = S - D = (S - T) - (D - T)$$

Then, one defines the experimental data error δ_D and the simulation error δ_S, as follows:

$$\delta_D = D - T$$

$$\delta_S = S - T$$

The simulation error δ_S has three components, the first one is the error due to the modelling process δ_{model}; the second is the numerical error δ_{num} produced by the numerical algorithm and the discrete mesh used to solve the modelling equations; and the third is inputs error (IC, BC, properties, …) δ_{input}. The standard uncertainty, u_S is an estimate of the standard deviation of the distribution of δ_S:

$$\delta_S = \delta_{model} + \delta_{num} + \delta_{input} \rightarrow u_S = \sqrt{u_{model}^2 + u_{num}^2 + u_{inp}^2}$$

Going back to the comparison error E, this can be written as:

$$E = \delta_{model} + (\delta_{input} + \delta_{num} - \delta_D)$$

thus, E is the overall result of all the errors coming from the experimental data and the simulation setup. From validation point of view, δ_{model} produced by the modelling is isolated:

$$\delta_{model} = E - (\delta_{input} + \delta_{num} - \delta_D)$$

where:

- E is known from the open tests;
- Signs and magnitude of δ_{num}, δ_{input}, and δ_D are unknown → estimated by standard uncertainties: u_{num} evaluated via Richardson extrapolation, u_{input} evaluated via uncertainty propagation method, and u_D which is known from open tests.

If these errors are really independent, the combined validation uncertainty is given by the expression:

$$u_{val} = \sqrt{u_{input}^2 + u_{num}^2 + u_D^2}$$

Finally, $\delta_{model} = [E - u_{val}, E + u_{val}]$ and we have assumed conservatively $u_{model} = |E| + u_{val}$.

In summary, for the blind test N318, we have evaluated the CFD simulation uncertainty for velocity, turbulent kinetic energy and concentration:

$$u_{S,blind} = \sqrt{u_{model}^2 + u_{num,blind}^2 + u_{inp,blind}^2}$$

u_{model} is obtained as a combination from open tests validation (N339, N337, N320):

$$u_{model} \equiv [u_{model}]_{open} = \left[u_{model,N339}, u_{model,N337}, u_{model,N320}\right]$$

$$[u_{model}]_{open} = [|E|]_{open} + [u_{val}]_{open}$$

$$[|E|]_{open} = [|S - D|]_{open}$$

$$[u_{val}]_{open} = \left[\sqrt{u_{input}^2 + u_{num}^2 + u_D^2}\right]_{open}$$

The data delivered from our side contain the simulated values S for velocity, turbulent kinetic energy and concentration at the requested y and x positions, as well as the symmetric uncertainty bands corresponding to $\pm 2\sigma$ around the mean, namely $S \pm u_S$.

3. Uncertainty in input parameters: u_{input}

The uncertainty of input parameters related to material properties, initial conditions and boundary conditions have been considered. The most relevant inputs are the velocity and turbulent kinetic energy profiles at the inlet. Since the $k - \varepsilon$ turbulence model is selected for the CFD simulations, the ε profile is

mapped together with k at the inlet, using Fluent's definition: $\varepsilon = C_\mu^{0.75} \frac{k^{1.5}}{l}$. In this definition, the turbulent length scale l appears, another input parameter.

The input uncertainties have been characterised by a PDF according to the available data provided and expert judgement. In order to propagate the uncertain input parameters according to their PDFs, the RAP++ software (Reliability Analysis Program) was used, which is able to extract both a set of random Monte Carlo (MC) samples and a set of deterministic samples, namely with the LHS. In a preliminary analysis by means of RAP++/Fluent loops we investigated the importance of each input parameter on the uncertainty in the results. The velocity, turbulent kinetic energy and turbulent length scale appeared the most dominant input parameters. These parameters were, therefore, selected to be applied in our UQ method.

With LHS the domain is first divided into sub-domains, instead of sampling random points in the whole domain, having equal probability content. Only one sample is taken in each sub-domain. In order to determine u_{input} we sampled 20 points as shown in Figure 2, i.e. 21 simulations including the mean point.

4. Numerical uncertainty: $\mathbf{u_{num}}$

We have evaluated as numerical uncertainty the combination of spatial discretisation errors and iteration errors: $u_{num} = \sqrt{u_{iter}^2 + u_{discret}^2}$.

The reference setup of fluent simulations is carachterised by residuals set to 1E-6 and a base mesh containing 62 418 cells. The iteration uncertainty $\mathrm{u_{iter}}$ is evaluated fetching the residuals up to 1E-8 for the base mesh.

The discretisation uncertainty $u_{discret}$ is evaluated via Richardson extrapolation using two additional more refined meshes in both x and y directions with grid spacing ratio $r = 1.6$, in agreement with ASME recommendation.

5. Summary and conclusions

The benchmark exercise has been executed according to the ASME V&V 20-2009 standard for validation & verification and uncertainty quantification for CFD applications. Uncertainty propagation method with deterministic-like sampling is used to evaluate uncertain input parameters (u_{input}), namely a LHS. Richardson extrapolation is used to evaluate the spatial discretisation uncertainty (u_{num}). CFD 2D steady state simulations are performed by ANSYS Fluent v14.0 with low Re Abid $k-\varepsilon$ turbulence model.

The data delivered from our side for the blind test N318 contain the simulated values S for velocity, turbulent kinetic energy and concentration at the requested y and x positions, as well as the symmetric uncertainty bands corresponding to $\pm 2\sigma$, namely $S \pm u_S$. Figure 2, Figure 3 and Figure 4 show our results for the blind test N318.

Figure 2. Blind N318 test computed velocity (S) with ±2σ uncertainty (uS)

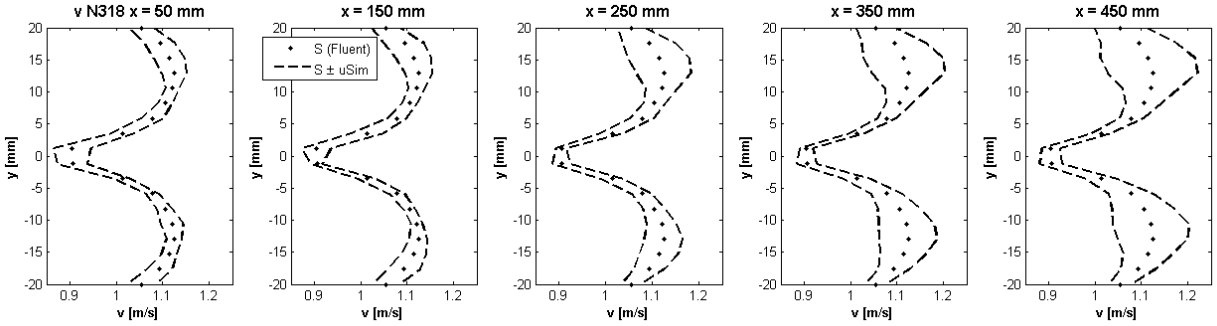

Figure 3. Blind N318 test computed turbulent kinetic energy (S) with ±2σ uncertainty (uS)

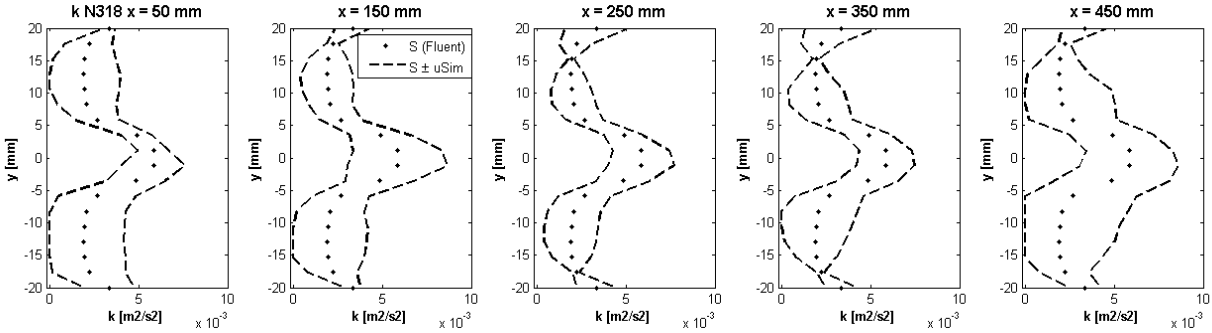

Figure 4. Blind N318 test computed concentration (S) with ±2σ uncertainty (uS)

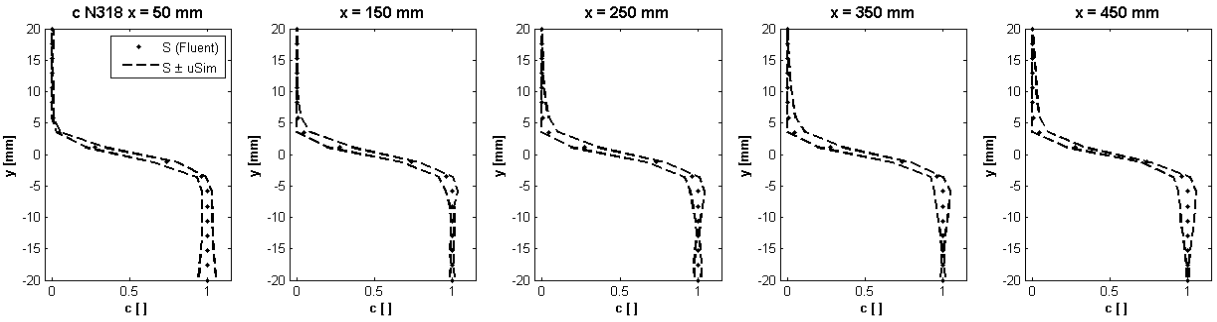

User-10

1. Source of the uncertainty: components of input velocity

Running simulations for open tests, namely N320, N337 and N339, we first checked several different criteria, e.g. we made mesh size sensitivity study, turbulence (RANS) model sensitivity study, in order to ensure that these elements have no or at most negligible influence on final results. The second step was to introduce variability of input parameters in the range given by organisers, in order to estimate uncertainties for considered cases.

In fact, we found strong dependence and great influence of input velocity profile on all output profiles (both measureable like velocities and concentration and derived like turbulence kinetic energy). However, very interesting for us was to observe the behaviour of XY (2D) output velocity profiles when varying only a input Z-velocity component keeping the two other fixed. This observation lead us to focus on effects occurring while treating the input velocity components separately.

2. Method for UQ quantification: Monte Carlo input error propagation

Having significant computing resources, we could easily handle and run hundreds of simulations, tens of them in parallel using 80 cores per each. Such conditions favoured us to choose robust Monte Carlo approach. We assumed to prepare more than hundred (exactly 144) of sets of input setup where 3 velocity components where generated separately for each case, but not entirely random. For each velocity component, we prepared a Gaussian distribution over a given range of velocities for every single input point, basing on the available data. The procedure for creating a single input setup was as follows:

1. We drew 3 random numbers (coefficients): $\boldsymbol{C_1}$, $\boldsymbol{C_2}$ and $\boldsymbol{C_3}$ – each one from a different (Gaussian) normal distribution (see Figure 5)

Figure 5. _ 3 random numbers

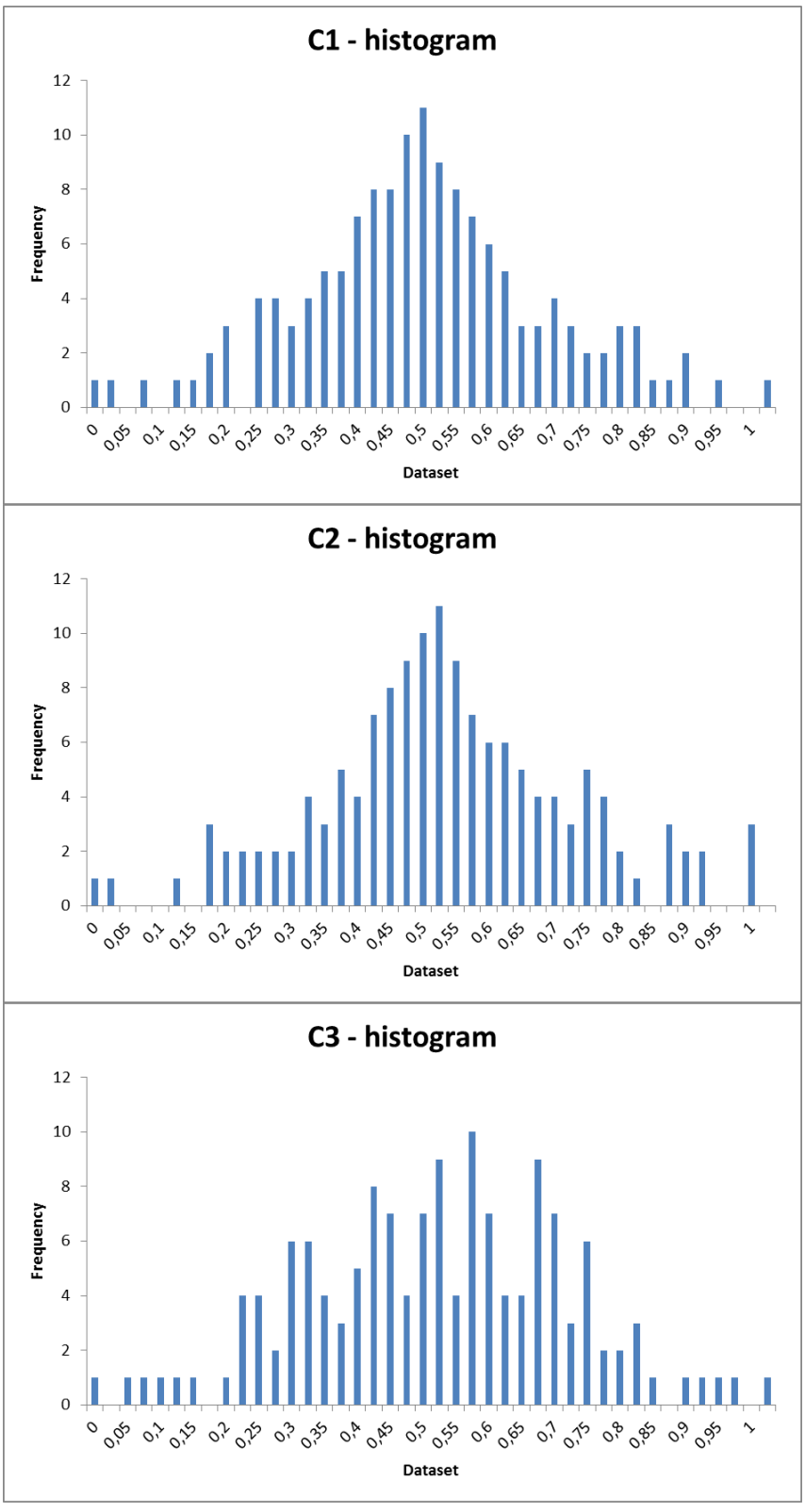

2. We calculated an exact value for an every single point in the particular velocity component profile (i.e. U_x, U_y or U_z). The set of equations for the i-th point is presented below:

$$U_{x,i} = V_{x,i} - RMS_{Vx,i} + 2 \times RMS_{Vx,i} \times C_1$$

$$U_{y,i} = V_{y,i} - RMS_{Vy,i} + 2 \times RMS_{Vy,i} \times C_2$$

$$U_{z,i} = V_{z,i} - RMS_{Vz,i} + 2 \times RMS_{Vz,i} \times C_3$$

In other words, all 144 input sets are based on 3 numbers (3 coefficients) drawn from 3 different Gaussian distributions. Each coefficient served as a multiplier for a whole velocity component profile, so it could not (at least significantly) change a shape of this profile, but it could shift this profile from its 'mean' (averaged) position to either min or max allowed value. Such a situation could lead to a case of increased Y or Z component influence on velocity magnitude in contrast to decreasing X-velocity influence.

3. Comments on results post-processing

In order to extract data, we had prepared a python-script that extracted min, mean and max-value for every single measurement point in the output profiles from over each of 144 simulations. The set of min-values become, finally, a U-dU or K-dK or C-dC depending on a parameter. The max-values become U+dU, K+dK, C+dC and for mean values a set of average result values become a U, K or C. When we refer to the 'average' we mean an arithmetical average calculated from a set of 144 result values obtained for a specific point and parameter, this mean there is no symmetry between upper and lower band.

User-11

The participants User 11 used deterministic sampling method for calculating sensitivity coefficients.

Sensitivity coefficients (uncertain parameters):

- - S1- turbulence models (LES or RANS-LES [RANS – inlet region, LES – mixed zone]);
- - S2- mesh size.

1. Short description of the deterministic sampling method

The goal of this method is to predict how the results from a simulation are affected by one or more uncertain input parameters. These uncertain parameters might be any physical model constant, the value of a fluid or solid property, boundary condition values, or geometric parameters. The term deterministic is used as opposed to random. Random sampling is used in the Monte Carlo simulation, where the parameter values are randomly generated to satisfy a specified probability distribution function (PDF). In the deterministic sampling (DS) method, the parameter values are instead calculated (Julier and Uhlmann, 2004; Hessling, 2013). Unlike the ensemble in the Monte Carlo method, which tries to represent a continuous PDF, the DS method represents the PDF with an ensemble that has the same statistical moments but contains much fewer samples. Each sample requires one simulation. In the DS method, the required number of simulations can be reduced substantially: by a factor of at least four orders of magnitude. This is key to be able to afford UQ in CFD and in all other simulations with long execution times.

2. Statistical moments

In DS, one tries to satisfy the statistical moments of a PDF. The first statistical moment is the mean, the second moment is the variance, the third is the skewness, and the fourth is the kurtosis or flatness. For a parameter, q, with an ensemble containing N samples, these can be written

$$mean = \frac{1}{N}\sum_{i=1}^{N} q_i = \bar{q}$$

$$\mathrm{var} = \frac{1}{N}\sum_{i=1}^{N} \left(q_i - \bar{q}\right)^2$$

$$\sigma = \sqrt{\mathrm{var}}$$

Arbitrarily higher moments can be represented with DS by adding new samples to the ensemble. To represent the mean and the variance of a parameter, q, a minimum of two samples is required.

User-15

1. Selection of the uncertainty sources

Since the uncertainties in the inlet boundary conditions and fluid properties were almost negligible, we selected the free coefficients of the Shear Stress Transport (SST) turbulence model as uncertain input parameters.

SST combines k-ω and *k-ε* turbulence models, using k-ω close to the walls and *k-ε* elsewhere. The SST model has 10 free coefficients: 2 global parameters (β* and a_1), 4 for the k-ω regime (σ_k1, σ_ω1, α_1 and β_1) and 4 for the k-ε regime (σ_k2, σ_ω2, α_2 and β_2). From all these coefficients, only the global and k-ω ones were considered, as the k-ε model was only active in a small region of the domain. These 6 coefficients can be linked to 4 parameters [Reference], which were eventually used as uncertain input parameters.

2. Propagation method

The method used was Polynomial Chaos (PC), which is based on projecting the response of the system into an orthogonal polynomial basis, selected in such a way that the mean and the variance of the response can be easily obtained.

The PC expansion was performed at first order, and the coefficients of the expansion computed by means of Gaussian quadrature. Sixteen simulations were used for the blind case.

3. Construction of uncertainty bands

The uncertainty bands correspond to ±2σ.

Reference

Margheri, L., M. Meldi, M.V. Salvetti and P. Sagaut (2014), "Epistemic uncertainties in RANS model free coefficients", *Computers and Fluids*, 102, pp. 315-335.

User-18

Uncertainty Quantification Method: Polynomial Chaos Expansion

Velocity profiles were parameterised by a linear spline function factored assuming a normal distribution of the velocity over the uncertainty range.

$$U = U_{mean} + X_U U_{95}/2$$

Here $X_U = \pm 1.653$.

The Reynolds stresses were parameterised by a cubic spline function assuming a uniform distribution of the Reynolds stresses over the uncertainty range.

$$R_{ii} = R_{ii,min} + X_K(R_{ii,max} - R_{ii,min})$$

Here $X_K = 0.488085$.

1. Input uncertainties

A process was completed using expert opinion to identify potential sources of uncertainty for the CFD model. These include geometric factors, modelling factors, the grid, boundary conditions, material properties, etc. Estimates of the potential uncertainty for each of these parameters were made using the test information if provided or engineering judgement if necessary. Sensitivity studies were conducted on each parameter to determine which input parameters could have a significant impact on the solution. The results were ranked according to their sensitivity and a total of 6 inputs (along with the mesh size) were found to be significant. The other inputs were not significant. Each of the 6 inputs, along with their estimated 95% (2 σ) confidence intervals is listed in Table .1.

Table .1. Inputs that contributed to solution uncertainty and their confidence intervals The abbreviations next to each input are used in the sensitivity documentation.

Input sensitivity		95% (2 s) Confidence Interval
TI	Turbulence Intensity	4.5% ± 2%
Sct	Turbulent Schmidt Number	0.475 ± 0.175
TopTilt	Upper channel Tilt*	-0.01 ± 0.02
BotTilt	Lower channel Tilt*	-0.01 ± 0.02
TopM	Upper channel mass flow rate	1.219 ± 0.024 kg/s
BotM	Lower channel mass flow rate	1.230 ± 0.025 kg/s
	Mesh	Determined via GCI

*The tilt was a linear variation, defined in Equation 1, applied to the experimental inlet velocity data. Its purpose was to account for possible asymmetry in the velocity inlet boundary condition.

Equation 1

$$\text{tilt factor (y)} = -2*\text{Tilt}*(y+0.025)/0.05 + 1 + \text{Tilt} \qquad y(m) \qquad (1)$$

The grid convergence index (GCI) was used to estimate the solution uncertainty due to the mesh. The refinement (r = 2) was accomplished by successively dividing each cell side in half. The resulting refined meshes had 13 102 272 and 104 818 176 cells starting from the base mesh of 1 637 784 cells. The rate of convergence, p, was calculated using Equation 2. The convergence rates for various points were found to be close to 1 and a final value of 1.0 was used for the GCI determination. The safety factor, Fs, was set to 1.25 which is considered reasonable due to the quality of the mesh and the refinement process. The GCI is used to estimate a bias in the results for the base mesh which is added into the uncertainty in the direction of the bias.

Equation 2

$$p = \ln[(f_m - f_c)/(f_f - f_m)]/\ln \qquad (2)$$

where f is the solution value and c, m, and f correspond to the coarse, medium, and fine meshes.

2. UQ method

It is assumed that each of the inputs that contributed to the solution uncertainty are independent. After calculating the second order sensitivity coefficient for each parameter using an input variation of ± 0.2 σ, an individual parameter uncertainty was calculated by multiplying the 2 σ uncertainty in the input parameter with the sensitivity coefficient. The 95% (2 σ) confidence interval based on the input parameter uncertainties is calculated by combining the individual parameter uncertainties using a root sum square approach (Equation 3).

Equation 3

$U = \text{sqrt (sum (ci2ui2))}$ (ui is the 2 σ uncertainty and ci is the sensitivity for the i-th input)

The uncertainty determined from the grid convergence index (GCI) was included in the total reported uncertainty by adding it to the uncertainty found from the input uncertainty parameters. In general, the GCI uncertainty was added to one side of the uncertainty band based on the direction of the grid convergence (increasing or decreasing values). In the few points where the convergence was oscillatory and a clear direction for the convergence was not found, the GCI uncertainty was added to both the positive and negative sides of the uncertainty band.

User-20

Short description of the UQ method

The uncertainty quantification method implemented was a Monte Carlo simulation to vary the inlet boundary conditions. The densities and inlet velocities of each fluid were the specific conditions varied. The implementation of the UQ on these boundary conditions was due to potential impact on the simulation results. This is especially important when the mesh was developed carefully to appropriate capture the physics involved. Further by carefully selecting an appropriate turbulence model, the inlet boundary conditions became the most sensitive to variation. The uncertainty reported for the measurement of the inlet conditions was provided. This provides a simple comparison based of the experimental and computational uncertainties.

Monte Carlo random sampling based on a normal distribution for velocity and a uniform distribution for density was chosen due to the simplicity of implementation with a commercial solver. By sampling different inlet velocities and densities for each inlet, the prorogation of uncertainty was able to be repeated many times. The large number (40) of samples provided for more accurate statistics to be produced. To illustrate this more clearly, if 40 inlet velocities sets and densities were sampled, there would be 40 CFD simulations. At every spatial data point requested in the mixing section, 40 values for velocity in the x direction, concentration, and turbulent kinetic energy (TKE) were extracted. This large data set was then imported into Matlab for statistical analysis. The mean, 5^{th} and 95^{th} values for velocity, concentration, and TKE were calculated and exported as data files for submission.

Sensitivity coefficients were not produced for this project.